2007

Theoretical Investigation of the Structure and Vibrational Frequencies of Water and Methanol Complexes

John Michael Craig
Virginia Commonwealth University

THEORETICAL INVESTIGATION OF THE STRUCTURE AND VIBRATIONAL FREQUENCIES OF WATER AND METHANOL COMPLEXES

A Thesis submitted in partial fulfillment of the requirements for the degree of Master of Science in Chemistry at Virginia Commonwealth University.
by

JOHN MICHAEL CRAIG
B.S., Virginia Commonwealth University, 1998
A.S., J. Sergeant Reynolds Community College, 1996

Directors: Donald D. Shillady
Professor, Department of Chemistry
Carl O. Trindle
Professor, Department of Chemistry
University of Virginia

Virginia Commonwealth University
Richmond, Virginia
May 2007

Acknowledgement

First of all, I would like to thank Jesus Christ for giving his life so that I might live, for providing the strength to carry on when weary, and for inspiring me to solve many problems that seemed to have no solution at the time.

I would also like to thank Dr. Donald Shillady for being my advisor, for his support and the many one-on-one sessions before important events, and for the important polynomial-variational HEG results. My thanks go out to Dr. Carl Trindle at the University of Virginia for his indispensable and generous advice and guidance, and also for his kind encouragement.

I thank Dr. Sarah Rutan for her patience when the original research and manuscript had to be scrapped after it was found that the foundational formulas from the literature were erroneous. I would also like to express my appreciation for her tireless editing, as we tried to get everything as perfect as possible. I would like to thank Dr. Sally Hunnicutt for those questions that make you use what you know (I love those).

Many thanks go out to Dr. Lidia Vallarino for her encouragement and motherly advice and support. I am also grateful to Dr. Bijan Rao of the Physics Department for having served on my committee until his passing, and for his inspiring remarks and enthusiasm. He is sorely missed. I thank Dr. Lemont Kier for his graciousness and good cheer and for coming on board my committee when needed.

Finally, but certainly not least, I would like to thank my dear parents for their love and support and for our inspiring conversations.

Table of Contents

Page

List of Tables

Page

List of Figures

Page

Abstract

THEORETICAL INVESTIGATION OF THE STRUCTURE AND VIBRATIONAL FREQUENCIES OF WATER AND METHANOL COMPLEXES

By John Michael Craig

A Thesis submitted in partial fulfillment of the requirements for the degree of Master of Science in Chemistry at Virginia Commonwealth University.

Virginia Commonwealth University, May 2007

Major Directors: Donald D. Shillady
Carl O. Trindle, Professors of Chemistry

Water and methanol are common solvents used in liquid chromatographic (LC) separations. It is highly desirable to model the interactions of these solvents in order to better understand the nature of analyte solvation and its effect on retention. Therefore, structure and frequencies of complexes of these solvent molecules have been studied from a theoretical perspective as a first step in this direction. Specifically, cluster structures have been optimized at the RHF and MP2 levels in various flexible basis sets and with the counterpoise correction for basis set superposition error, and trends in the

structure and binding energies of several clusters are described. Good agreement was obtained for the water dimer with the experimental value for the binding energy of D_2O using MP2 energies from 6-311G**/6-31+G** basis sets in conjunction with counterpoise optimizations and full counterpoise corrections. In this investigation harmonic frequencies have been calculated and corrected for the effects of anharmonicity by several methods, two of which are original. The first new method fits a Morse potential function to the energy computed along each normal mode. A second new method is based on fitting a quartic polynomial to energies computed along each normal mode. In cases where the quartic potential function is not very different from the harmonic well, a second order perturbation formula provides a reasonable approximation to the anharmonic vibrational frequencies. When the quartic potential is very far from the harmonic potential, a variational treatment of the vibrations is required. We find that the Morse method delivers reasonable estimates of frequencies of anharmonic motions at lower cost than multi-point potential mapping/multiple geometry optimization/Taylor series methods, and is more successful at predicting intermolecular frequencies than the anharmonic VSCF methods found in GAMESS software. Variational calculations using the quartic polynomials produce estimates of frequencies comparable to the more costly VSCF method. Both the Morse method and polynomial method are very fast computationally relative to these and other methods found in the literature.

CHAPTER I. Overview and Objectives

The goal of the work reported here is the fast prediction of experimental vibrational spectra with reasonable accuracy, using quantum mechanical computational methods. These predicted spectra can give insight into the structure of liquids and into the nature of solvation. This work is the basis for future investigations into analyte solvation and liquid structure because analyte solubility is a thermodynamic property, which can be calculated by statistical mechanics from molecular properties, including vibrational frequencies. This work provides two fast methods that improve calculated frequencies for this purpose. In the future, improved understanding of mobile phases should give rise to improved prediction of LC retention characteristics, in particular, the retention factor k.

In high-performance liquid chromatography, analytes interact with the mobile phase components and the stationary phase according to attractive forces (hydrogen bonding, van der Waals forces, etc.). They partition themselves among these components to varying degrees -- affecting the retention time of the analyte. Understanding how a solute is solvated should therefore lead to a better understanding of separations.

Ab initio optimized geometry calculations of solvent clusters can be used to study solvent-solvent relationships. One of the most important solvent systems from a liquid chromatographic point of view is that of methanol-water. In this work, dimers of pure

water and pure methanol have been examined, as well as the 1:1 molecular complexes of water and methanol. These clusters were chosen to represent some of the cluster compositions suggested by experimental vibrational spectra, analyzed using multivariate curve resolution methods [1]. The optimized structures of these clusters, their hydrogen-bonding energies, hydrogen-bond lengths, angular relationships between atoms participating in a hydrogen-bond, and the harmonic vibrational frequencies have been calculated. Two unique methods for adjusting the harmonic frequency for anharmonicity are presented in detail, calibrated for performance (using experimental data for the water dimer), and compared to the unmodified harmonic frequencies for all clusters and to other approaches from the literature. These improved gas-phase frequencies (and other molecular properties) can later be used to generate bulk liquid-phase thermodynamic data via statistical thermodynamic computations. With improved frequencies, better estimates of bulk thermodynamic properties can then be used to make reliable predictions of relative chromatographic retention times.

Low frequency vibrations and vibrations due to hydrogen bonding may be *very anharmonic* in nature. The computed "static mode" potential of the water dimer, describing the enegy as a function of the position of the bridging, hydrogen bonded hydrogen atom between the two static oxygen atoms, is broad, shallow, and very anharmonic for SCF and correlated SCF potentials (6-311G** and 6-311GL** basis sets, respectively) [2]. Because the potentials of many normal modes vary significantly from the harmonic potential model, it is important to correct for the effects of anharmonicity in these solvent systems. A Morse potential describes the true potential for bond stretching much better than a harmonic function [3]. The improved frequency predictions in this

work have been obtained by employing a distinct Morse or quartic polynomial potential for each vibrational potential.

Many applications can benefit from improved theoretical calculations of vibrations. Computed vibrational spectra can be used to assist in interpreting IR and Raman spectra and as a tool to make assignments of experimental bands [4]. In ranges that are difficult for experimental instruments to obtain frequencies, theory can provide good frequency values in their absence. Also theoretical transitions can be employed to make spectral predictions of new, possibly short-lived and complex, structures as well.

Calculated frequencies and intensities are important for the computation of thermodynamic properties of gas-phase hydrogen bonded complexes. Usually the molecules involved are sufficiently small that it becomes practical to employ the methods of quantum mechanics. It is easier to model thermodynamic quantities of gas phase species than to model solutions because the effects due to hydrogen bonding are not obscured by other factors operating in solution.

Ab intio structure, energy, and frequency calculations are useful for a first-principles determination of solvent effects on hydrogen bonding in the condensed phase. They also shed light on the energetics of the hydrogen bonds themselves, from the values of complexation energies, which are very difficult to derive from condensed phase thermodynamic measurements. These values are important for obtaining state equations for gases. Theoretical values of gas-phase energies and frequencies also allow direct calculation of thermodynamic properties such as the enthalpy of association (directly related to complex stability and the free energy of formation) and the entropy of formation of the gas-phase hydrogen bonded complexes [5].

One method to arrive at thermodynamic properties of gas-phase complexation is to measure and interpret relative vibrational intensities of free monomers and the dimer complex and the temperature dependence of these intensities [5]. Thomas [6] handled IR bands like charge-transfer bands, using the Benesi-Hildebrand approximation [7] to obtain the equilibrium constant (via peak intensity) from the extinction coefficient. Pine and Howard [8] employed absolute IR intensities to arrive at dissociation energies, using statistical thermodynamic total partition functions of monomers and dimers, where the input consists of rotational and vibrational parameters. With a similar approach, Legon et al. [9, 10] found dissociation energies from intermolecular vibrational frequencies. Experimental spectra are sometimes difficult to interpret owing to the overlapping of broadened bands; theoretical calculations can give guidance for distinguishing the position and intensity of spectral peaks. All of these approaches can benefit from employing calculated spectra, and the more accurate the theory the better. Also, fast theoretical treatments are of great value when the complexes of interest are large or when many spectra must be calculated.

CHAPTER II. Anharmonicity Correction Approaches to Vibrational Frequencies

Efforts have been made to improve computational vibrational spectroscopy beyond the frequency predictions of the standard harmonic model. This is especially important for chemical systems having very anharmonic frequencies such as those of hydrogen bonded water and methanol complexes. Several correction approaches are outlined here: simple scaling of harmonic frequencies [11, 12], is the least demanding, while attempts to solve the vibrational Schroedinger equation require much more elaborate efforts. These include treating a series expansion of the Hessian matrix by perturbation theory [13], solving a self-consistent approximation to the vibrational problem (VSCF) [4, 14, 15], treating coupling of the normal modes which are the basis of that method by perturbation theory (cc-VSCF) [4, 14, 15] and variational treatments of the vibrational potential [16].

2.1 Scaling Factors for Harmonic Frequencies

Pople et al. [11, 12] created the first general scaling factors to adjust the harmonic frequencies for systematic errors (relative to observed vibrational frequencies) due to anharmonicity. These include the familiar 0.8929 factor for use for the HF/6-31G(d) model chemistry and the 0.9427 factor for MP2/6-31G(d) calculations.

Scott and Radom [17] have developed sets of scaling factors for various model chemistries. Their factors were developed using a set of 122 molecules including water for a total of 1066 frequencies for the fundamental frequency scaling factors and 1062 frequencies for low frequency mode scaling factors. Scaling factors were calculated for

the individual molecules (which are not reported in that work) en route to developing the general scaling factors for various levels of theory and basis sets. The optimum scaling factor, λ, for the fundamental frequencies is determined through a least-squares approach where the residual (Δ) is minimized

$$\Delta = \sum_{i}^{all} (\lambda \omega_i^{theor} - \omega_i^{expt})^2 \tag{2.1}$$

and ω_i^{theor} is the ith harmonic frequency and ω_i^{expt} is the ith experimental frequency of the 1066 frequency set. This leads to the following expression for the optimized scaling factor

$$\lambda = \frac{\sum_{i}^{all} \omega_i^{theor} \omega_i^{expt}}{\sum_{i}^{all} (\omega_i^{theor})^2} \tag{2.2}$$

Root mean square errors relative to the entire frequency set are calculated for each scaling factor according to

$$rms_{ov} = \left(\frac{\sum_{l}^{n_{all}} \Delta_{\min}}{n_{all}} \right)^{\frac{1}{2}} \tag{2.3}$$

where $\Delta_{\min}$ is the minimized residual for each mode. The fundamental scaling factors derived from this approach are presented in Table 1 below for various levels of conventional *ab initio* theory, with the root-mean-square error for each factor.

Table 1. Scaling Factors for Fundamental Harmonic Vibrational Modes [17].

Method	Scale Factor	rms_{ov} (cm^{-1})
HF / 3-21G	0.9085	87
HF / 6-31G(d)	0.8953	50
HF / 6-31+G(d)	0.8970	49
HF / 6-31G(d,p)	0.8992	53
HF / 6-311G(d,p)	0.9051	54
HF / 6-311G(df,p)	0.9054	56
MP2-fu / 6-31G(d)	0.9427	61
MP2-fc / 6-31G(d)	0.9434	63
MP2-fc / 6-31G(d.p)	0.9370	61
MP2-fc / 6-311G(d,p)	0.9496	60
QCISD-fc / 6-31G(d)	0.9537	37

Fc means frozen core: excitations from cores are not included in the perturbation theory; fu refers to calculations including such excitations.

The scaling factors for density functional methods ranged from 0.9558 to 0.9986 (rms_{ov} 34 - 45 cm^{-1}). The authors [17] found that only 8 % of the frequencies derived from using the MP2-fc / 6-311G(d,p) method were beyond their arbitrary target accuracy of ±10 % relative to experimental values.

Frequency corrections were also developed [17] to minimize the error of the low-frequency, fundamental vibrations using an inverse scaling factor and a least-squares fit. (The previous scaling factor was weighted to favor minimization of errors for high frequencies). This time, the residuals are calculated according to

$$\Delta = \sum_{i}^{all} \left(\frac{1}{\lambda \omega_i^{thoer}} - \frac{1}{\omega_i^{expt}} \right)^2 \qquad (2.4)$$

for 1062 frequencies from the 122 molecule set.

The optimized low frequency scaling factor is found from

$$\lambda = \frac{\sum_{i}^{all}\left(\frac{1}{\omega_i^{thoer}}\right)^2}{\sum_{i}^{all}\frac{1}{\omega_i^{thoer}\omega_i^{expt}}} \tag{2.5}$$

The resulting optimized scaling factors for conventional *ab initio* theory are given in Table 2 below.

Table 2. Scaling Factors for Low-frequency Harmonic Vibrational Modes [17].

Method	Scale Factor	rms_{ov} (10^{-5} cm^{-1})
HF / 3-21G	1.0075	39
HF / 6-31G(d)	0.9061	15
HF / 6-31+G(d)	0.9131	15
HF / 6-31G(d,p)	0.9089	15
HF / 6-311G(d,p)	0.9110	15
HF / 6-311G(df,p)	0.9085	15
MP2-fu / 6-31G(d)	1.0214	24
MP2-fc / 6-31G(d)	1.0485	29
MP2-fc / 6-31G(d.p)	1.0229	23
MP2-fc / 6-311G(d,p)	1.0127	23
QCISD-fc / 6-31G(d)	1.0147	20

In this work, the factors defined by Scott and Radom [17] are used to correct harmonic frequencies which were previously calculated at the MP2/6-311G(d,p) level to evaluate the effectiveness of their method. These are displayed in Table 3 below. The authors [17] use a frozen core approximation in their MP2 calculations, while my harmonic frequencies are obtained by full calculations. It is still possible to use Scott and Radom's scaling in this case because the difference in the root mean square errors (rms_{ov}) was only about 2 cm^{-1} for full and frozen core calculations [17] in a similar basis set.

Throughout Chapter II (anharmonic frequency methods), the latest available experimental data has been provided alongside the authors' frequency results in each table.

Table 3. MP2/6-311G(d,p) Frequencies of the Water Dimer Using Scaling Factors.

Mode	Harm v (cm^{-1}) [a]	Scaled Harm v (cm^{-1}) [b]	Experiment (cm^{-1})	% Dev vs Exp
Donor rotation about O-O	115	116	88 [c]	31.8
	143	145	103 [c]	40.8
	143	145	108 [c]	34.5
O-O stretch	157	159	143 [d]	10.9
	306	310	311 [e]	0.270
	566	573	523 [e]	9.59
Acceptor O-H bend	1673	1694	1599 [e]	5.94
Donor O-H bend	1701	1723	1616 [e]	6.62
Donor O-H sym stretch	3869	3674	3601 [f]	2.02
Acceptor O-H sym stretch	3906	3709	3660 [f]	1.34
Donor O-H asym stretch	3990	3789	3735 [f]	1.44
Acceptor O-H asym stretch	4010	3808	3745 [f]	1.68

[a] Harmonic frequencies this work, Gaussian 03. [b] Harmonic frequencies scaled using Scott and Radom's 1.0127 factor for low-frequency, fundamental vibrations and intermolecular modes (lowest eight modes) and the 0.9496 factor for high-frequency, fundamental vibrations (highest four modes). [c] Reference [18], planar supersonic molecular beam expansion (terahertz laser vibration-rotation-tunneling spectroscopy), 5 K. [d] Reference [19], planar supersonic molecular beam expansion (terahertz laser vibration-rotation-tunneling spectroscopy), 5 K. [e] Reference [20], Neon matrix, 10 K. [f] Reference [21], molecular beam depletion spectroscopy with size selection by momentum transfer in scattering experiment (atoms under single collision conditions).

The intramolecular frequencies for the water dimer as scaled by Scott and Radom are in good agreement with the experimental data provided, especially for the high-frequency, fundamentals. The scaling factors handle the intermolecular vibrations less well, especially in the case of the lowest three vibrational modes. These three calculated modes do not agree well with the experimental values probably because the harmonic vibrational model is the basis for the scaling factors, and these modes are more akin to relative rotations or torsions of the two water molecules rather than to vibrations.

2.1.1 Experimental Frequencies

The frequencies for vibrational transitions in water dimer and related systems are not very well established. It should be noted that experimentally determined frequencies vary by the techniques and conditions used to obtain them, as can be seen from the range of frequencies measured for each mode in Table 4. Matrix effects perturb experimental frequencies, so molecular beam work is deemed more accurate. Though not an absolute standard, experimental bands make a good benchmark for comparison with theoretical spectral values.

Table 4. Experimental Frequencies of the Water Dimer (cm^{-1})

Mode	Molecular Beam		Neon Matrix		Nitrogen Matrix	Argon Matrix	Range	Description
1	88 [a]		93 [g]	106 [h]			88-106	PD torsion
2	103 [a]		115 [g]	128 [h]			103-128	PA wag
3	108 [a]		123 [g]				108-123	PA twist
4	143 [b]	150 [d]					143-150	Intermolec str
5			311 [g]		310 [i,j]	300 [j,m]	300-311	In-plane bend
6			523 [g]	514 [h]	520 [i,j]	500 [j,m]	500-523	Out-of-plane bend
7			1599 [g]		1601 [j,k]	1593 [j,m]	1593-1601	PA OH bend
8			1616 [g]		1619 [j,k]	1612 [j,m]	1612-1619	PD OH bend
9	3601 [c]	3480 [e], 3530 [f]	3591 [g]				3480-3601	PD sym OH str
10	3660 [c]	3600 [f]	3661 [g]		3627 [j,l]	3634 [j,n]	3600-3661	PA sym OH str
11	3735 [c]	3730 [f]	3734 [g]		3699 [j,l]	3709 [j,n]	3699-3735	PD asym OH str
12	3745 [c]	3745 [f]	3750 [g]		3715 [l]	3726 [n]	3715-3750	PA asym OH str

[a] Reference [18], planar supersonic molecular beam expansion (terahertz laser vibration-rotation-tunneling spectroscopy), 5 K. [b] Reference [19], planar supersonic molecular beam expansion (terahertz laser vibration-rotation-tunneling spectroscopy), 5 K. [c] Reference [21], molecular beam depletion spectroscopy with size selection by momentum transfer in scattering experiment (atoms under single collision conditions). [d] Reference [22], molecular beam electric resonance spectroscopy. [e] Reference [23], molecular beam, coherent anti-Stokes Raman spectroscopy. [f] Reference [24], high resolution near-IR, molecular beam. [g] Reference [20], neon matrix, 4 K. [h] Reference [20], neon matrix, 8 K. [i] Reference [25], nitrogen matrix. [j] Descriptions assigned on the basis of harmonic frequencies. [k] Reference [26], nitrogen matrix, 20 K. [l] References [27, 28], nitrogen matrix. [m] [25], argon matrix. [n] References [27, 28], argon matrix.

2.2 Taylor Expansions, Fourier Series, and Morse Potential

Muñoz-Caro and Niño [29] studied the water monomer and dimer at the MP2/6-311++G(2d,2p) level using a variety of methods for correcting frequencies for anharmonic effects. They state that there is a fine line between translation and large amplitude vibrations, and suggest that the low frequency intermolecular vibrations often are in excited states at room temperature. Therefore, the kinetic elements of their vibrational Hamiltonian include the effects of coupling between translation and large amplitude vibrations.

The authors [29] separate the vibrational motions into normal modes, and define potentials for each mode q_k (each normal coordinate). The vibrational potentials are usually represented by a Taylor series in q_k. For some frequencies they take special measures, employing a Morse potential, a Fourier series, or (for coupled modes) a double Taylor series. They generate their mode potentials by calculating single-point energies along normal mode coordinates r_i according to

$$r_i = r_e + \Delta W_i \tag{2.6}$$

where r_e is the equilibrium position of the atoms, and ΔW_i is the displacement along the normal mode potential in the direction W_i. ΔW_i is an arbitrary factor, usually 0.1 and 0.2 so the depth of the well probed varies inconsistently from potential to potential and can result in the probing of high-energy regions of the potential for one mode and only low-energy regions of the potential for another mode. The problems with this type of probing have been remedied by a novel technique presented later (this work). Once the potentials

have been defined by their sets of single-point energies, Munoz-Caro and Nino [29] solve their vibrational Hamiltonian variationally.

Below, in Table 5, are the theoretical frequency results for the water dimer as reported by Muñoz-Caro and Niño [29]. A detailed description of the methods employed for each of the frequencies follows.

Table 5. Anharmonic Frequencies of the Water Dimer [29].

Mode	Anharmonic v (cm^{-1}) [a]	Expt (cm^{-1})	% Dev vs Exp
Donor rotation about O-O	105	88 [b]	19.3
	NA	103 [b]	NA
	158	108 [b]	46.3
O-O stretch	153	143 [c]	6.99
	371	311 [d]	19.3
	639	523 [d]	22.2
O-H bend	1654	1599 [d]	3.44
O-H bend	1680	1616 [d]	3.96
Donor O-H stretch	3548	3601 [e]	1.47
Acceptor O-H stretch	3803	3660 [e]	3.91
Donor O-H stretch	3905	3735 [e]	4.55
Acceptor O-H stretch	3769	3745 [e]	0.641

[a] Frequencies after various anharmonic corrections by Muñoz-Caro and Niño [29]as described in this text at MP2/6-311++G(2d,2p); NA indicates that no anharmonic frequency was attempted. [b] Reference [18], planar supersonic molecular beam expansion (terahertz laser vibration-rotation-tunneling spectroscopy), 5 K. [c] Reference [19], planar supersonic molecular beam expansion (terahertz laser vibration-rotation-tunneling spectroscopy), 5 K. [d] Reference [20], Neon matrix, 10 K. [e] Reference [21], molecular beam depletion spectroscopy with size selection by momentum transfer in scattering experiment (atoms under single collision conditions). In order to match all frequencies, assignments for modes without descriptions (not available from Muñoz-Caro and Niño [29]) are based on matching the order of their harmonic frequencies with those of Dunn, et al. [30], as both authors used sufficiently large basis sets to make these assignments good assumptions.

For the higher, fundamental frequencies [29], a Taylor expansion is fitted to the single-point energies, and coupling between modes is not considered. The asymmetric

O-H stretch of the water acceptor molecule is given special consideration. The Taylor series was found to produce a frequency that was higher even than the harmonic frequency, which is known to overestimate stretching fundamental frequencies. Muñoz-Caro and Niño [29] rationalize that the asymmetric vibration has an instantaneous potential like a Morse potential while one O-H bond expands and the other O-H bond contracts. However, for the second half of the vibration where the first O-H bond contracts and the second expands, the potential would need to be reversed for this situation. This translates into a positive quartic correction in the Taylor expansion relative to the harmonic potential and, thus a higher frequency. They solved the problem by simple scaling, reducing the compression motions of both O-H bonds by 4 % and obtained better agreement with experimental results. All water O-H stretches not involved in H-bonding were treated in this manner.

The donor O-H symmetric stretch which is influenced by the H-bonding was treated by mapping a relaxed scan along the O-H bond length [29]. The hydrogen was moved incrementally in steps of 0.2 Å, and the energy at each point was optimized with respect to the remaining coordinates. These energy points were then used to generate a Taylor series as before, resulting in a polynomial with quartic terms in the displacement. As can be seen from Table 5, this method generated a frequency about 1.5 % lower than that of the quoted experimental value for this mode.

The intermolecular vibrational mode that is mainly the rotation of the donor water molecule about the O-O axis [29] was handled by changing the geometry configuration of the dimer by rotating the donor water molecule in steps of 30° about the O-O axis. The energy was optimized with respect to other degrees of freedom for each angle effectively

mapping the rotational potential. A Fourier expansion was fit to the grid as a function of torsional angle. The vibrational energy levels were then calculated variationally in the free-rotor basis.

The O-O intermolecular stretching mode is also handled [29] with a special procedure. Nine single-point energies are calculated along the O-O distance in addition to the energy at the equilibrium geometry. The O-O distance is adjusted in increments of 0.2 Å, and the geometry is fully optimized at each step (fixed O-O distance). Most of these points describe the dissociative portion of the vibration beyond the equilibrium length (about 2.9 Å), including one point beyond the systematic stepping at about 4.4 Å. The remaining points arise from compression of the O-O distance. The resulting energies are then used to construct a Morse potential to describe this mode. The O-O stretching frequency generated is in good agreement with the listed experimental frequency (about 7 % higher than and within 10 cm^{-1} of the experimental value).

Muñoz-Caro and Niño [29] also investigated the technique of 2-dimensional potential grid mapping as a means of accounting for the coupling between vibrational modes. They studied the coupling of the donor O-H stretch with the O-O stretch using a surface grid of 12 points and re-optimized the geometry of the remaining coordinates not involved in these motions for every point. A double Taylor series in the two normal modes $q_{O\text{-}O}$ and $q_{O\text{-}H}$ was then fitted to those points, and the resulting 2-dimensional oscillator potential with coupling terms was solved variationally. The resulting frequencies for the donor O-H stretch and the O-O stretch were 3321 cm^{-1} and 176 cm^{-1}, respectively, as seen in Table 6 below.

Table 6. Donor O-H stretch and O-O stretch using One-Dimensional and Two-Dimensional Grid-Mapping [29].

Mode	Anharmonic v (cm^{-1})	Expt (cm-1)	% Dev vs Exp
One-Dimensional Models			
O-O stretch	153 [a]	143 [c]	6.99
Donor O-H stretch	3548 [b]	3601 [d]	1.47
Two-Dim. Coupled Model			
O-O stretch	176	143 [c]	23.1
Donor O-H stretch	3321	3601 [d]	7.78

[a] 10-point potential mapping at MP2/6-311++G(2d,2p) with fit of Morse potential. [b] Five-point mapping at MP2/6-311++G(2d,2p) with fit of Taylor series polynomial. [c]Reference [19], planar supersonic molecular beam expansion (terahertz laser vibration-rotation-tunneling spectroscopy), 5 K. [d] Reference [21], molecular beam depletion spectroscopy with size selection by momentum transfer in scattering experiment (atoms under single collision conditions).

Given that the independent mode models used initially in this study [29] yield more reliable results than the coupled model, it seems that a two-dimensional grid potential is not the best approach for describing the coupling between these two stretching modes of the water dimer.

With this assortment of techniques and approaches for handling the frequencies of the water dimer, Muñoz-Caro and Niño [29] arrive at frequencies that are significantly higher than those found experimentally for the low frequency intermolecular vibrations. However, their methods result in good agreement with experimental values for the intramolecular modes, producing generally only slight overestimates in these frequencies.

2.3 Vibrational Self-Consistent Field (VSCF) Approximation

Chaban, Jung, and Gerber [14, 15, 31] present a method that uses input from *ab initio* electronic structure calculations to directly calculate corrected frequencies for all vibrational modes and includes the effects due to pair-wise mode coupling of each mode

with all of the others, treating the very anharmonic water monomer and dimer. Like Muñoz-Caro and Niño, they make the assumption that the total vibrational wave function, Ψ_n, of all modes Q_N is given by the product of the vibrational wave functions in the state (n) of each individual mode as follows

$$\Psi_n(Q_1,\ldots,Q_N) = \prod_{j=1}^{N} \psi_j^{(n)}(Q_j) \tag{2.7}$$

The self-consistent field equation for one mode is given by

$$\left[\frac{-1}{2}\frac{\partial^2}{\partial Q_j^2} + \overline{V_j^{(n)}}(Q_j)\right]\psi_j^{(n)} = \varepsilon_j^{(n)}\psi_j^{(n)} \tag{2.8}$$

where the harmonic potential of the Hamiltonian is replaced by

$$\overline{V_j^{(n)}}(Q_j) = \left\langle \prod_{l\neq j}^{N} \psi_l^{(n)}(Q_l) \middle| V(Q_1,\ldots,Q_N) \middle| \prod_{l\neq j}^{N} \psi_l^{(n)}(Q_l) \right\rangle \tag{2.9}$$

This is a "mean field" or self- consistent approximation analogous to the Hartree-Fock method for electronic motions. Equations (2.7) and (2.8) must be solved iteratively until self-consistency is reached, resulting in the calculations of the single-mode energies, wave functions, and potentials.

The total vibrational energy in the VSCF approximation is represented by

$$E_n = \sum_{j=1}^{N} \varepsilon_j^{(n)} - (N-1)\times\left\langle \prod_{j=1}^{N} \psi_j^{(n)}(Q_j) \middle| V(Q_1,\ldots,Q_n) \middle| \prod_{j=1}^{N} \psi_j^{(n)}(Q_j) \right\rangle \tag{2.10}$$

It is possible to go beyond the mean-field approximation. The potential operator from equation (2.10) can be written

$$V(Q_1,\ldots,Q_N) = \sum_{j=1}^{N} V_j(Q_j) + \sum_{i}\sum_{i<j} V_{ij}(Q_i,Q_j) \tag{2.11}$$

where the single mode potential $V_j(Q_j)$ is perturbed by the pair-wise interaction of mode j with all other modes i. The coupling integrals have the form

$$V_j^{coup,n}(Q_j) \equiv \langle \psi_i(Q_i) | V_{ij}(Q_i, Q_j) | \psi_i(Q_i) \rangle \tag{2.12}$$

where the pair-wise interaction potential from (2.11) is the operator. Both terms in the potential are recovered from a grid of energy values. The VSCF method is generally used in conjunction with *ab intio* potential surfaces. A number N ranging from 8 to 32 single-point energies are calculated for mode j, and if coupling is to be described a two-dimensional grid of points for displacements along modes i and j is generated [14]. This results in a N x N potential grid representation of $V_{ij}(Q_i, Q_j)$, the interaction between the two modes. It was found that a 16 x 16 point grid (256 points) was sufficient to describe two-mode coupling in the water monomer and dimer [15].

2.4 Correlation Corrected VSCF (CC-VSCF)

A more advanced form of VSCF [14, 15, 31] involves the correction of the VSCF vibrational energy to second order using the expression below

$$E_n^{cc2} = E_n^{VSCF} + \sum_m \sum_n \frac{\left| \left\langle \prod_{j=1}^{N} \psi_j^{(n)}(Q_j) \middle| \Delta V \middle| \prod_{j=1}^{N} \psi_j^{(m)}(Q_j) \right\rangle \right|^2}{E_n^{(0)} - E_m^{(0)}} \tag{2.13}$$

where E_n^{cc2} is the final cc-VSCF energy (correlation-corrected VSCF vibrational energy). The correlation effects are defined by the quantity

$$\Delta V(Q_1, \ldots, Q_N) = V(Q_1, \ldots, Q_N) - \sum_{j=1}^{N} \overline{V_j^{(n)}}(Q_j) \tag{2.14}$$

It is possible to treat only a subset of frequencies if desired for either VSCF or cc-VSCF. The VSCF and cc-VSCF methods are available in the GAMESS software package, and the authors [15] estimate that chemical systems as large as 15 atoms can be fully treated.

In Table 7, the frequency results from the VSCF and CC-VSCF methods [31] are shown for the water dimer, where all potential surface calculations were done at the MP2/TZP level. The harmonic frequencies overestimate the fundamental stretching frequencies, while the VSCF and CC-VSCF methods do correct the high frequency, intramolecular modes to the red and are in very good agreement with experimental values. The VSCF model slightly underestimates the frequencies of bending modes, while the CC-VSCF method slightly underestimates the intramolecular frequencies in general. However, for the low frequency, intermolecular modes, the VSCF and CC-VSCF frequencies are not very consistent with one another or with the harmonic frequencies and are much larger than the harmonic frequencies.

Table 7. Anharmonic Frequencies of the Water Dimer by VSCF and cc-VSCF

Mode	Harm (cm^{-1})	VSCF (cm^{-1})	CC-VSCF (cm^{-1})	Expt (cm^{-1})	% Dev vs Exp VSCF	% Dev vs Exp CC-VSCF	Description
1	142	545	419				
2	161	414	309				
3	179	259	147	143 [a]	81	2.8	O-O str
4	191	451	409				
5	366	550	521				
6	674	769	732				
7	1618	1565	1564	1599 [b]	2.13	2.19	acceptor bend
8	1646	1612	1605	1616 [b]	0.248	0.681	donor bend
9	3799	3560	3565	3601 [c]	1.14	1.000	donor sym str
10	3874	3689	3647	3660 [c]	0.792	0.355	acceptor sym str
11	3982	3733	3745	3735 [c]	0.0535	0.268	donor asym str
12	4005	3763	3724	3745 [c]	0.481	0.561	acceptor asym str

[a] Reference [19], planar supersonic molecular beam expansion (terahertz laser vibration-rotation-tunneling spectroscopy), 5 K. [b] Reference [20], Neon matrix, 10 K. [c] Reference [21], molecular beam depletion spectroscopy with size selection by momentum transfer in scattering experiment (atoms under single collision conditions).

Table 8 provides a closer look at the low frequency vibrations. Each mode and the harmonic, VSCF, and CC-VSCF frequencies correspond to one another, according to the assignments of Chaban, et al. [31].

Table 8. Overall Comparison with Available Experimental Low Frequency Vibrations for the Water Dimer [4].

Mode	Harm (cm^{-1})	VSCF (cm^{-1})	CC-VSCF (cm^{-1})	Expt (cm^{-1})
1	142	545	419	88 [a]
2	161	414	309	103 [a]
3	179	259	147	108 [a]
4	191	451	409	143 [b]
5	366	550	521	311 [c]
6	674	769	732	523 [c]

[a] Reference [18], planar supersonic molecular beam expansion (terahertz laser vibration-rotation-tunneling spectroscopy), 5 K. [b] Reference [19], planar supersonic molecular beam expansion (terahertz laser vibration-rotation-tunneling spectroscopy), 5 K.
[c] Reference [20], Neon matrix, 10 K.

Due to the sparse mode descriptions provided by the authors [31] for the low modes, it is difficult to assign experimental frequencies (including newer observed values that have now become available) on a mode per mode basis, so these experimental values are listed in ascending order to provide a means of comparison with the theoretical intermolecular frequencies as a whole.

As can be seen, the VSCF frequencies are in the 400 cm^{-1} and 500 cm^{-1} range, or more, for five of the six modes, greatly overestimating the experimental frequencies of the low mode vibrations where five of the six frequencies are found between 88 cm^{-1} and 311 cm^{-1}. The CC-VSCF low frequencies are a modest improvement over the VSCF predictions, but these also, as a whole, overestimate the experimental results by a large margin. The harmonic frequencies, however, do provide a more reasonable agreement with the experimental values as a group.

Chaban et al. [31] also investigated the frequencies of both the water-methanol configuration (where water donates the proton in the hydrogen bond) and the methanol-water configuration (where methanol donates the proton) of the water/methanol mixed dimer. As before, all potential surface calculations were done at the MP2/TZP level. In Table 9 for the water-donor complex, where experimental data is available, the VSCF and CC-VSCF frequencies agree very well with the experimental values of the fundamental frequencies. However, the VSCF and CC-VSCF methods generally blue-shift frequencies to a large extent relative to the harmonic frequencies for the intermolecular vibrations. This suggests that they may be largely overestimating physically measurable frequencies as was the case for the water dimer.

The red-shifting of the bonded water OH-stretch in this mixed complex relative to that in the water dimer gives evidence (both from the VSCF and CC-VSCF calculations, as well as from the experimental data) that the hydrogen bonding is stronger in the water-methanol conformer of the mixed dimer than in the water dimer.

Table 9. Anharmonic Frequencies of the Water(donor)-Methanol Dimer [4].

Mode	Harm (cm^{-1})	VSCF (cm^{-1})	CC-VSCF (cm^{-1})	Expt [a] (cm^{-1})	% Dev vs Exp VSCF	% Dev vs Exp CC-VSCF	Description
1	55	252	174				
2	75	279	142				
3	130	578	575				
4	200	195	172				O-O str
5	306	579	546				
6	402	623	592				
7	678	827	799				
8	1065	1039	1037	1032	0.678	0.484	CO str
9	1098	1104	1093	1078	2.41	1.39	Methanol bend
10	1210	1203	1201				Methanol bend
11	1390	1371	1366				Methanol bend
12	1532	1503	1500	1466	2.52	2.32	CH_3 bend
13	1540	1531	1532				CH_3 bend
14	1552	1539	1539				CH_3 bend
15	1641	1593	1582	1614	1.30	1.98	H_2O bend
16	3093	2955	2907	2974	0.639	2.25	CH_3 str
17	3172	2975	2935	3018	1.42	2.75	CH_3 str
18	3229	3050	3026				CH_3 str
19	3760	3530	3501	3539	0.254	1.07	H_2O str (bonded OH)
20	3911	3683	3713	3663	0.546	1.37	Methanol OH str
21	3975	3742	3792	3704	1.03	2.38	H_2O str (free OH)

[a] Reference [32], Argon matrix, 12 K.

In Table 10 the frequencies for the methanol-donor configuration of the water/methanol dimer are given. Good agreement with the experimental frequencies was obtained with both the VSCF method and the CC-VSCF for the fundamental vibrational modes. For the intermolecular modes, the VSCF method still exhibits some

inconsistency with the harmonic frequencies. In all cases, the VSCF and CC-VSCF methods produce frequencies that are higher (and usually much higher) than the harmonic values for each mode.

Table 10. Anharmonic Frequencies of the Methanol(donor)-Water Mixed Dimer

Mode	Harm (cm^{-1})	VSCF (cm^{-1})	CC-VSCF (cm^{-1})	Expt [a] (cm^{-1})	% Dev vs Exp VSCF	% Dev vs Exp CC-VSCF	Description
1	75	215	192				
2	81	350	102				
3	99	413	270				
4	188	309	284				
5	209	496	432				
6	252	652	614				
7	721	851	827				
8	1094	1067	1064	1048	1.81	1.53	CO str
9	1141	1135	1128	1103	2.90	2.27	OCH bend
10	1209	1192	1189				OCH bend
11	1456	1428	1420	1380	3.48	2.90	COH bend
12	1531	1497	1495	1448	3.38	3.25	CH_3 bend
13	1536	1515	1516	1464	3.48	3.55	CH_3 bend
14	1555	1524	1523	1475	3.32	3.25	CH_3 bend
15	1619	1617	1625	1601	0.999	1.50	H_2O bend
16	3061	2930	2891	2835	3.35	1.98	CH_3 str
17	3123	2934	2904				CH_3 str
18	3194	3020	3007	2982	1.27	0.838	CH_3 str
19	3812	3572	3595	3536	1.02	1.67	Methanol OH str
20	3874	3689	3645	3627	1.71	0.496	H_2O sym str
21	4005	3705	3661	3714	0.242	1.43	H_2O asym str

[a] Reference [33], Nitrogen Matrix, 10 K.

The authors [31] remark that their VSCF and CC-VSCF methods will predict the intermolecular vibrational frequencies of hydrogen bonded systems with less accuracy than for the fundamental frequencies and that the greatest inaccuracy would be found for low frequency modes involving large nuclear motions.

2.5 Taylor Series Transformation into Morse and Gauss Potentials

Taylor series force fields do not predict strong anharmonicity features when they are present in the potentials of large displacement vibrations [16]. Because Taylor expansions do not always describe vibrational potentials very well, especially in the case of stretching modes involving hydrogen atoms [34], Burcl, Carter, and Handy [16] transformed a quartic, Taylor series polynomial potential to expansions in Morse coordinates or in Gauss coordinates and tested the resulting potentials on water, formaldehyde, and methane molecules.

The initial quartic, polynomial force fields are calculated using density functional theory. The single mode (uncoupled) Taylor polynomial used for symmetric vibrations is

$$V(Q_k) = \frac{1}{2}\omega_k^2 Q_k^2 + \frac{1}{6}F_{kkk}Q_k^3 + \frac{1}{24}F_{kkkk}Q_k^4 \tag{2.15}$$

where Q_k are the normal coordinates, ω_k is the harmonic frequency, and F_{kkk} and F_{kkkk} are the cubic and quartic force constants, respectively. The authors [16] assume that these vibrations can be associated with the Morse potential

$$V(Q_k) = D_e(1 - e^{-\alpha_k Q_k})^2 \tag{2.16}$$

where D_e is the dissociation energy. The parameter α , which governs the width of the potential, can be found by setting equations (2.15) and (2.16) equal to each other and then expanding $e^{-\alpha_k Q_k}$. Then the mass-weighted normal coordinates Q_k of the force fields for these symmetric vibrations are substituted by Morse-like coordinates of the form

$$y_k = 1 - e^{-\alpha_k Q_k} \tag{2.17}$$

Burcl, et al. [16] propose that the asymmetric vibrations, which they describe with the polynomial

$$V(Q_k) = \frac{1}{2}\omega_k^2 Q_k^2 + \frac{1}{24}F_{kkkk}Q_k^4 \tag{2.18}$$

may be associated with some degree of dissociation and therefore can be modeled by a Gauss potential

$$V(Q_k) = D_e(1 - e^{-\beta_k Q_k^2}) \tag{2.19}$$

By equating (2.18) and (2.19) β_k is found to be

$$\beta_k = \frac{\omega_k^2}{2D_e} \tag{2.20}$$

An initial guess for D_e in equation (2.20) is guided by the dissociation energies for the symmetric modes and a rough estimate of β_k is obtained which can be fine tuned.

Now the Q_k for asymmetric vibrations are substituted by Gauss-like coordinates

$$z_k = \left(1 - e^{-\beta_k Q_k^2}\right)^{\frac{1}{2}} \tag{2.21}$$

After the normal coordinate substitutions for all vibrations, the Taylor series force constants remain unchanged for the quartic polynomial.

Finally, the frequencies are found variationally by a vibrational SCF calculation followed by configuration interaction (CI). These calculations are done in conjunction with a maximum of four potential grids, so up to four vibrational modes may be coupled. The method is designed for use on small, polyatomic molecules, and is computationally expensive.

In the case of the water monomer frequencies shown in Table 11 below, Morse-like and Gauss-like potentials used in place of Taylor series polynomials in variational/CI

vibrational calculations with multi-dimensional grid mapping provided improved frequency prediction.

Table 11. Water Monomer Vibrational Frequencies [16].

Mode	MM-T [a] (cm^{-1})	MM-MG [b] (cm^{-1})	Expt [c] (cm^{-1})	% Dev vs Exp (MM-T)	% Dev vs Exp (MM-MG)
Asym OH str	3810	3765	3756	1.44	0.240
Sym OH str	3712	3666	3652	1.64	0.383
OH bend	1586	1592	1595	0.564	0.188

[a] MM-T is the authors' [16] computer program "MULTIMODE" used to execute the calculations as described in this section above. T indicates that Taylor expansion potentials were used. [b] MM-MG indicates the use of MULTIMODE where the normal coordinates have been replaced by Morse-like coordinates for the symmetric vibrations and by Gauss-like coordinates for the asymmetric modes. [c] Reference [31]

2.6 Perturbation Theory with Multi-Dimensional Potential Surfaces

In order to account for anharmonic vibrational effects and improve anharmonic frequencies, Barone [13, 20] has developed a perturbative evaluation of vibro-rotational parameters which makes use of an anharmonic, force constant building technique. Vibrational levels are computed from multidimensional potential surfaces in conjunction with second-order perturbation theory and takes into account vibrational resonances. The effects of which are incorporated into the anharmonicity coefficients, χ_{ij}, as found in the vibrational energy levels

$$G(n) = \sum_i \omega_i \left(n_i + \frac{1}{2} \right) + \sum_{i \le j} \chi_{ij} \left(n_i + \frac{1}{2} \right) \left(n_j + \frac{1}{2} \right) \tag{2.22}$$

All values for χ_{ij} are calculated from the frequencies (υ and 2υ transitions). Barone's approach is available in the latest version of Gaussian.

In Table 12 below, it can be seen that Barone's [13] method is not quite as accurate as that of Burcl et al. [16] for the stretching frequencies of the water monomer. Both methods, however, arrive at about the same excellent estimation for the OH bend. Barone's treatment still yields very good agreement with observed values for all three frequencies.

Table 12. Water Monomer Frequencies as Calculated by Bouteiller and Perchard [20]

Mode	Calculated (cm^{-1}) [a]	Expt (cm^{-1}) [b]	% Dev vs Exp
Asym OH str	3794	3756	1.01
Sym OH str	3674	3652	0.602
OH bend	1598	1595	0.188

[a] Theoretical method of Barone [13] as found in Gaussian03 at MP2 level using D95++(2d,2p) basis set. [b] Reference [31].

Testing Barone's approach on the water dimer, Bouteiller and Perchard [20] arrived at the frequencies shown in Table 13. The upper six intramolecular modes and the out-of-plane bend are very well reproduced, and the in-plane bend and intermolecular stretch agree fairly well with observed values. The frequencies of the lowest three intermolecular modes agree within 20 % of their experimental counterparts, which is an improvement over the estimations of many methods, including the ones already discussed in detail in this text.

Table 13. Water Dimer Frequencies as Calculated by Bouteiller and Perchard [20]

Mode	Calculated (cm^{-1}) [a]	Expt (cm^{-1})	% Dev vs Exp
PD torsion	78	88 [b]	11.4
PA wag	122	103 [b]	18.4
PA twist	120	108 [b]	11.1
Intermolec str	150	143 [c]	4.90
In-plane bend	323	311 [d]	3.86
Out-of-plane bend	525	523 [d]	0.382
PA OH bend	1608	1599 [d]	0.563
PD OH bend	1618	1616 [d]	0.124
PD sym OH str	3599	3601 [e]	0.056
PA sym OH str	3666	3660 [e]	0.164
PD asym OH str	3772	3735 [e]	0.991
PA asym OH str	3779	3745 [e]	0.908

[a] Theoretical method of Barone [13] as found in Gaussian03 at MP2 level using D95++(2d,2p) basis set. [b] Reference [18], planar supersonic molecular beam expansion (terahertz laser vibration-rotation-tunneling spectroscopy), 5 K. [c] Reference [19], planar supersonic molecular beam expansion (terahertz laser vibration-rotation-tunneling spectroscopy), 5 K. [d] Reference [20], Neon matrix, 10 K. [e] Reference [21], molecular beam depletion spectroscopy with size selection by momentum transfer in scattering experiment (atoms under single collision conditions).

CHAPTER III. Morse Method for Correcting Frequencies for Anharmonicity

3.1 Theory

Vibrational spectra of solvent complexes bound by hydrogen bonding and weak van der Waals forces can be described poorly by the harmonic oscillator model. Figure 1 gives an idea of what the potential well looks like for a hydrogen atom moving between two oxygen atoms in an uncharged hydrogen bonded water dimer. Note that these are *static* potentials where the O atoms are held fixed.

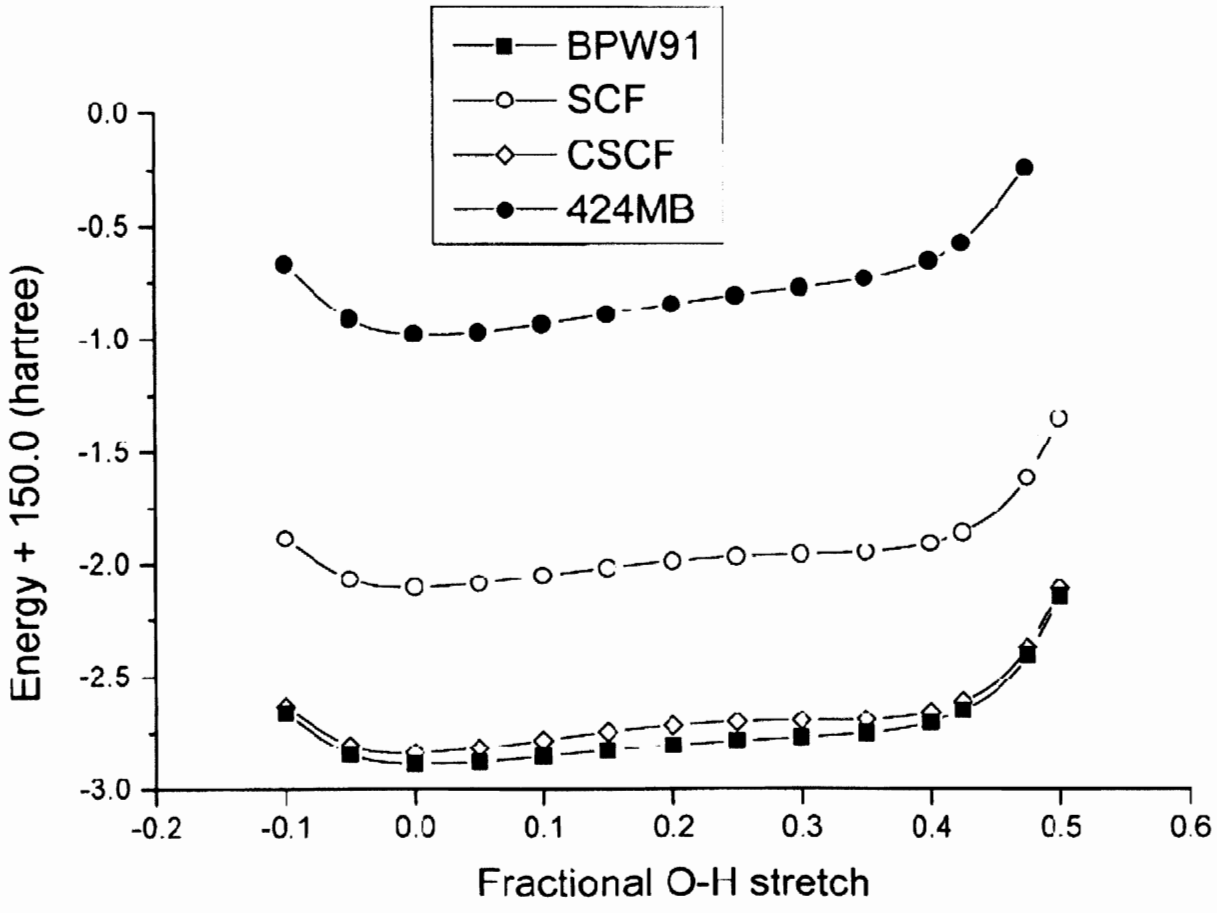

Figure 1. Static Mode Potential Simulating the Hydrogen-Bond Vibration of the Water Dimer [2].

Chaban and co-workers' VSCF method [15] to calculate frequencies corrected for anharmonicity uses *16 points* along the potential for each vibration in addition to the equilibrium energy (the minimized structural energy). The results for intramolecular modes in weakly bound clusters are quite good, without the use of scaling factors. However, this method requires enormous amounts of computational time, and may not be suitable for strongly coupled intermolecular motions.

Here we present a method that requires only 3 points along the potential for each vibrational mode, which is to say, *only two single-point energy calculations* plus the global minimum (equilibrium energy). Our method provides a tool that not only gives accurate frequencies, but does so relatively quickly. A method with these characteristics is greatly desired for research projects that demand a large quantity of good, theoretical frequency data, for large cluster systems, as well as for projects that require reasonable calculation times coupled with sufficient accuracy.

Three different potential energy curves are discussed in this section. First is the harmonic potential (Figure 2), parabolic in shape and symmetric about the point r_e with r_e as its minimum, which is the model that is used to compute harmonic frequencies. The advantage of a perfectly harmonic potential is that it can be exactly separated. The energies of the normal modes Q_j are each a solution of a one-dimensional problem.

$$V = \frac{1}{2}\sum\left(\frac{\partial^2 E}{\partial x_i \partial x_j}\right)_0 x_i x_j = \frac{1}{2}\sum K_{tt} Q_t^2 \qquad (3.1)$$

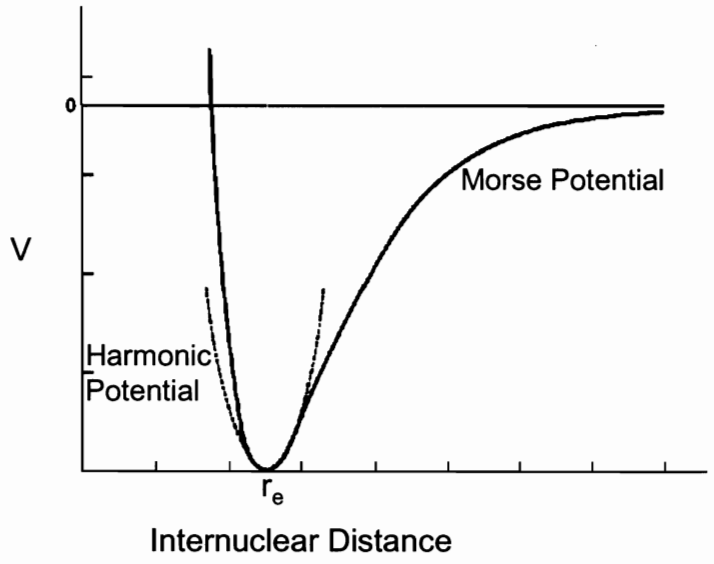

Figure 2. Potential Curves. In this figure, the dashed curve is the harmonic potential while the solid curve is the Morse model potential. V is the internuclear potential energy, r is the instantaneous internuclear distance, and r_e is the equilibrium internuclear distance.

The second curve we shall discuss is the potential that could be constructed if one calculated the MP2 single point energies for a large number of displacements of the atoms. This would provide the exact shape of the MP2 vibrational potential. However, it is not practical to generate even one of these potentials as you would need many energy points along the curve to map it out. Even this curve is an approximation of the true potential because it originates from the MP2 method, which itself makes an approximation to the exact energy.

The third potential curve is a Morse potential and has the shape of the solid curve in Figure 3. Because a Morse potential more accurately describes the true potential (especially for weak intermolecular interactions and hydrogen-bonding) than does the harmonic parabola and has an *exact solution*, this is the curve that we will use to simulate

the true potential. To do this, we will assume that the bottom of the Morse well maps directly onto the bottom of the harmonic and true potential wells, and that the energy at r_e is the same on all curves.

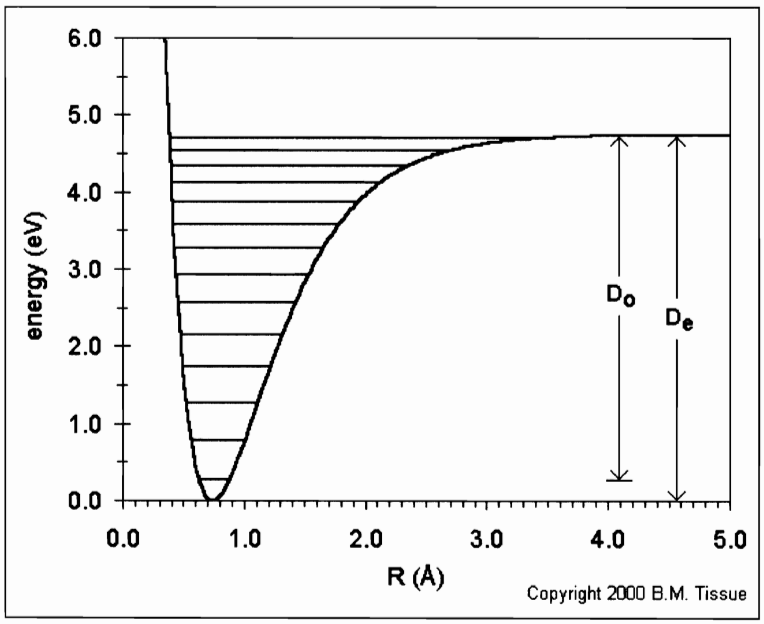

Figure 3. Anharmonic Potential Well. Taken from reference [35].

The Morse curve is of the general form

$$V = D_e\left(1 - e^{-a(r-r_e)}\right)^2 \tag{3.2}$$

where D_e is the depth of the potential (relative to the energy of the separated atoms), i.e., the dissociation energy. Here again, r is any internuclear distance on the potential, r_e is

the point on the curve with the lowest energy (at the equilibrium, internuclear distance), and V is the corresponding energy of r. The energy levels of the Morse potential are not spaced equally and are given by

$$E_{Morse} = hc\omega_e\left(n+\frac{1}{2}\right) - hc\mathrm{X}_e\omega_e\left(n+\frac{1}{2}\right)^2 \tag{3.3}$$

where X_e is the anharmonicity constant. Unfortunately, the Morse potential for molecules with more than one vibrational mode is not separable; there is no direct analogy to the separate normal modes of the harmonic oscillator and the energies associated with each mode. The Morse potential (and its energy levels) is not solvable for the polyatomic case. Therefore, an indirect means must be found to solve it.

The well-known wave functions and energies of the harmonic oscillator can serve as a starting point for a perturbation treatment of the Morse oscillator. The energy levels of the harmonic oscillator are given by the following equation

$$E_{harm} = h\nu_0\left(n+\frac{1}{2}\right) \tag{3.4}$$

where h is Planck's constant, ν_0 is the harmonic frequency, and n is the selected energy level of interest.

According to Pauling and Wilson [3], the energy levels of the harmonic oscillator can be perturbed and constrained to fit a new set of energy levels defined by another energy level model (in our case, that of the Morse potential) using first order perturbation theory. The perturbed energy levels of the harmonic oscillator are:

$$E_{pert} = h\nu_0\left(n+\frac{1}{2}\right) + \left(\frac{3}{64\pi^4}\right)\left(2n^2+2n+1\right)\left(\frac{h^2 b}{m^2\nu_0^2}\right) \tag{3.5}$$

(where b is the perturbation parameter and m is the reduced mass) which can then be set equal to the formula for the energy levels of a Morse potential [36] (equation (3.6) below):

$$E_{Morse} = hc\omega_e\left(n+\frac{1}{2}\right) - hc\mathrm{X}_e\omega_e\left(n+\frac{1}{2}\right)^2 \tag{3.6}$$

where c is the speed of light and

$$\omega_e = \frac{a}{\pi c}\sqrt{\frac{D_e}{2m}} \tag{3.7}$$

and

$$\mathrm{X}_e = \frac{hc}{4D_e}\omega_e \tag{3.8}$$

a is a parameter that governs the width of the Morse potential. D_e represents the spectroscopic dissociation energy. With E_{pert} and E_{Morse} set equal to each other, the energy levels of a quartic approximation to the Morse potential can be solved for each normal mode in terms of the harmonic energy levels. In order to accurately solve for these energy levels, we reexamined the work of Zhang [37] and proceed with the following modified derivation.

After setting equation (3.5) and equation (3.6) (E_{pert} and E_{Morse} respectively) equal to each other, and after manipulation we solve for b as follows

$$h\nu_0\left(n+\frac{1}{2}\right) + \left(\frac{3}{64\pi^4}\right)\left(2n^2+2n+1\right)\left(\frac{h^2 b}{m^2\nu_0^2}\right) = hc\omega_e\left(n+\frac{1}{2}\right) - hc\mathrm{X}_e\omega_e\left(n+\frac{1}{2}\right)^2 \tag{3.9}$$

We isolate the factor that contains b

$$\left(\frac{h^2 b}{m^2 \nu_0^2}\right) = \frac{hc\omega_e\left(n+\frac{1}{2}\right) - hcX_e\omega_e\left(n+\frac{1}{2}\right)^2 - h\nu_0\left(n+\frac{1}{2}\right)}{\left(\frac{3}{64\pi^4}\right)\left(2n^2+2n+1\right)} \tag{3.10}$$

Simplifying the denominators and isolating perturbation parameter b gives

$$b = \frac{64m^2\nu_0^2\pi^4\left[hc\omega_e\left(n+\frac{1}{2}\right) - hcX_e\omega_e\left(n+\frac{1}{2}\right)^2 - h\nu_0\left(n+\frac{1}{2}\right)\right]}{\left(3h^2\right)\left(2n^2+2n+1\right)} \tag{3.11}$$

and may be further simplified to

$$b = \frac{64m^2\nu_0^3\pi^4\left(n+\frac{1}{2}\right)\left[-X_e\left(n+\frac{1}{2}\right)\right]}{3h\left(2n^2+2n+1\right)} \tag{3.12}$$

Furthermore,

$$b = -\frac{\left(n+\frac{1}{2}\right)^2}{\left(2n^2+2n+1\right)}\frac{64m^2\nu_0^3\pi^4}{3h}\chi_e = -\frac{\left(n+\frac{1}{2}\right)^2}{\left(2n^2+2n+1\right)}F = -\frac{\left(4n^2+4n+1\right)}{\left(2n^2+2n+1\right)}\frac{F}{4} \tag{3.13}$$

where is F represents $\frac{64m^2\nu_0^3\pi^4}{3h}\chi_e$. In other words b depends on n. The vast majority of vibrational transitions which occur during infrared spectroscopy are from the n=0 to n=1 quantum states, so we must compute the perturbed energy levels for both the n=0 and the n=1 levels. For n=0, b = -F/4, and for n=1, b = -9F/20, taking note that $c\omega_e$ is equal to ν_0,

the harmonic frequency in Hz. From here a numerical calculation is carried out to find a value for b (which is in units of $kg^2s^{-4}J^{-1}$) by substituting in the various values for the variables that define b for each n. Now with the value of b in hand, it can be substituted into the equation for E_{pert} (equation (3.5)), and because all other quantities are known, the perturbed energy of the harmonic oscillator at the desired energy level (n=0 or n=1) may now be calculated. This is the approximation to that energy level in a Morse potential.

We now arrive at the anharmonically corrected frequency, ν_{Morse} (equation (3.14)), based on the Morse curve in terms of the solvable harmonic treatment (for vibrational transitions from n=0 to n=1).

$$\nu_{Morse} = \frac{E_1 - E_0}{h} \tag{3.14}$$

3.2 Derivation of D_e and variable a

In order to represent the D_e formulation accurately, we reexamined the work of Zhang [37] and derive a new expression as follows.

Recall, the Morse potential is defined by the expression

$$V(x) = D_e\left(1 - e^{-ax}\right)^2 \tag{3.15}$$

where $x = r - r_e$. Taking the first derivative of the potential function, we have

$$\frac{dV(x)}{dx} = 2D_e\left(1 - e^{-ax}\right)ae^{-ax} \tag{3.16}$$

The second derivative follows

$$\frac{d^2V(x)}{dx^2} = 2D_e a^2\left(e^{-ax}\right)^2 - 2D_e\left(1 - e^{-ax}\right)a^2e^{-ax} \tag{3.17}$$

The force constant for the Morse curve can be calculated at the equilibrium position using the second derivative, by setting x (the step size, r-r_e) equal to zero. This results in

$$k = 2D_e a^2 \tag{3.18}$$

for the Morse potential. The step size along the *harmonic* potential, x, originates from

$$V = \frac{1}{2}kx^2 \tag{3.19}$$

where

$$x = \sqrt{\frac{2V}{k}} \tag{3.20}$$

And at the n=0 energy level,

$$x = \sqrt{\frac{h\nu}{k}} \tag{3.21}$$

Interestingly, the difference in energy at the points +x and -x depends only upon D_e and so does not depend on the Morse parameter "a".

The cubic term for the Morse potential can be found by taking the third derivative of the Morse potential function

$$\frac{d^3V(x)}{dx^3} = -6D_e a^3\left(e^{-ax}\right)^2 + 2D_e\left(1-e^{-ax}\right)a^3e^{-ax} \tag{3.22}$$

and evaluating at x = 0. This gives the cubic term the value $-6D_e a^3$.

The difference in energy at the turning points is given by (notice that a will cancel):

$$\Delta E = -2D_e a^3\left(\frac{h\nu}{2D_e a^2}\right)^{\frac{3}{2}} \tag{3.23}$$

or

$$\Delta E^2 = \frac{(h\nu)^3}{2D_e} \tag{3.24}$$

As ΔE approaches zero, D_e increases. This makes sense because the potential is approaching that of a pure harmonic oscillator, for which no dissociation energy is defined. The harmonic frequency, ν, is known, leaving the value for D_e as the only unknown. Solving for D_e, the dissociation energy, we find

$$D_e = \frac{(h\nu)^3}{2(\Delta E)^2} \tag{3.25}$$

Having obtained this estimate for D_e, it is now possible to evaluate the a parameter of the Morse curve.

As before, $k = 2D_e a^2$ for the Morse curve, and for the harmonic oscillator, $k = \mu\omega^2$. Because the force constant for the Morse potential has the same meaning as the force constant of the harmonic potential at the equilibrium position (r_e), we may set the two equal to each other to find a:

$$\mu\omega^2 = 2D_e a^2 \tag{3.26}$$

Solving for a, we have

$$a = \sqrt{\frac{\mu\omega^2}{2D_e}} \tag{3.27}$$

Now all parameters are known, and first-order perturbation theory can be used to calculate the energy for a given normal mode.

3.3 Determination of Displacement x

We use a method which provides a *non-subjective* way to determine ± x that is based on the selected energy value down in the harmonic well of the given vibration and as such is *self-adjusting* to the depth of each potential (see below).

The displacement ± x, about r_e, is based on the potential of the harmonic oscillator. From Hooke's Law, the energy of the classical (and quantum mechanical) oscillator is given by

$$V = \frac{1}{2}kx^2 \tag{3.28}$$

Therefore,

$$x = \pm\left(\frac{2V}{k}\right)^{\frac{1}{2}} \tag{3.29}$$

where k is the harmonic force constant and V is the selected energy level in the well. To determine x, the n=0 energy level in the well was chosen for this study. A large value for V can describe the asymmetry of the vibration more accurately, however, this may also be at the expense of an accurate description for the bottom of the well. Furthermore, at higher energy values, some molecules (especially hydrogen-bonded complexes) will dissociate. The n=0 energy level was found to be a suitable choice for the hydrogen-bonded systems in this work.

The equilibrium coordinates of the atoms are moved by this fractional displacement Δx along the normal coordinate (i.e., by Δx times the normalized, normal mode displacements). Because the displacements are adjusted by the naturally occurring

fluctuations in depth and width of the harmonic potential from mode to mode, this renders the choice of x objective and self-adjusting (to the depth). Finally, single-point energies at the new geometries are calculated to obtain energies V_+ (at $+\Delta x$) and V- (at $-\Delta x$) along the MP2 coordinate.

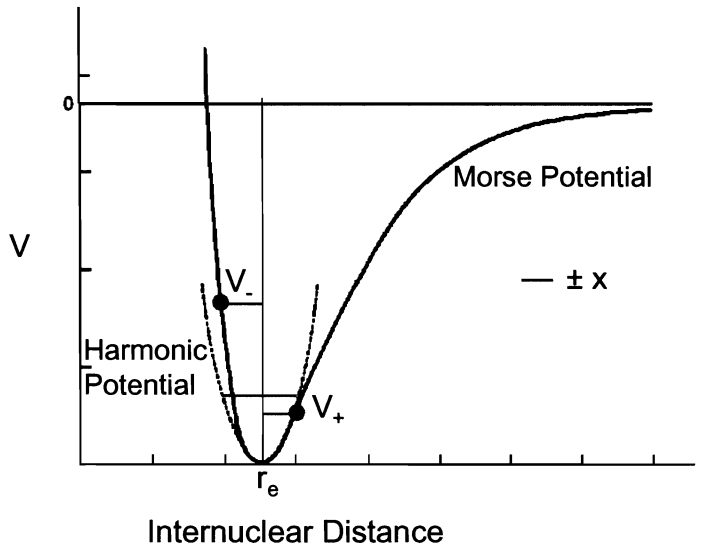

Figure 4. Potential Curves demonstrating the x step and corresponding V_+ and V_- single point energies. The n=0 level intersects the harmonic potential at ± x. This allows a novel approach for determining an objective and self-adjusting Δx for each and every vibration that results in a good fit of the true potential by the Morse curve. Also, using Δx in this fashion will lead to single point energies $V_\pm$ that automatically fit an asymmetric potential.

With Δx for each mode in hand, we are now able to calculate the single-point energies, $V_\pm$, along the potential. The values $V_\pm$ in turn allow for the solving of D_e, and, D_e, in turn, is used to obtain the Morse parameter a, which is the range of the Morse curve and is in units of cm^{-1} as discussed above. Finally, the frequency is corrected for

anharmonicity using first-order perturbation theory, and we arrive at the Morse frequency, ν.

3.4 Illustration of the Morse Method with Data

Using the water dimer (counterpoise optimized in a 6-311G** basis set with full CP corrections for energies and frequencies) as an example for each mode, the step-size (in the positive x and negative x directions) is determined as shown in Table 14. For mode 9, which is the O-H stretch vibration of the hydrogen in the hydrogen bond, x comes out to be 0.09108149 Å. The equilibrium energy, V_{re}, which is the energy at the bottom of the well, is -6.650154 x 10^{-9} ergs. V_+, the single-point energy at the n=0 turning point stepping "forward" (in the positive x direction) is -6.649830 10^{-9} ergs. Likewise, V_- is the second turning point stepping "backward" (in the negative x direction) and has the value -6.649692 10^{-9} ergs.

The energies at the turning points must be calculated relative to the baseline, the energy minimum. V_{re} now becomes zero, and V_+ and V_- now have positive energy values.

Table 14. Displacement x and Single-Point Energy Values.

Mode	x Step	x (Å)	V_{re} (ergs)	$V_{\pm}$ (ergs)	$V_{\pm}$ (ergs) [relative to V_{re}]
9	Pos	0.091081	-6.650154 x 10^{-09}	-6.649830 x 10^{-09}	3.239225 x 10^{-13}
9	Neg	0.091081	-6.650154 x 10^{-09}	-6.649692 x 10^{-09}	4.614672 x 10^{-13}

ΔE, the change in energy at the turning points is the simple difference in energy between the two single-point energies, V_+ and V_- relative to the baseline (Table 15). The equilibrium dissociation energy, D_e, is calculated from

$$D_e = \frac{(h\nu)^3}{2(\Delta E)^2} \tag{3.30}$$

Table 15. Difference in Energy of the Turning Points (ΔE), Harmonic Frequency (ν), and D_e .

Mode	ΔE (ergs)	ν (Hz)	D_e (ergs)
9	1.375×10^{-13}	1.160×10^{14}	1.200×10^{-11}

Next, we calculate a as shown in Table 16. a^2 is given by the relation $\mu\omega^2 = 2D_e a^2$, where

$$a^2 = \frac{\mu\omega^2}{2D_e} \tag{3.31}$$

Recall, that ω is equal to $2\pi\nu$.

Table 16. Anharmonicity Constant, χ_e and Computed Values for ω_e and a.

Mode	μ (g)	ω^2 (cm^{-2})	a (cm^{-1})	ω_e (cm^{-1})	χ_e
9	1.744×10^{-24}	5.909×10^{8}	1.965×10^{8}	3.869×10^{3}	1.602×10^{-2}

ω_e calculated by $\omega_e = \frac{a}{\pi c}\sqrt{\frac{D_e}{2m}}$ provides a good check of the parameters, as the result should be the harmonic frequency as calculated in Gaussian. The anharmonicity constant χ_e is given by $\chi_e = \frac{hc}{4D_e}\omega_e$.

Using first-order perturbation theory, as discussed before, we arrive at the following values for b and E for mode nine (Table 17). The subscripts of 0 and 1 for b and E indicate the n=0 and n=1 energy levels, respectively. From $\nu_{Morse} = \frac{E_1 - E_0}{hc}$, we arrive at the Morse frequency in wavenumbers.

Table 17. Calculated b and E Values and Arrival at the Morse Frequency.

Mode	b_0 (g^2/s^4ergs)	E_0 (ergs)	b_1 (g^2/s^4ergs)	E_1 (ergs)	ν Morse (cm^{-1})
9	-5.962×10^{20}	3.812×10^{-13}	-1.073×10^{21}	1.125×10^{-12}	3745

3.5 Results from Morse Illustration

From Table 18 below, it can be seen that the Morse frequency approximates the experimental frequency fairly well for the upper nine of the twelve modes of the water dimer. Modes 1-3 are too high (30%-33% above the experimental values) owing to the fact that their energies at the turning points are quite high for low frequency modes, having the same order of magnitude as those of the upper five frequencies. Modes 1 and 3 also appear to be high partly because the expression for D_e approaches infinity when ΔE approaches zero (the harmonic oscillator has an effective "D_e" that approaches

infinity, hence it's lesser success in modeling a dissociation energy), and modes 1-3 are rovibrational modes which are not well characterized by a potential with this characteristic. The reasoning regarding D_e approaching infinity also applies to modes six and twelve, the error being 7%-8%. The low, soft modes are expected to exhibit shallow, wide potentials. Therefore, the 6-311G** basis may need to be upgraded to include diffuse functions.

Table 18. Comparison of Morse Frequencies with Experimental Values.

Mode	ν Morse (cm^{-1})	Experiment (cm^{-1})	Deviation from Expt (cm^{-1})	% Deviation from Experiment
1	115	88 [a]	27	30.19
2	143	103 [a]	40	38.77
3	143	108 [a]	35	32.84
4	149	143 [b]	6	4.32
5	305	311 [c]	-6	-1.92
6	566	523 [c]	43	8.21
7	1668	1599 [c]	69	4.31
8	1697	1616 [c]	81	4.98
9	3745	3601 [d]	144	3.99
10	3815	3660 [d]	155	4.25
11	3912	3735 [d]	177	4.73
12	4010	3745 [d]	265	7.08

[a] Reference [18], planar supersonic molecular beam expansion (terahertz laser vibration-rotation-tunneling spectroscopy), 5 K. [b] Reference [19], planar supersonic molecular beam expansion (terahertz laser vibration-rotation-tunneling spectroscopy), 5 K. [c] Reference [20], Neon matrix, 10 K. [d] Reference [21], molecular beam depletion spectroscopy with size selection by momentum transfer in scattering experiment (atoms under single collision conditions).

A look at the values for D_e (in eV's) for all modes, as shown in Table 19, reveals the extreme dissociation energies for Modes 1,3, 6, and 12 provided by the Morse potential,

which contributes to the error in these bands (except for mode 2, whose D_e seems reasonable here despite significant error in the resulting Morse frequency).

Table 19. Computed D_e Values for all Modes.

Mode	D_e(eV)
1	206201.3
2	5.1
3	27060.3
4	0.2
5	4.7
6	14278750.3
7	35.8
8	37.2
9	7.5
10	10.5
11	12.6
12	560675805.0

3.6 The Morse Potential and Symmetric Potentials

When the two single-point energies for a given mode are exactly equivalent, this suggests a symmetric MP2 potential. Recall the expression for D_e in the Morse potential

$$D_e = \frac{(h\nu)^3}{2(\Delta E)^2} \tag{3.32}$$

When the single-point energies are equal, as must happen in this system for the motions of symmetry species A", ΔE equals zero. Such modes are better expressed in even powers of the displacement for symmetry reasons, than by using the intrinsically asymmetric Morse function to describe the potential. Never the less, it is possible to fit a Morse potential for these modes.

Normally, the Morse method would be unable to predict a frequency in this case due to division by zero. In this situation, we introduced an insignificant departure from perfect equivalence; ΔE remains effectively unchanged (but nonzero), and the calculation can proceed, and the results processed by Morse analysis. These frequency predictions are based on Morse potentials with a high degree of symmetry. As D_e of the Morse potential becomes very large, the Morse curve is very nearly quadratic and strongly resembles that of the harmonic potential (producing frequencies akin to the harmonic bands). This can be seen from figures 5 and 6, which illustrate how the Morse frequencies approach the harmonic frequencies in these cases.

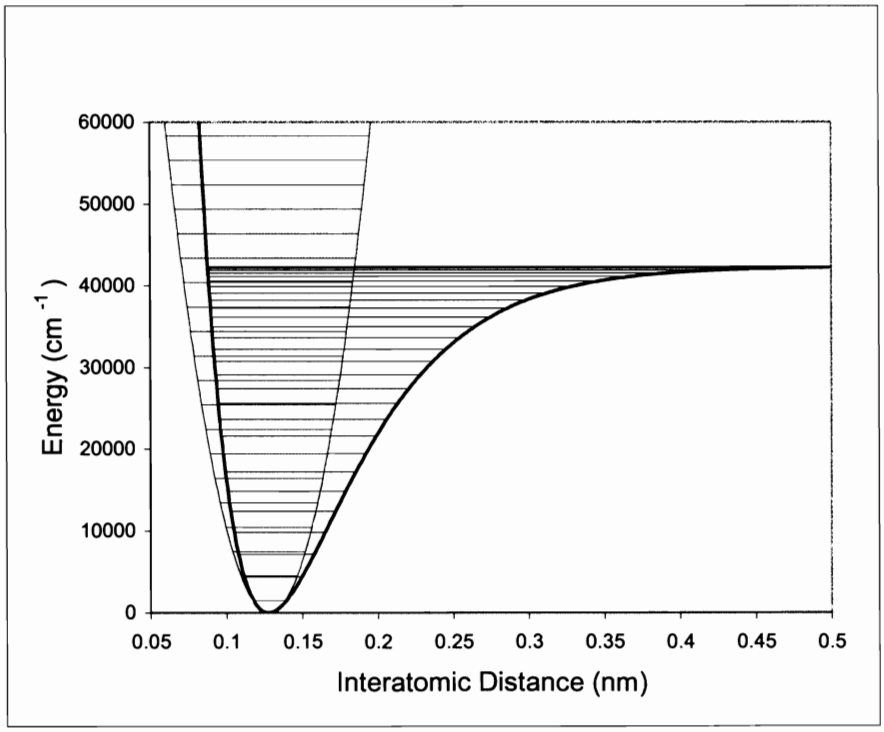

Figure 5. Harmonic (blue) and Morse (black) potentials overlayed with their respective energy levels for HCl [38]. Note the distinctive form of the Morse potential with its highest degree of asymmetry for large ΔE.

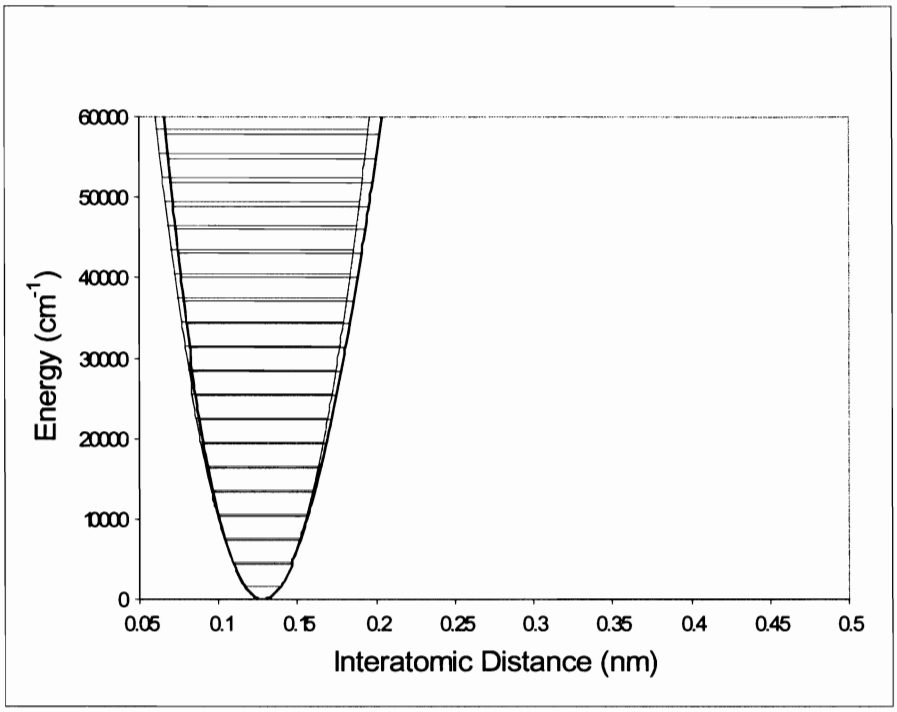

Figure 6. Harmonic (blue) and Morse (black) potentials overlayed with their respective energy levels for HCl [38]. Note the very symmetric Morse potential with only a 3 % anharmonic factor similar to the case when single-point energy values are close in energy (very small ΔE).

CHAPTER IV. The Polynomial Method

4.1 Basic Theory

In an attempt to provide an alternative method for calculating vibrational frequencies and to improve upon the Morse method, while maintaining the same computational speed advantage, a polynomial fitting technique was investigated. A three-term polynomial potential may be thought of as an harmonic potential (first term) followed by two terms that are perturbations of the harmonic potential. We have chosen to approximate the vibrational potentials as follows, where V is the polynomial potential

$$V = \frac{Ax^2}{2} + \frac{Bx^3}{6} + \frac{Cx^4}{24} \tag{4.1}$$

As before with x, the turning point is given by

$$x = \sqrt{\frac{h\nu}{k}} \tag{4.2}$$

Stepping forward (in the positive x direction) along the potential, we have the single-point energy, V_+

$$V_+ = \frac{Ah\nu}{2k} + \frac{B\left(\frac{h\nu}{k}\right)^{\frac{3}{2}}}{6} + \frac{Ch^2\nu^2}{24k^2} \tag{4.3}$$

And stepping backward (in the negative x direction) gives the single-point energy V_-

$$V_- = \frac{Ah\nu}{2k} - \frac{B\left(\frac{h\nu}{k}\right)^{\frac{3}{2}}}{6} + \frac{Ch^2\nu^2}{24k^2} \tag{4.4}$$

To define the B coefficient, we subtract V_+ from V_-. This leaves only the B term

$$\Delta E = -\frac{B\left(\frac{h\nu}{k}\right)^{\frac{3}{2}}}{3} \tag{4.5}$$

The values of all variables are known (except for the coefficient B). Here, ν is the harmonic frequency calculated in Gaussian, and k is the corresponding force constant. ΔE, of course, is the difference in energy of the single-point energies. One may now solve for B.

We may also eliminate the B term entirely by calculating the mean or average of the two single-point energies, E

$$E = \frac{Ah\nu}{2k} + \frac{Ch^2\nu^2}{24k^2} \tag{4.6}$$

By making the slight approximation that the coefficient A equals k, forcing the first term to equal the harmonic potential, the only unknown variable is the coefficient C, and so C may now be calculated.

A better representation of A in the polynomial than the harmonic force constant can be found by using the force constant of a Morse potential

$$k_{Morse} = 2D_e a^2 = A \tag{4.7}$$

Now all coefficients of the polynomial are known.

It is necessary to employ second-order perturbation theory when arriving at frequencies generated by a polynomial potential. First-order perturbation theory is not adequate because the cubic term (B term) is annihilated, and it is this term that provides significant reduction of energy of the harmonic frequency, bringing it closer to the frequency observed experimentally.

4.2 First and Second Order Perturbation Corrections

The polynomial method presented in this work makes use of perturbation theory to correct vibrational frequencies to second order. In perturbation theory, for a vibrational system whose energy and wavefunction are unknown, as given by the equation

$$H\psi = E\psi \tag{4.8}$$

and for a reference vibrational system that has already been solved,

$$H^0\psi_n^0 = E_n^0\psi_n^0 \tag{4.9}$$

where n is the ground state, a perturbation of the reference system can be defined, and the components of the system to be solved may be written in terms of the perturbed reference system.

After manipulation, the first order correction of the vibrational energy is given by

$$E_n^{(1)} = \left\langle \psi_n^{(0)} \middle| V \middle| \psi_n^{(0)} \right\rangle \tag{4.10}$$

where V is the potential operator.

The second order correction to the energy is calculated according to

$$E_n^{(2)} = \left\langle \psi_n^{(0)} \middle| V \middle| \psi_n^{(1)} \right\rangle = -\sum_{k \neq n} \frac{\left\langle \psi_n^{(0)} \middle| V \middle| \psi_k^{(0)} \right\rangle \left\langle \psi_k^{(0)} \middle| V \middle| \psi_n^{(0)} \right\rangle}{E_k^{(0)} - E_n^{(0)}} \tag{4.11}$$

Here, the first order correction to the wave function, $\psi_n^{(1)}$, is given by

$$\psi_n^{(1)} = \left[-\sum_{k \neq n} \frac{\left\langle \psi_k^{(0)*} \middle| V \middle| \psi_n^{(0)} \right\rangle}{(E_k^{(0)} - E_n^{(0)})} \right] \left| \psi_k^{(0)} \right\rangle \tag{4.12}$$

Detailed derivations of first and second order perturbation corrections are presented in the appendix.

4.3 Polynomial Method in Detail

4.3.1 Perturbing the Harmonic Oscillator

Here we present in detail the polynomial method developed in this work. We begin with the Schroedinger equation for the quantum mechanical harmonic oscillator [39]

$$\left(-\frac{\hbar^2}{2m}\frac{d^2}{dx^2}+\frac{kx^2}{2}\right)\psi = E\psi \tag{4.13}$$

where the quadratic potential operator, $\frac{kx^2}{2}$, is separable from the kinetic operator, m is the effective mass, and k is the force constant. The quadratic potential describes the normal mode motions according to the harmonic model. The harmonic frequencies are computed from the diagonalized mass-weighted Hessian (force constant) matrix represented by

$$k_{ij} = \left(\frac{d^2V}{dx_i dx_j}\right) \tag{4.14}$$

The resulting eigenvectors are the normal mode motions of each atom, and the eigenvalues provide the vibrational energies.

For the perturbed harmonic oscillator

$$\left(\frac{-\hbar^2}{2m}\frac{d^2}{dx^2}+\frac{kx^2}{2}+\beta x^3+\gamma x^4\right)\Psi = E\Psi \tag{4.15}$$

We define the unit of energy as $\hbar\omega/2$ and define the quantity ε to be $\left(\frac{2E}{\hbar\omega}\right)$ and after manipulation ultimately arrive at

$$\left(\frac{-\hbar}{m\omega}\frac{d^2}{dx^2}+\frac{kx^2}{\hbar\omega}+\left(\frac{2}{\hbar\omega}\right)\beta x^3+\left(\frac{2}{\hbar\omega}\right)\gamma x^4\right)\Psi=\varepsilon\Psi \tag{4.16}$$

In equation (4.16) above, we simplify terms by gathering constants and the variable x into a single variable q. More importantly we do this to put x in terms of the unitless length, q, similar to the same q used by Fowler [40]. We find q to be

$$q=\sqrt{\frac{m\omega}{\hbar}}x \tag{4.17}$$

From equation (4.17) x must be

$$x=\sqrt{\frac{\hbar}{m\omega}}q \tag{4.18}$$

Substituting this expression wherever x appears eventually produces

$$\left(\frac{-d^2}{dq^2}+q^2+\beta\left(\frac{2}{\hbar\omega}\right)\left(\frac{\hbar}{m\omega}\right)^{\frac{3}{2}}q^3+\gamma\left(\frac{2}{\hbar\omega}\right)\left(\frac{\hbar}{m\omega}\right)^2q^4\right)\Psi=\varepsilon\Psi \tag{4.19}$$

Our perturbation takes the form of a polynomial

$$V(q)=Bq^3+Cq^4 \tag{4.20}$$

This is the same form as in equation (4.19) above, where

$$B=\beta\left(\frac{2}{\hbar\omega}\right)\left(\frac{\hbar}{m\omega}\right)^{\frac{3}{2}} \tag{4.21}$$

and

$$C=\gamma\left(\frac{2}{\hbar\omega}\right)\left(\frac{\hbar}{m\omega}\right)^2 \tag{4.22}$$

The perturbed harmonic oscillator is now in terms of energy units of $\hbar\omega/2$ and in terms of q, the desired unitless length (unitless displacement along the normal mode coordinate):

$$\left(\frac{-d^2}{dq^2} + q^2 + Bq^3 + Cq^4\right)\Psi = \varepsilon\Psi \tag{4.23}$$

A more detailed treatment is presented in the appendix.

4.3.2 q Matrices

Let our perturbation again be expressed in cubic and quartic terms

$$V(q) = Bq^3 + Cq^4 \tag{4.24}$$

Using our unit of energy, $\left(\frac{\hbar\omega}{2}\right)$, the energy states of the oscillator become $\varepsilon_n = 2n+1$, and the working integral is

$$\langle n|q|n+1\rangle = \left[(n+1)/2\right]^{1/2} \tag{4.25}$$

Variable q, in the reference (unperturbed) system, then becomes the matrix of these integrals.

The matrices for all powers of q are as follows:

$$q = \begin{bmatrix} 0 & \frac{\sqrt{2}}{2} & 0 & 0 & 0 & 0 & 0 & 0 \\ \frac{\sqrt{2}}{2} & 0 & 1 & 0 & 0 & 0 & 0 & 0 \\ 0 & 1 & 0 & \frac{\sqrt{3}\sqrt{2}}{2} & 0 & 0 & 0 & 0 \\ 0 & 0 & \frac{\sqrt{3}\sqrt{2}}{2} & 0 & \sqrt{2} & 0 & 0 & 0 \\ 0 & 0 & 0 & \sqrt{2} & 0 & \frac{\sqrt{5}\sqrt{2}}{2} & 0 & 0 \\ 0 & 0 & 0 & 0 & \frac{\sqrt{5}\sqrt{2}}{2} & 0 & \sqrt{3} & 0 \\ 0 & 0 & 0 & 0 & 0 & \sqrt{3} & 0 & \frac{\sqrt{7}\sqrt{2}}{2} \\ 0 & 0 & 0 & 0 & 0 & 0 & \frac{\sqrt{7}\sqrt{2}}{2} & 0 \end{bmatrix}$$

For q^2 we have the matrix below. Notice that the diagonal elements are $\frac{(2n+1)}{2}$. This is the fraction of energy in units of $\frac{\hbar\omega}{2}$ in each state. The pattern fails for the 8,8 element. This presents no error in our calculations though as we are only interested in the ground state (n=0) mixing with states k=1-4 and the first excited state (n=1) mixing with states k=2-5. So the 8,8 element is never needed.

$$q^2 = \begin{bmatrix} \frac{1}{2} & 0 & \frac{\sqrt{2}}{2} & 0 & 0 & 0 & 0 & 0 \\ 0 & \frac{3}{2} & 0 & \frac{\sqrt{3}\sqrt{2}}{2} & 0 & 0 & 0 & 0 \\ \frac{\sqrt{2}}{2} & 0 & \frac{5}{2} & 0 & \sqrt{3} & 0 & 0 & 0 \\ 0 & \frac{\sqrt{3}\sqrt{2}}{2} & 0 & \frac{7}{2} & 0 & \sqrt{5} & 0 & 0 \\ 0 & 0 & \sqrt{3} & 0 & \frac{9}{2} & 0 & \frac{\sqrt{5}\sqrt{2}\sqrt{3}}{2} & 0 \\ 0 & 0 & 0 & \sqrt{5} & 0 & \frac{11}{2} & 0 & \frac{\sqrt{3}\sqrt{7}\sqrt{2}}{2} \\ 0 & 0 & 0 & 0 & \frac{\sqrt{5}\sqrt{2}\sqrt{3}}{2} & 0 & \frac{13}{2} & 0 \\ 0 & 0 & 0 & 0 & 0 & \frac{\sqrt{3}\sqrt{7}\sqrt{2}}{2} & 0 & \frac{7}{2} \end{bmatrix}$$

The values from the q^3 and q^4 matrices may be used in approximating first and second order perturbations. Diagonal elements are used for calculating first order effects and off-diagonal elements are used in calculating second order corrections. q^3 is represented by

$$q^3 = \begin{bmatrix} 0 & \frac{3\sqrt{2}}{4} & 0 & \frac{\sqrt{3}}{2} & 0 & 0 & 0 & 0 \\ \frac{3\sqrt{2}}{4} & 0 & 3 & 0 & \sqrt{3} & 0 & 0 & 0 \\ 0 & 3 & 0 & \frac{9\sqrt{3}\sqrt{2}}{4} & 0 & \frac{\sqrt{5}\sqrt{2}\sqrt{3}}{2} & 0 & 0 \\ \frac{\sqrt{3}}{2} & 0 & \frac{9\sqrt{3}\sqrt{2}}{4} & 0 & 6\sqrt{2} & 0 & \sqrt{5}\sqrt{3} & 0 \\ 0 & \sqrt{3} & 0 & 6\sqrt{2} & 0 & \frac{15\sqrt{5}\sqrt{2}}{4} & 0 & \frac{\sqrt{5}\sqrt{3}\sqrt{7}}{2} \\ 0 & 0 & \frac{\sqrt{5}\sqrt{2}\sqrt{3}}{2} & 0 & \frac{15\sqrt{5}\sqrt{2}}{4} & 0 & 9\sqrt{3} & 0 \\ 0 & 0 & 0 & \sqrt{5}\sqrt{3} & 0 & 9\sqrt{3} & 0 & \frac{13\sqrt{7}\sqrt{2}}{4} \\ 0 & 0 & 0 & 0 & \frac{\sqrt{5}\sqrt{3}\sqrt{7}}{2} & 0 & \frac{13\sqrt{7}\sqrt{2}}{4} & 0 \end{bmatrix}$$

Lastly, we have q^4

$$q^4 = \begin{bmatrix} \frac{3}{4} & 0 & \frac{3\sqrt{2}}{2} & 0 & \frac{\sqrt{3}\sqrt{2}}{2} & 0 & 0 & 0 \\ 0 & \frac{15}{4} & 0 & \frac{5\sqrt{3}\sqrt{2}}{2} & 0 & \frac{\sqrt{5}\sqrt{2}\sqrt{3}}{2} & 0 & 0 \\ \frac{3\sqrt{2}}{2} & 0 & \frac{39}{4} & 0 & 7\sqrt{3} & 0 & \frac{3\sqrt{5}\sqrt{2}}{2} & 0 \\ 0 & \frac{5\sqrt{3}\sqrt{2}}{2} & 0 & \frac{75}{4} & 0 & 9\sqrt{5} & 0 & \frac{\sqrt{5}\sqrt{3}\sqrt{7}\sqrt{2}}{2} \\ \frac{\sqrt{3}\sqrt{2}}{2} & 0 & 7\sqrt{3} & 0 & \frac{123}{4} & 0 & \frac{11\sqrt{5}\sqrt{2}\sqrt{3}}{2} & 0 \\ 0 & \frac{\sqrt{5}\sqrt{2}\sqrt{3}}{2} & 0 & 9\sqrt{5} & 0 & \frac{183}{4} & 0 & \frac{9\sqrt{3}\sqrt{7}\sqrt{2}}{2} \\ 0 & 0 & \frac{3\sqrt{5}\sqrt{2}}{2} & 0 & \frac{11\sqrt{5}\sqrt{2}\sqrt{3}}{2} & 0 & \frac{199}{4} & 0 \\ 0 & 0 & 0 & \frac{\sqrt{5}\sqrt{3}\sqrt{7}\sqrt{2}}{2} & 0 & \frac{9\sqrt{3}\sqrt{7}\sqrt{2}}{2} & 0 & \frac{91}{4} \end{bmatrix}$$

4.3.3 First Order Effects

For the n = 0 state the first order correction to the energy is

$$E_0^{(1)} = \langle 0|Cq^4|0\rangle = \frac{3}{4}C \tag{4.26}$$

The $\frac{3}{4}$ constant before the C coefficient is taken straight from the q^4 matrix where the 0^{th} state mixes with itself to form the diagonal element 0,0. Vibrational mixing with other states does not occur for first order perturbations. The n =1 state has the first order correction

$$E_1^{(1)} = \langle 1|Cq^4|1\rangle = \frac{15}{4}C \tag{4.27}$$

The constant before the C coefficient in this case comes from the element 1,1 of the q^4 matrix. There are no first order corrections from the cubic term as can be seen from the q^3 matrix. All diagonal elements are 0.

4.3.4 Second Order Effects

In the second order there exists both cubic and quartic corrections to the vibrational energy as follows (from equation (4.11)). For the n = 0 state

$$\frac{\langle 0|Bq^3|1\rangle\langle 1|Bq^3|0\rangle}{E_0^{(0)} - E_1^{(0)}} + \frac{\langle 0|Bq^3|3\rangle\langle 3|Bq^3|0\rangle}{E_0^{(0)} - E_3^{(0)}} = -\frac{\left(3\sqrt{2}/4\right)^2}{2} - \frac{\left(\sqrt{3}/2\right)^2}{6} = -\frac{11}{16}B^2 \tag{4.28}$$

and

$$\frac{\langle 0|Cq^4|2\rangle\langle 2|Cq^4|0\rangle}{E_0^{(0)}-E_2^{(0)}}+\frac{\langle 0|Cq^4|4\rangle\langle 4|Cq^4|0\rangle}{E_0^{(0)}-E_4^{(0)}}=-\frac{\left(3\sqrt{2}/2\right)^2}{4}-\frac{\left(\sqrt{6}/2\right)^2}{8}=-\frac{21}{16}C^2 \quad (4.29)$$

In the denominators, the energy level differences are doubled because we use energy units of one-half the quantum. For the $v=1$ state

$$\begin{aligned}&\frac{\langle 1|Bq^3|0\rangle\langle 0|Bq^3|1\rangle}{E_1^{(0)}-E_0^{(0)}}+\frac{\langle 1|Bq^3|2\rangle\langle 2|Bq^3|1\rangle}{E_1^{(0)}-E_2^{(0)}}+\frac{\langle 1|Bq^3|4\rangle\langle 4|Bq^3|1\rangle}{E_1^{(0)}-E_4^{(0)}}\\&=+\frac{\left(3\sqrt{2}/4\right)^2}{2}-\frac{(3)^2}{2}-\frac{\left(\sqrt{3}\right)^2}{6}=-\frac{71}{16}B^2\end{aligned} \quad (4.30)$$

and

$$\frac{\langle 1|Cq^4|3\rangle\langle 3|Cq^4|1\rangle}{E_1^{(0)}-E_3^{(0)}}+\frac{\langle 1|Cq^4|5\rangle\langle 5|Cq^4|1\rangle}{E_1^{(0)}-E_5^{(0)}}=-\frac{\left(5\sqrt{6}/2\right)^2}{4}-\frac{\left(\sqrt{30}/2\right)^2}{8}=-\frac{165}{16}C^2 \quad (4.31)$$

The energy difference between the two states becomes

$$E_1-E_0=2+\left(\frac{15}{4}-\frac{3}{4}\right)C+\left(-\frac{71}{16}+\frac{11}{16}\right)B^2+\left(-\frac{165}{16}+\frac{21}{16}\right)C^2 \quad (4.32)$$

or

$$\Delta E=2+3C-\frac{15}{4}B^2-9C^2 \quad (4.33)$$

The first term on the right hand side of equation (4.33) would normally be one (one times the harmonic energy), however, we are using units of $\left(\frac{\hbar\omega}{2}\right)$ so we must multiply the one by two. For the polynomial method, equation (4.33) above is used to calculate each frequency after multiplying through by our unit of energy $\left(\frac{\hbar\omega}{2}\right)$.

4.3.5 Calculating β and γ from B and C

Recall that

$$B = \beta\left(\frac{2}{\hbar\omega}\right)\left(\frac{\hbar}{m\omega}\right)^{\frac{3}{2}} \tag{4.34}$$

and

$$C = \gamma\left(\frac{2}{\hbar\omega}\right)\left(\frac{\hbar}{m\omega}\right)^{2} \tag{4.35}$$

The only unknowns left to solve are β and γ. We know that the single point energy V_+ (relative to the baseline equilibrium energy) must be

$$V_+ = \frac{1}{2}kx^2 + \beta x^3 + \gamma x^4 \tag{4.36}$$

and that, likewise, the single point energy V_- (relative to the baseline equilibrium energy) must be

$$V_- = \frac{1}{2}kx^2 - \beta x^3 + \gamma x^4 \tag{4.37}$$

To isolate β, we subtract equation (4.37) from equation (4.36).

$$V_+ - V_- = 2\beta x^3 \tag{4.38}$$

So β must be

$$\beta = \frac{V_+ - V_-}{2x^3} \tag{4.39}$$

To find γ we add equation (4.36) to equation (4.37) as follows

$$V_+ + V_- = kx^2 + 2\gamma x^4 \tag{4.40}$$

This provides γ as

$$\gamma = \frac{V_+ + V_- - kx^2}{2x^4} \tag{4.41}$$

So to calculate β and γ, we only need the single point energies V_+ and V_- computed in Gaussian at the points on the potential at our chosen step, x. (k is the harmonic force constant). Now we may calculate B and C and substitute these into equation (4.42) below

$$\Delta E = 2 + 3C - \frac{15}{4}B^2 - 9C^2 \tag{4.42}$$

and arrive at frequencies corrected from second order perturbation theory in cm^{-1}, where

$$\nu = \frac{\Delta E}{hc} \tag{4.43}$$

CHAPTER V. Computational Resources

For various parts of the calculations, the following computational resources were employed when available: an SGI Origin 2000 supercomputer with sixteen 250-MHz processors; a Paralogic Beowulf cluster with thirty-two 600-MHz processors and a Linux operating system; one 833-MHz single processor personal computer; and one 2.4-GHz single processor PC (both PC's were running under the Linux operating system). A Linux Beowulf cluster with 64 3.06 GHz PIV processors was later used, as this equipment replaced the SGI and the Beowulf cluster.

Electronic structure calculations were carried out at the MP2 level in the 6-311G** and 6-31+G** basis sets using the Gaussian 03 software package. Optimizations employing counterpoise (CP) corrections for each iteration were used to calculate the structure of each complex at the minimum potential energy. The harmonic frequencies were then generated at the same levels of theory after the completion of the optimizations.

From there, an in-house FORTRAN 77 program was developed in this work and was used to move the cluster atoms to probe the potential at the two turning points. Gaussian 03 was then employed again to obtain these single-point energies. These energies in conjunction with the third point, the energy of the equilibrium geometry, provided enough information to fit a Morse potential to each normal mode. Afterward, the parameters for the custom Morse potential were calculated and then used to arrive at frequencies corrected for anharmonicity. The calculated variables used for input with the polynomial method were worked up in Excel spreadsheets and the above same

FORTRAN 77 program was employed to set up Gaussian single-point energy calculations.

CHAPTER VI. Structures and Energy

6.1 Background

A significant amount of theoretical research has been done to obtain optimized geometries of water and methanol solvent clusters [41-50], to predict and measure their binding energies [45, 48, 51-57], and to calculate their vibrational spectra [42, 44, 46, 57-73]. Structures and frequencies are typically determined from the Hartree-Fock method, Møller-Plesset (MP) perturbation theory, or density functional theory. Optimized cluster structures for pure water (up to 12 molecules) include linear and cyclic conformations, as well as "books", "bags", "cages", "prisms", and even a ten molecule "butterfly" [74-76]. GAUSSIAN computational software predicts solvent clusters of MeOH-H_2O (having a stoichiometry of 1 methanol to 2 waters) in a HF/6-311G(2d,2p) basis set, where the atoms participating in hydrogen bonding form a highly stable six-membered ring (work done in this lab) [77]. Low and Kjaergaard have found a similar six-membered ring for the water trimer, using a HF/6-311++G(2d,2p) basis set [78].

A less stable seven-membered ring for a methanol-water 2:1 cluster was also found [2, 79]. Studies have not been limited to neutral species. Ionic clusters are also possible; a highly stable anionic water hexamer has been found via high-level *ab initio* calculations [80].

6.2 Basis Sets Used

In this work two basis sets were employed as part of the model chemistries used for electronic structure calculations: the 6-311G** basis set and the 6-31+G** basis set.

The 6-311G** basis set uses a single linear combination 6 Gaussian functions (primitives) called a "contraction" for the basis function used to describe the 1s orbital of each atom except for hydrogen [81]. Using three contractions to describe the valence shell (triple-split valence or triple-zeta), this basis set provides a flexible description of the bonding region [82]. The inner basis function consists of a linear combination of three primitives. The outer two basis functions (short and long range) are described by one Gaussian function each [81]. The "**" designation indicates that polarization functions were used as well: d-functions were added to the basis set for nonhydrogen atoms and p-functions were added to the basis functions for hydrogens [82].

The 6-31+G** basis set uses two basis functions to describe each valence shell (double-split valence or double-zeta) [82]. The inner valence basis function is described by a linear combination of three Gaussian functions, while the outer valence basis function is represented by one Gaussian function. The "+" indicates that, on all atoms other than hydrogen, diffuse functions (s-functions and p-functions larger than valence s and p-functions) were added to the basis. Diffuse functions, like those of the 6-31+G** basis set, are important for chemical systems involving electrons that are separated from nuclei by a relatively large distance as in the cases of anions, molecules with electron lone pairs, and hydrogen bonded systems.

6.3 Counterpoise Calculations and BSSE

In electronic structure energy calculations, the orbitals from all distinct molecules form a basis set which is effectively larger in a cluster than in the infinitely-separated fragments. This can lead to an artifactual lowering of the energy of the cluster relative to

the isolated fragments, and an over-estimation of the binding energy. This is called the Basis Set Superposition Error (BSSE). In an attempt to compensate for BSSE, the counterpoise method is often employed [83]. Without the counterpoise correction the energy of complexation of molecule A and molecule B to form complex AB is usually simply estimated as

$$E_{complexation} = E(AB)^{*}_{ab} - E(A)_{a} - E(B)_{b} \tag{6.1}$$

which is to say, the total energy of the complex E(AB) less the energies of each isolated, optimized monomer E(A) and E(B) gives the energy of complexation. The "*" denotes that the geometry of the complex is optimized. The geometry of A and B in the optimized cluster may be different from the geometries of free A and B. The subscripts a and b represent the basis sets of molecules A and B, respectively, and the subscript "ab" means that the basis set for the cluster is the union of the fragments' basis sets.

To calculate the BSSE from the counterpoise method, the energy of monomer A in the geometry assumed in the complex is calculated in the presence of its own basis set *and* the basis set of monomer B. This is called $E(A)_{ab}$*. In that same geometry the energy of A is evaluated with its own basis; this is called $E(A)_{a}$*. Analogous energies are defined for fragment B. The BSSE is then

$$BSSE = E(A)^{*}_{ab} + E(B)^{*}_{ab} - E(A)^{*}_{a} - E(B)^{*}_{b} = E_{CP} \tag{6.2}$$

Then the corrected complexation energy is.

$$E_{complexation(corrected)} = E_{complexation} - E_{CP} \tag{6.3}$$

Normally, during a geometry optimization, the norm of the energy gradient – the vector of derivatives of the energy with respect to atomic positions – is minimized. In counterpoise optimizations, it is the norm of the counterpoise-corrected energy gradient that is minimized. This generally improves the predicted energies, structures, and harmonic frequencies. Counterpoise corrections permit calculation of weak binding energies that approach experimental values. For example, our calculated binding energy of the hydrogen bond in the water dimer (MP2/6-311G**) was 0.1 kcal/mole just outside of the experimental range (see the results later in this chapter) and within the experimental range using MP2/6-31+G**.

6.4 Cluster Properties using a 6-311G** Basis Set

Gas phase optimizations with the 6-311G** basis set at the MP2 level were carried out and the harmonic frequencies computed for the water and methanol monomers, the water dimer as shown in figure 7, the methanol dimer as shown in figure 8, and two complexes with one water and one methanol each, as shown in figures 9 and 10. In the last case, when water is donating the hydrogen in the H-bond, it is designated as water-methanol. When methanol is the donor, the cluster is denoted methanol-water. Optimizations and computation of the harmonic frequencies for these configurations were carried out in conjunction with the counterpoise correction for basis-set superposition error. The counterpoise runs provided the improved geometries and vibrational frequencies necessary for use in the in-house anharmonicity correction program.

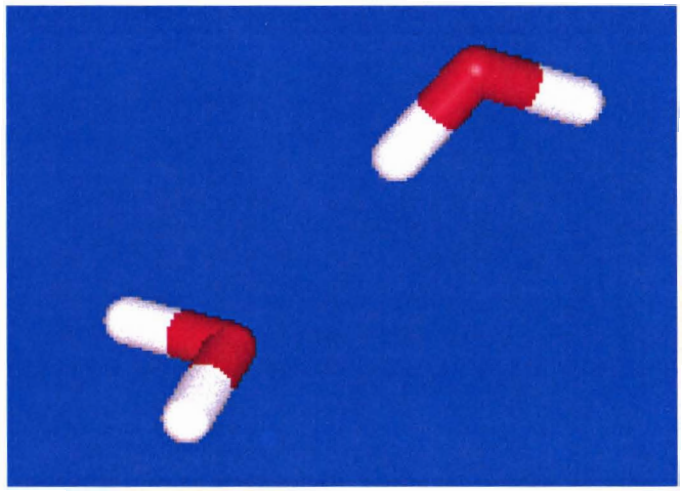

Figure 7. The water dimer optimized at the MP2/counterpoise level in a 6-311G** basis set.

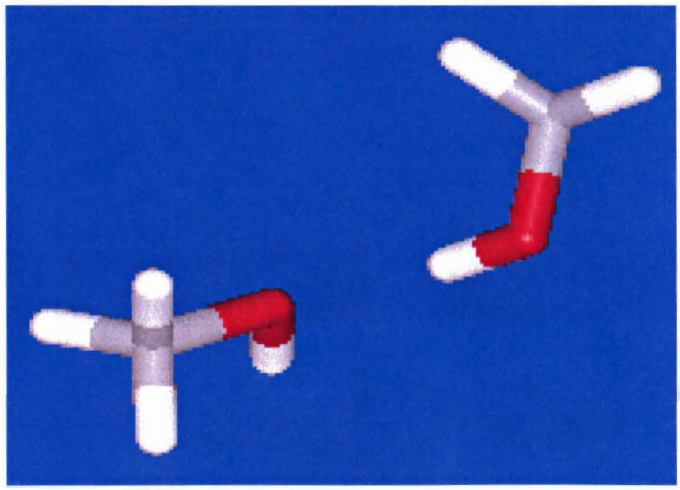

Figure 8. The methanol dimer optimized at the MP2/counterpoise level in a 6-311G** basis set.

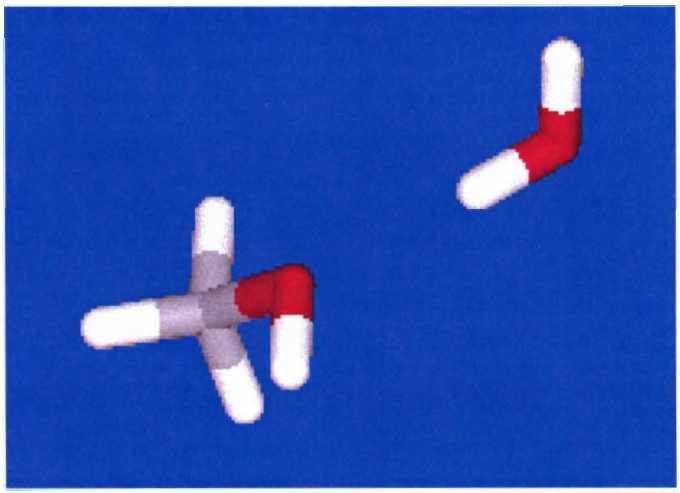

Figure 9. The 1:1 water-methanol complex (water donor) optimized at the MP2/counterpoise level in a 6-311G** basis set.

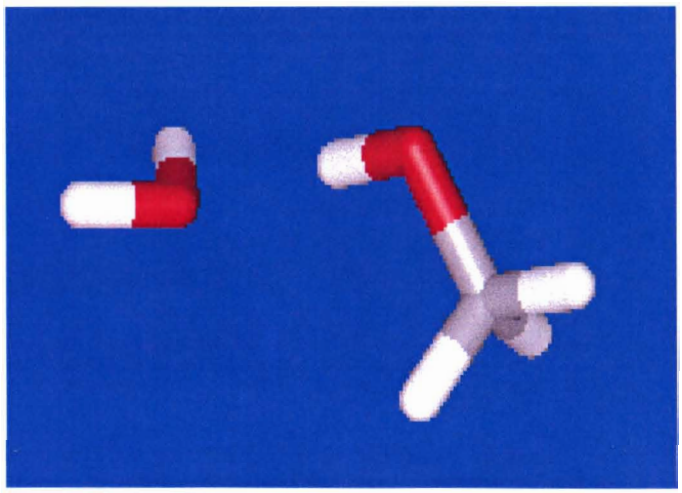

Figure 10. The 1:1 methanol-water complex (methanol donor) optimized at the MP2/counterpoise level in a 6-311G** basis set.

6.4.1 Cluster Binding Energies

Using the MP2/6-311G** model chemistry, the donor O-H distance was found to be a consistent 0.96 Å in all complexes; only the water monomer differed, having a value of 0.99 Å for the OH participating in the H-bond.

Table 20 shows the expected overestimation of the interaction energy for MP2 optimized species, owing to the basis set superposition error (BSSE) and electron correlation. The counterpoise MP2 optimizations provide the lowest interaction energies of all methods.

Table 20. Calculated Dimer Binding Energies (kcal/mol) for the RHF, MP2, and MP2 CP Opt Levels of Theory Using a 6-311G Basis Set.**

	RHF	MP2	MP2 CP Opt
water dimer	-5.58	-7.03	-4.60
methanol dimer	-5.67	-8.20	-4.84
(PD)water-(PA)methanol complex	-5.65	-7.72	-4.58
(PD)methanol-(PA)water complex	-5.65	-7.51	-4.78

Note: For the 1:1 water-methanol complexes, the hydrogen bond donor molecule is listed first in the label (e.g., water-methanol indicates that water is the donor).

Whether water or methanol is the acceptor, a methanol donor exerts a stronger interaction than a water donor. The methanol dimer always has the strongest interaction energy of all clusters, regardless of the level of theory used, and whether or not the counterpoise correction is applied. The strongest H-bonds occur in complexes where methanol is the donor. For the water dimer the counterpoise optimization with a medium-sized 6-311G** basis set has provided a calculated interaction energy, 4.6 kcal/mol, that is almost within the range for experimental error (the low end of the experimental range is 4.7 kcal/mol) [77].

6.4.2 Angle about Acceptor Oxygen (HOH) in Hydrogen Bond

An inspection of Table 21 reveals that MP2 calculations give smaller angles about the acceptor O (HOH) angle than RHF calculations and that the counterpoise, MP2 optimizations yield angles about the acceptor O that are very consistent from cluster to cluster.

Table 21. Angle about Acceptor Oxygen in Hydrogen Bond (°).

	RHF	MP2	MP2 CP Opt
water dimer	113	108	119
methanol dimer	133	133	124
(PD)water-(PA)methanol complex	133	127	122
(PD)methanol-(PA)water complex	115	110	121

A methanol acceptor always provides larger angles about the acceptor oxygen (vs. a water acceptor), whether the donor is a methanol or a water molecule. Also, regardless of which is the acceptor, this angle is larger when a methanol is the H-bond donor. These last two observations are likely the result of additional electron density about methanol's oxygen (relative to that of water's oxygen).

6.4.3 Hydrogen Bond Length

Table 22 shows that MP2 produces the shortest H-bonds (the H…O distance) due to additional BSSE from electron correlation, while the counterpoise MP2 optimizations provide the longest H-bonds.

Table 22. Hydrogen Bond (H...O) Distances (Å).

	RHF	MP2	MP2 CP Opt
water dimer	2.03	1.94	2.07
Methanol dimer	2.00	1.88	2.01
(PD)water-(PA)methanol complex	2.03	1.91	2.04
(PD)methanol-(PA)water complex	2.01	1.90	2.04

This agrees well with the trends found for the binding energies in Table 7. Also, the longest H-bond is found in the water-methanol complex, while the shortest H-bond occurs in the methanol dimer. For a given acceptor (either water or methanol), the shorter H-bond is observed when methanol is the donor, while for a given donor, the shorter H-bond occurs when methanol is the acceptor.

6.5 Theoretical Structure Work using a 6-31+G** Basis Set

6.5.1 Water Dimer

The structure of the water dimer is well characterized in flexible basis sets in the MP2 correlation model. Full optimization with the counterpoise correction has a significant impact. In Table 23, the computed structures of the water dimer in the MP2 correlation model in five different basis sets and with and without CP correction are compared.

Table 23. Computational Structural Results for the Water Dimer

Model Chemistry Geometric Parameter	MP2/ TZP [a]	MP2/ 6-311G (d,p) [b]	MP2/ 6-311+G (d,p) [b]	MP2/ 6-31+G (d,p)-CP [b]	MP2/ 6-311+G (d,p)-CP [b]	MP2/ 6-31+G(d,p)-CP-opt [c]
O-H free PD (Å)	0.957	0.9570	0.9585	0.9627	0.9588	0.962
O-H bonded PD (Å)	0.964	0.9635	0.9654	0.969	0.9646	0.969
H-bond (Å)	1.925	1.9393	1.9478	2.0458	2.0555	2.043
O-H PA (Å)	0.959	0.9593	0.9606	0.9641	0.9601	0.964
H-O-H PD (°)	105.0	102.39	103.62	105.57	103.51	105.6
H-O-H PA (°)	105.4	103.35	104.02	105.8	104.07	105.8
O-H-O (°)		174.22	176.69	172.65	176.69	172.8

[a] Reference [4]. [b] Reference [84], with frozen core MP2. [c] This work. PD is proton donator and PA is proton acceptor.

In all basis sets the OH bond participating as a donor in the H-bond is extended and longer than all other OH distances. The remaining OH bond in the donor water molecule is contracted relative to the other OH bonds, while the acceptor water molecule's OH bonds are of intermediate length. The hydrogen bond length O....HO is roughly twice the length of the intramolecular OH bonds. Acceptor HOH angles exhibit a slight opening relative to their donor counterparts, and the OH...O angle involving the hydrogen bond is almost linear.

From the Pople basis sets (all but TZP), those with a triple-split valence gave larger OHO angles, while the doubly split valence set gave the largest HOH angles of the donor and acceptor molecules. The addition of diffuse functions typically results in larger angles (both HOH and OH...O). The Dunning (TZP) basis set, lacking diffuse functions, produces fairly large HOH angles. Optimizing the structure with the counterpoise correction method produces a significant increase in hydrogen bond O...HO distance. This is because the bonding regions are over emphasized due to BSSE during standard electronic structure calculations. This effect is enhanced by the electron correlation of

MP2, and leads to the prediction of shorter (and stronger) bonds. Removing BSSE during the counterpoise optimizations results in more accurate (and longer/weaker) bond properties.

A quasi-experimental binding energy (D_e) for the deuterated water dimer $(D_2O)_2$ has been found by Curtiss, Frurip, and Belander [85-87]. D_0 is measured from thermal conductivity experiments (ranging from 358 K - 386 K with pressures between 100 and 1,000 Torr) and is added to the calculated value of the zero-point energy to arrive at an estimation of D_e of -5.40 ± 0.7 kcal/mol. This figure is most likely an upper bound because of the very anharmonic nature of the water dimer potential [87].

6.5.2 Water/Methanol Mixed Dimers

The structure of the 1:1 water/methanol complex from various sources in the literature and from this work is detailed in Table 24.

Table 24. Computational Structural Results for the Water Donor Conformer

Model Chemistry	MP2/ 6-31G(d) [a]	MP2/ TZP [b]	MP2/ aug-cc -pVTZ [c]	MP2/ 6-311+ G(d,p) [d]	MP2/ aug-cc -pVDZ [e]	MP2/ 6-311++ G(2d,2p) [e]	MP2/ 6-31+G (d,p)- CP-opt [g]
Geometric Parameter							
C-O (Å)	1.434	1.431	1.431				1.435
H-bond (Å)	1.929	1.884	1.888		1.904	1.911	1.992
Free O-H (Å)	0.968	0.957	0.960				0.962
Bonded O-H (Å)	0.976	0.966	0.971	0.965			0.97
O-O (Å)	2.867		2.840	2.906	2.844	2.860	2.951
O-H Meth (Å)		0.959	0.962				0.965
O-H-O (°)	162.3		166.1	179.7			169.2
C-O-Hbond (°)		107.3					110.1
Water H-O-H (°)		105.1	104.6	107.0			105.7
C-O-H Meth (°)			108.3				108.8

[a] Reference [88]. [b] Reference [4] . [c] Reference [89]. [d] Reference [90]. [e] Reference [91]. [g] This work.

The (water)OH…O(methanol) distance is shorter than the OH…O distance in the water dimer, suggesting a stronger hydrogen bond in the mixed dimer. The remaining O-H bond in water (listed as "Free OH" in the table) is the shortest O-H bond in the mixed complex, while the methanol O-H has intermediate length. This pattern is similar to that found in the water dimer. Despite the hydrogen bond, the donor water HOH angle does not change relative to the water monomer. Optimization with CP correction extends the OH…O bond length and the O…O distance, and has an impact on the OH…O angle as well.

Table 25 provides data on the calculated structures of the 1:1 methanol-water mixed dimer.

Table 25. Computational Structural Results for the Methanol Donor Conformer

Model Chemistry	MP2/ 6-31G(d) [a]	MP2/ TZP [b]	MP2/ aug-cc -pVTZ [c]	MP2/ 6-311+ G(d,p) [d]	MP2/ aug-cc -pVDZ [e]	MP2/ 6-311++ G(2d,2p) [e]	MP2/ 6-31+G(d,p)-CP-opt [g]
Geometric Parameter							
C-O (Å)	1.417	1.416	1.418				1.424
H-bond (Å)	1.930	1.907	1.938		1.942	1.948	2.048
O-H Meth (Å)	0.976	0.964	0.967	0.967			0.969
O-O (Å)	2.898		2.905	2.855	2.912	2.911	3.017
O-H Water (Å)		0.959	0.962				0.964
C-O-H (°)	107.2	107.2	107.8	103.6			108.3
O-H-O (°)	180.1		177.1	173.8			178.1
H-O-H Water (°)			104.5				105.8

[a] Reference [88]. [b] Reference [4] . [c] Reference [89]. [d] Reference [90]. [e] Reference [91]. [g] This work.

The C-O bond is shorter in this conformer than in the water donor version of the complex. The hydrogen bond length and the O-O distance are longer than that in the water-methanol complex. This implies a weaker hydrogen bond in the methanol donor conformer. The O-H bond participating in hydrogen bonding in the methanol-water cluster is longer than the O-H bonds of the water molecule. The OH…O angle of the hydrogen bond in the methanol donor complex is more nearly linear than the corresponding angle in the water donor complex. Once again, the CP-correction extends the OH…O bond and the O…O distance.

6.5.3 Methanol Dimer

Structural parameters for the methanol dimer can be found in Table 26. Of the four dimers the hydrogen bond has the shortest length in the methanol dimer, suggesting that it also has the strongest hydrogen bond. (In the 6-31+G(d,p) basis set with full

counterpoise treatment the hydrogen bond of the water-methanol conformer has about the same length as the hydrogen bond in the methanol dimer). The donor O-H distance in the methanol dimer is about the same as the length of the methanol donor O-H bond found in the 1:1 methanol-water pair, and the OH…O angle is about the same in the two complexes (6-311+G(d,p)). However, with full counterpoise treatment in the 6-31+G** basis set (this work), the dimer with the most linear hydrogen bond is the methanol donor complex.

Table 26. Computational Structural Results for the Methanol Dimer

Model Chemistry	MP2/ 6-311+G (d,p) [a]	MP2/ Aug -cc-pVDZ [b]	MP2/ 6-311++G (2d,2p) [b]	MP2/ VTZ (2df,2p) [c]	MP2/ 6-31+G(d,p)-CP-opt [e]
Geometric Parameter					
H-bond (Å)		1.887	1.895		1.993
O-O (Å)	2.847	2.846	2.852	2.831	2.956
O-H Donor (Å)	0.966				0.970
Donor C-O (Å)					1.424
Acceptor C-O (Å)					1.435
Acceptor O-H (Å)					0.965
Donor C-O-H (°)	106.9				108.3
O-H-O (°)	172.5				171.2
Acceptor C-O-Hbond (°)					110.7

[a] Reference [90]. [b] Reference [91] . [c] Reference [92]. [e] This work.

In general, for complexes other than the water dimer, the order of increasing O-O length is methanol dimer < 1:1 water-methanol < 1:1 methanol-water. Similarly for all dimers, the ordering of the hydrogen bond length is methanol dimer < 1:1 water-methanol < 1:1 methanol-water < water dimer. The structural data points to a stonger H-bond in the water-methanol complex than in the methanol-water conformer and suggests that the water-methanol complex is more energetically stable as well. The longest and

presumably weakest hydrogen bond is found in the water dimer, and the shortest in the methanol dimer.

Computational studies in the literature do not conclusively identify the preferred conformer of the 1:1 water/methanol complex. Depending on the method and basis set used, computational evidence can be found to support either isomer. Experimental IR studies in gas matrices has led to conflicting conclusions as well [32, 33]. However, microwave rotation-tunneling spectroscopy of 1:1 water/methanol complexes formed in molecular beam adiabatic expansion experiments gave evidence strongly supporting the water-methanol complex as the lower energy conformer [93].

6.5.4 Complex Binding Energies

In Table 27, the binding energies for each of the dimer complexes are shown as calculated from counterpoise-corrected single-point energies from a variety of methods. CP-corrected binding energies are always smaller than values uncorrected for BSSE.

Table 27. Counterpoise-Corrected Binding Energies of the Four Dimer Complexes (kcal/mol).

Complex	Water Dimer	Water-Methanol	Methanol-Water	Methanol Dimer
Model Chemistry				
MP2/aug-cc-pVDZ [a]	-4.39			
MP2/aug-cc-pVTZ [a]	-4.74			
MP2/aug-cc-pVQZ [a]	-4.87			
CBS [a]	-4.95			
MP2(FC)/cc-pVQZ [b]	-4.67			
MP2(FC)/aug-cc-pVQZ [b]	-4.79			
MP2/VTZ(2df,2p) [c]	-4.68			-5.21
MP2/6-311+G(2df,2p) [d]	-4.47	-4.50	-5.07	-5.15
MP2/aug-cc-pVDZ [e]		-5.15	-4.48	-5.22
MP2/6-311++G(2d,2p) [e]		-5.15	-4.45	-5.19
MP2/6-31+G(d,p)-CP-opt [g]	-4.89	-5.39	-4.70	-5.26

[a] Geometry optimized at MP2(FC)/aug-cc-pVTZ, Reference [94]. [b] MP2/6-311++G(2d,2p) geometry, Reference [95]. [c] Reference [92]. [d] Geometry optimized at 6-311+G(d,p), Reference [90] . [e] Reference [91] . [g] Counterpoise geometry optimization as well as full counterpoise treatment of binding energy, This work.

Our calculations employ the counterpoise-corrected energy gradient, which guides the geometry optimization. Also, our geometries and binding energies are calculated with the same basis set, and we make use of full MP2 calculations instead of freezing the core electrons, all of which leads to enhanced results.

The reported binding energies are not zero-point-energy corrected and range from -4.39 to -4.95 kcal/mol for the water dimer, -4.50 to -5.39 kcal/mol for the water-methanol complex, -4.45 to -5.07 kcal/mol for the methanol-water complex, and -5.15 to -5.26 kcal/mol for the methanol dimer. In general, the methanol-water complex has the lowest binding energy, and the methanol dimer exhibits the strongest hydrogen bond. Chemically this makes some sense, as the methyl group is an electron donating group and makes the oxygens of acceptor methanol molecules more electron rich, strengthening the hydrogen bond.

Comparing our calculated energies to available experimental work, our MP2/6-31+G(d,p)-CP-opt binding energy of -4.89 kcal/mol for the water dimer is in good agreement with the 5.4±0.7 kcal/mol [85-87] reported by Curtiss et al. for $(D_2O)_2$. Also, our energy is below the 5.4 kcal/mol figure thought to be an upper bound as discussed above [87]. Furthermore, we also found that the water-methanol complex (-5.39 kcal/mol) is more energetically preferred than the methanol-water complex (-4.70 kcal/mol) which agrees well with the microwave spectroscopy experiments of Stockman et al. [93] that found that only the water-methanol conformer is formed in molecular beam expansions. Our data also show the water-methanol complex and the methanol dimer to have the strongest hydrogen bonds of the dimers -- in other words, whenever a methanol molecule is the proton acceptor. These stronger hydrogen bonds again make sense from the perspective that a methyl, electron donating group is attached to the oxygen of the acceptor methanol molecule.

6.5.5 Conclusions

Counterpoise corrected structures resulted in longer hydrogen bonds and correspondingly lower (and more accurate) binding energies. From our calculations the methanol-water complex exhibited the longest O-O length, the shortest donor O-H distance, and the longest hydrogen bond, all consistent with the weakest calculated binding energy. The next shorter O-O and hydrogen bond distances (and longer donor O-H bonds) and next strongest binding energy were displayed by the water dimer. The dimers with the strongest hydrogen bonds were found to be the water-methanol complex and the methanol dimer. The shortest hydrogen bond and O-O distances and the longest

donor O-H bond lengths were calculated to be those of the water-methanol pair. These results are consistent with our estimates of binding energies, strongest for the water-methanol complex. The computed structural parameters (hydrogen bond length, O-O distance, and donor O-H length) for the methanol dimer corresponded directly to the complex with the second strongest hydrogen bond. Our calculations predicted the methanol dimer to have a binding energy of -5.26 kcal/mol, slightly smaller than that of the water-methanol complex, -5.39 kcal/mol.

CHAPTER VII. Frequency Results and Discussion

7.1 Morse, Harmonic, and Polynomial Frequencies

*7.1.1 Water Dimer in 6-311G** Basis Set*

In Tables 28 and 29, the results from the Morse and polynomial methods are compared to experimental gas phase and matrix frequency data, as well as to the harmonic frequencies produced by Gaussian using the MP2 level of theory in a 6-311G** basis set. All electronic structure calculations employed counterpoise optimizations and full counterpoise treatment of single-point energies and frequencies. The Morse method compares well to the harmonic method, and to a lesser extent, the polynomial method is an improvement beyond the harmonic model and provides the best treatment for certain frequencies of water molecules.

Table 28. Water Dimer Frequencies using MP2/6-311G-CP-opt Model Chemistry.**

Mode	Morse v (cm^{-1})	Experimental v (cm^{-1})	% Dev of Morse vs Exp % : Δ v(cm^{-1})	Harmonic v (cm^{-1})	% Dev of Harm vs Exp % : Δ v(cm^{-1})	Description
1:A"	115	88 [a]	30.2	115	30.2: 27	PD torsion
2:A'	143	103 [a]	38.8	143	39.0: 40	PA wag
3:A"	143	108 [a]	32.8	143	32.8: 35	PA twist
4:A'	149	143 [b]	4.32: 6	157	9.51: 14	Intermolec str
5:A'	305	311 [c]	-1.92: -6	306	-1.52: -5	In-plane bend
6:A"	566	523 [c]	8.21	566	8.21: 43	Out-of-plane bend
7:A'	1668	1599 [c]	4.31: 69	1673	4.61: 74	PA OH bend
8:A'	1697	1616 [c]	4.98: 81	1701	5.28: 85	PD OH bend
9:A'	3745	3601 [d]	3.99: 144	3869	7.44: 268	PD sym OH str
10:A'	3815	3660 [d]	4.25: 155	3906	6.71: 246	PA sym OH str
11:A'	3912	3735 [d]	4.73: 177	3990	6.83: 255	PD asym OH str
12:A"	4010	3745 [d]	7.08	4010	7.08: 265	PA asym OH str

[a] Reference [18], planar supersonic molecular beam expansion (terahertz laser vibration-rotation-tunneling spectroscopy), 5 K. [b] Reference [19], planar supersonic molecular beam expansion (terahertz laser vibration-rotation-tunneling spectroscopy), 5 K. [c] Reference [20], Neon matrix, 10 K. [d] Reference [21], molecular beam depletion spectroscopy with size selection by momentum transfer in scattering experiment (atoms under single collision conditions).

All assignments have been made according to the mode descriptions offered by the experimentalists referenced in the table and match the mode motions as calculated from Gaussian (this work). From Table 28, computed harmonic frequencies are generally higher than the experimental values. This arises from systematic error in the computational model, and anharmonicities inherent in the experimental data. The Morse method significantly corrects A' symmetry modes but applies negligible corrections to A" modes (these modes have single-point energies at the turning points that are extremely close in value or are exactly the same). We class modes 7-12 as intramolecular, and 1-6 as intermolecular motions. On the whole, it does not appear that the Morse method affords systematic improvements over the harmonic calculation of the

intermolecular frequencies. The strongest Morse corrections are for the A' OH-stretching modes 9, 10, and 11.

Table 29. Polynomial Method Frequencies for the Water Dimer (MP2/6-311G-CP-opt).**

Mode	Experimental v (cm^{-1})	Polynomial v (cm^{-1})	Harmonic v (cm^{-1})	% Dev P:P vs Exp
1 A"	88 [a]	-448657	115	
2:A'	103 [a]	-143393	143	
3:A"	108 [a]	-100497	143	
4:A'	143 [b]	152	157	6.40
5:A'	311 [c]	-1716	306	-652
6:A"	523 [c]	370	566	-29.2
7:A'	1599 [c]	1665	1673	4.11
8:A'	1616 [c]	1692	1701	4.70
9:A'	3601 [d]	3755	3869	4.29
10:A'	3660 [d]	3823	3906	4.45
11:A'	3735 [d]	3968	3990	6.23
12:A"	3745 [d]	4102	4010	9.54

We fit polynomials to the energies computed along normal modes for the water dimer, and treated the departure from the perfect harmonic potential as a perturbation, as described in Chapter IV. We found that the departure from the harmonic frequency values for the intramolecular modes 7-12 was minor. The frequencies of most intermolecular modes could not be represented reasonably by treating the polynomial potential as a perturbation, with state energy differences usually so seriously shifted that the method often produced negative frequencies. Like those of the Morse and harmonic methods, the positive frequencies produced by the polynomial method are almost always higher than the experimental frequencies and on occasion for the polynomial method even higher than the harmonic vibrations.

Assignments of the OH stretching frequencies have been made by molecular beam depletion spectroscopy with size selection from momentum transfer in scattering experiments (atoms under single collision conditions) by Buck and Huisken [96]. The acceptor water asymmetric stretch and donor water asymmetric stretch occur at 3745 cm^{-1} and 3735 cm^{-1}, respectively, and the acceptor symmetric stretch and donor symmetric stretch occur at 3660 cm^{-1} and 3601 cm^{-1}, respectively. The Morse method has the best agreement with the experimental values for these stretching vibrations. The experimental assignments for the OH bending modes from Bouteiller and Perchard [20] (neon matrix, 10 K) are 1616 cm^{-1} for the donor water and 1599 cm^{-1} for the acceptor water molecule. Despite participating in the hydrogen bond, the bonded OH bending vibration is actually higher in frequency than the free (acceptor) OH bending vibration.

The harmonic frequencies do a fairly good job of representing the measured values of the intermolecular modes on an absolute basis. The discrepancies, however, are still high on a relative basis. On the other hand, the agreement for the intramolecular modes is fairly good on a relative basis, but the harmonic frequencies tend to be blue-shifted by 200 cm^{-1} or more for the majority of these modes.

The most difficult task for this system is to model the low-frequency intermolecular motions. No method does an entirely satisfactory job with the lowest three modes.

*7.1.2 Water Dimer in 6-31+G** Basis Set*

The water dimer was examined in the 6-31+G** basis set, and these results are shown in Tables 30 and 31.

Table 30. Water Dimer Frequencies using MP2/6-31+G-CP-opt Model Chemistry.**

Mode	Morse v (cm^{-1})	Experimental v (cm^{-1})	% Dev vs Exp	Harm v (cm^{-1})	% Dev vs Exp
1	102	88 [a]	16.2	102	16.2
2	128	103 [a]	24.5	129	25.1
3	152	108 [a]	41.0	152	41.0
4	168	143 [b]	17.8	170	19.1
5	332	311 [c]	6.80	335	7.65
6	596	523 [c]	14.0	596	14.0
7	1630	1599 [c]	1.97	1633	2.12
8	1648	1616 [c]	1.95	1650	2.09
9	3669	3601 [d]	1.88	3804	5.65
10	3768	3660 [d]	2.96	3864	5.57
11	3899	3735 [d]	4.38	3983	6.65
12	4006	3745 [d]	6.96	4006	6.96

[a] Reference [18], planar supersonic molecular beam expansion (terahertz laser vibration-rotation-tunneling spectroscopy), 5 K. [b] Reference [19], planar supersonic molecular beam expansion (terahertz laser vibration-rotation-tunneling spectroscopy), 5 K. [c] Reference [20], Neon matrix, 10 K. [d] Reference [21], molecular beam depletion spectroscopy with size selection by momentum transfer in scattering experiment (atoms under single collision conditions).

The Morse method once again has a significant impact on A' modes only, most dramatically on the OH stretching modes 9-11. Despite the use of a basis set with diffuse functions, both the Morse and harmonic methods in MP2/6-31+G** predict experimental frequencies less well than in MP2/6-311G**. This suggests that employing a triple-zeta basis set as well as including the important diffuse functions may be necessary for best results.

Table 31. Polynomial Method Results for the Water Dimer (MP2/6-311G-CP-opt).**

Mode	Experimental v (cm^{-1})	Harmonic v (cm^{-1}): Δ v	Polynomial v (cm^{-1}): Δ v	P:P % Dev vs Exp
1	88 [a]	102: 14	negative	
2	103 [a]	129: 26		
3	108 [a]	152: 44		
4	143 [b]	170: 27		
5	311 [c]	335: 24		
6	523 [c]	596: 73	542: 19	3.62
7	1599 [c]	1633: 34	1620: 21	1.34
8	1616 [c]	1650: 34	1638: 22	1.33
9	3601 [d]	3804: 203	3677: 76	2.12
10	3660 [d]	3864: 204	3776: 116	3.16
11	3735 [d]	3983: 48	3953: 18	5.83
12	3745 [d]	4006: 264	4099: 354	9.45

The polynomial frequencies from MP2/6-31+G**-CP-opt agree well with experimental values for modes 6-12 (Table 31). However, the frequencies of modes 1-5 are negative, suggesting that the polynomial method is inappropriate. On the whole it appears that when a perturbative treatment of the polynomial potential is relevant (i.e., for small corrections), it improves on the harmonic frequencies. This is certainly the case for the high frequency modes.

The Morse method provides improved OH intramolecular stretching frequencies over the polynomial method because it better models dissociative motions (i.e., stretches). However, the polynomial method better predicts the bending vibrations as these are more correctly represented by a potential having a series of even-powered terms. For the upper eight modes, the Morse method predicts half of these vibrations better than the polynomial method, and both methods are more capable than the harmonic method for the water dimer in the 6-31+G** basis set. The lowest four vibrations were predicted

poorly by all methods probably because all methods have their basis in the harmonic model which does not account for the rotational character that contributes to the frequencies of the lowest modes.

*7.1.3 Water Donor Mixed Dimer in 6-31+G** Basis Set*

The mixed water-methanol dimer (water donor configuration) has been studied using the above three methods and the results are compared to experimental data when possible.

Table 32. Water-Methanol Complex (water donor) Frequencies (MP2/6-31+G-CP-opt).**

Mode	Expt (cm^{-1}) [a]	Morse (cm^{-1})	Harm (cm^{-1})	Poly (cm^{-1})	% Dev from Expt			Description
					Morse	Harm	Poly	
1		36	38	negative				
2		46	47					
3		124	125					
4		162	169	164				OO stretch
5		297	297	negative				
6		362	363					
7		602	602	493				
8	1032	1046	1061	1050	1.38	2.82	1.75	CO stretch
9	1078	1087	1088	1113	0.837	0.906	3.23	methanol bend
10		1200	1200	1217				methanol bend
11		1378	1379	1392				methanol bend
12	1466	1523	1523	1528	3.90	3.92	4.23	CH_3 bend
13		1549	1549	1549				CH_3 bend
14		1560	1560	1559				CH_3 bend
15	1614	1648	1651	1638	2.13	2.28	1.46	H_2O bend
16	2974	3070	3119	3076	3.22	4.86	3.41	CH_3 stretch
17	3018	3205	3205	3275	6.20	6.20	8.53	CH_3 stretch
18		3179	3263	3206				CH_3 stretch
19	3539	3620	3776	3624	2.28	6.70	2.41	H_2O str (bonded OH)
20	3663	3692	3895	3694	0.789	6.34	0.839	methanol OH str
21	3704	3867	3978	3909	4.40	7.40	5.54	H_2O str (free OH)

[a] Reference [32], Argon matrix, 12 K.

For the water-methanol mixed dimer, the Morse method provides frequencies that agree well with the experimental values, as shown in Table 32. The harmonic frequencies agree reasonably well with the experimental frequencies, but the Morse method achieves better agreement -- eight of the nine available experimental values are predicted better by the Morse method. (The methyl stretch at 3018 cm^{-1} is predicted to have the same value in both methods). For this cluster, the Morse method appears to almost always best the harmonic method and never provides a value in lesser agreement with the measured data. Given that the Morse method is also computationally inexpensive, it seems worthwhile to employ the Morse method as a correction to the harmonic approximation, based on its success thus far.

The polynomial method achieves good agreement with the intramolecular experimental frequencies for this cluster. Using the measured data as a benchmark, the polynomial method evaluates two-thirds of these modes better than does the harmonic method. However, the Morse method yields even greater accuracy than the polynomial method for eight of the nine experimental frequencies. The water bending frequency is still predicted better by the polynomial method. In contrast the Morse method actually performs even better than the polynomial method for the two methanol bending modes. The Morse method is clearly the best overall method of the three for use with this cluster, based on the available experimental frequencies, and the prediction of negative values by the polynomial method for frequencies of the intermolecular modes.

*7.1.4 Methanol Donor Mixed Dimer in 6-31+G** Basis Set*

As can be seen in Table 33, the Morse method once again produces the best agreement with experimental data. The harmonic evaluations agree less well with the experimental frequencies. For the vast majority of experimental values, the Morse method gives a better prediction than the harmonic approximation. (For the few modes that it does not, the predictions are about the same -- the Morse method is not less accurate for any mode).

Table 33. Methanol-Water Complex (methanol donor) Frequencies (MP2/6-31+G-CP-opt).**

Mode	Expt (cm^{-1}) [a]	Morse (cm^{-1})	Harm (cm-1)	Poly (cm^{-1})	% Dev from Expt			Description
					Morse	Harm	Poly	
1		56	56	negative				
2		60	60					
3		84	84					
4		136	143	144				
5		182	182	negative				
6		203	217					
7		643	643	628				
8	1048	1069	1085	1071	2.00	3.57	2.24	CO str
9	1103	1122	1122	1143	1.72	1.74	3.59	OCH bend
10		1200	1200	1216				OCH bend
11	1380	1422	1423	1440	3.03	3.11	4.36	COH bend
12	1448	1521	1521	1525	5.04	5.07	5.32	CH_3 bend
13	1464	1548	1548	1548	5.73	5.73	5.71	CH_3 bend
14	1475	1561	1562	1560	5.86	5.91	5.77	CH_3 bend
15	1601	1629	1632	1619	1.77	1.96	1.10	H_2O bend
16	2835	3041	3093	3047	7.28	9.09	7.49	CH_3 str
17		3166	3166	3237				CH_3 str
18	2982	3142	3235	3165	5.36	8.47	6.14	CH_3 str
19	3536	3623	3820	3623	2.46	8.04	2.47	methanol OH str
20	3627	3773	3864	3782	4.02	6.55	4.28	H_2O sym str
21	3714	4006	4006	4099	7.86	7.86	10.38	H_2O asym str

[a] Reference [33], Nitrogen Matrix, 10 K.

The polynomial method also provides frequencies that achieve good agreement with the experimental values, mainly for the higher frequencies. However, the Morse method again improves accuracy beyond the polynomial method (greater accuracy for three-fourths of the vibrations). For the methanol-water mixed dimer, there is no clear winner, Morse or polynomial method, for evaluating bending frequencies.

*7.1.5 Methanol Dimer in 6-31+G** Basis Set*

Table 34 is a complete listing of the calculated frequencies of the methanol dimer in each of the three methods. The relatively sparse experimental data is discussed below.

Table 34. Methanol Dimer Frequencies (MP2/6-31+G-CP-opt).**

Mode	Morse (cm^{-1})	Harm (cm^{-1})	Poly (cm^{-1})
1	24	24	negative
2	35	36	
3	39	41	
4	91	91	50
5	124	124	negative
6	165	170	172
7	343	344	negative
8	652	652	612
9	1047	1061	1051
10	1082	1086	1090
11	1086	1088	1097
12	1126	1127	1147
13	1200	1200	1212
14	1200	1200	1211
15	1377	1378	1391
16	1429	1430	1448
17	1521	1521	1525
18	1523	1523	1528
19	1548	1548	1547
20	1549	1549	1549
21	1560	1561	1559
22	1562	1562	1560
23	3040	3091	3045
24	3069	3118	3075
25	3164	3164	3235
26	3204	3204	3274
27	3139	3233	3162
28	3178	3262	3205
29	3576	3791	3568
30	3693	3896	3695

The proportion of negative frequencies to positive frequencies from the polynomial method decreases with increasing cluster size, with the smallest fraction of negative frequencies being present in the methanol dimer. This is due to the decrease in the

fraction of intermolecular modes which are difficult for the polynomial potential to model.

In Tables 35 and 36, the Morse and polynomial methods give frequencies that are in excellent agreement with experimental data where they are available. The harmonic frequencies, are significantly higher in these cases.

Table 35. Methanol Dimer O-H Stretching Frequencies (MP2/6-31+G-CP-opt).**

Mode	Experimental (cm^{-1}) [a]	Morse (cm^{-1})	% Dev from Exp	Harm (cm^{-1})	% Dev from Exp
29	3574	3576	0.0463	3791	6.08
30	3684	3693	0.243	3896	5.77

[a] Reference [97], complexes of methanol dimer with chromophore formed in supersonic expansion; laser induced fluorescence and IR/UV double resonance spectroscopy.

Table 36. Methanol Dimer O-H Stretching Frequencies (MP2/6-31+G-CP-opt).**

Mode	Poly (cm^{-1})	% Dev from Exp [a]
29	3568	-0.159
30	3695	0.290

[a] Reference [97], complexes of methanol dimer with chromophore formed in supersonic expansion; laser induced fluorescence and IR/UV double resonance spectroscopy.

7.1.6 Conclusions

The Morse method provides inexpensive and effective improvement on harmonic frequencies, and treats vibrational modes on the whole better than the polynomial method. In general, the Morse treatment is the method of choice among these three methods for calculating frequencies. This is illustrated in Table 37 which shows the RMS error for each method in every study where experimental data is available.

The polynomial method usually gives better predictions than the harmonic model especially for water bending frequencies.

Table 37. RMS Error (cm^{-1}) Relative to Experimental Frequencies for All Methods.

	Water Dimer	Water Dimer	Water Donor	Methanol Donor	Methanol Dimer
Model Chemistry	MP2/6-311G**	MP2/6-31+G**	MP2/6-31+G**	MP2/6-31+G**	MP2/6-31+G**
Morse	404	216	288	453	9
Polynomial	515	440	364	534	12
Harm	535	474	497	614	304

Note, the polynomial negative frequencies are ignored in the water dimer statistics as some of the negative frequencies are so large that a meaningful comparison of the polynomial frequencies to those of the other methods would not be possible. Also, all model chemistries employed counterpoise optimization and frequency calculations.

7.2 Improvement of Polynomial Method Low Frequencies

Many of the low frequency, intermolecular vibrations for each of the complexes were calculated to be negative using a second order perturbation treatment of our polynomial fit to the energy changes along normal modes of the water dimer. Intermolecular frequencies are the least well characterized and are the most difficult to determine experimentally and theoretically. Recall our perturbation-theoretic equation for transition energies (in units of $\frac{1}{2}h\nu$), equation (7.1) below

$$\Delta E = 2 + 3C - \frac{15}{4}B^2 - 9C^2 \qquad (7.1)$$

An analysis of the negative frequencies in the water dimer on a mode per mode basis showed that the size of B (the coefficient of the cubic term in the polynomial) did not significantly impact the sign of the transition energy (values for B were always less than

one), although the B term will always be negative. However, large values of C (the coefficient of the quartic term in the polynomial) produce negative frequencies. Specifically for equation (7.1), when B is zero, the energy change will be negative when C is greater than 2/3. When B is nonzero, C can be even smaller and still have this effect. In such cases the perturbation assumption that the potential departs only slightly from the reference harmonic fails, and another approach to estimation of the transition energies is required.

7.3 Alternative Methods

Perturbation theory can produce energies, and therefore frequencies, that are either too high or too low even to the point of being negative (as was found for the intermolecular, soft modes). An alternative polynomial method is presented here which eliminates negative values for the low frequency, intermolecular modes. Specifically, the MP2 potentials of the six intermolecular vibrational modes for the water dimer have been mapped with eight single-point MP2/6-31+G(d,p) calculations at points 0.5, 1.0, 1.2, and 1.5 times the turning point value, ±x. A ninth point is provided from the equilibrium geometry optimization employing the same model chemistry. A quartic polynomial was fit, using Microsoft Excel, to these energies producing potential curves for each mode (Figures 11-16). By taking the second derivative of the resulting polynomial functions at x=0, effective force constants, k, were found for each vibrational mode. The frequencies were recovered by

$$\nu = \frac{1}{2\pi}\left(\frac{k}{\mu}\right)^{\frac{1}{2}} \tag{7.1}$$

where μ is the reduced mass reported from the harmonic frequency calculations. This method used for the soft modes in tandem with the previous polynomial method for the fundamental bands we dub the "dual polynomial method". To avoid confusion, the previous method alone will now be referred to as the polynomial-perturbational method.

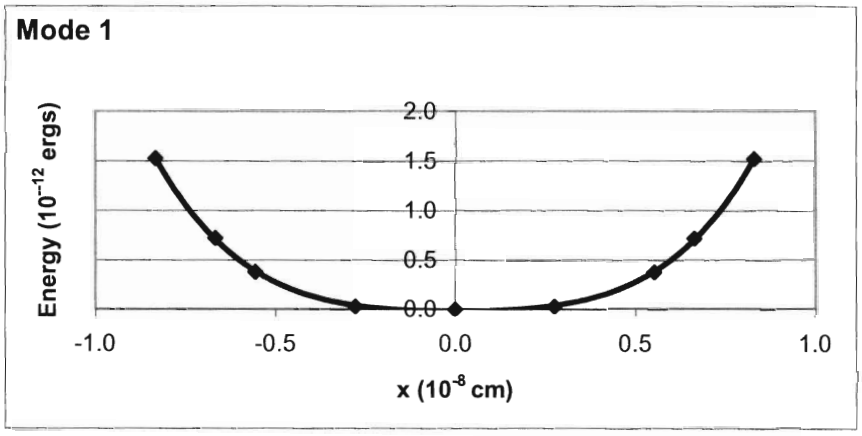

Figure 11. Water Dimer Vibrational Potential Map for Donor Molecule Rotation about O-O. Polynomial: $y = 2.3765x^4 - 6 \times 10^{-11}x^3 + 0.5877x^2 + 2 \times 10^{-11}x - 0.0189$, $R^2 = 0.9996$.

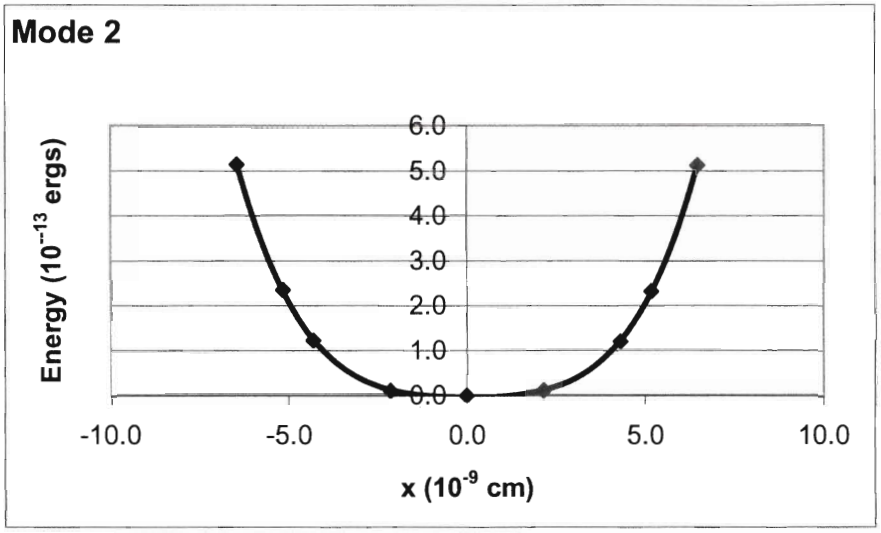

Figure 12. Water Dimer Vibrational Potential Map for Proton Acceptor Wag.
Polynomial: $y = 0.0024x^4 - 3 \times 10^{-05}x^3 + 0.0233x^2 - 0.0014x - 0.0347$, $R^2 = 0.9999$.

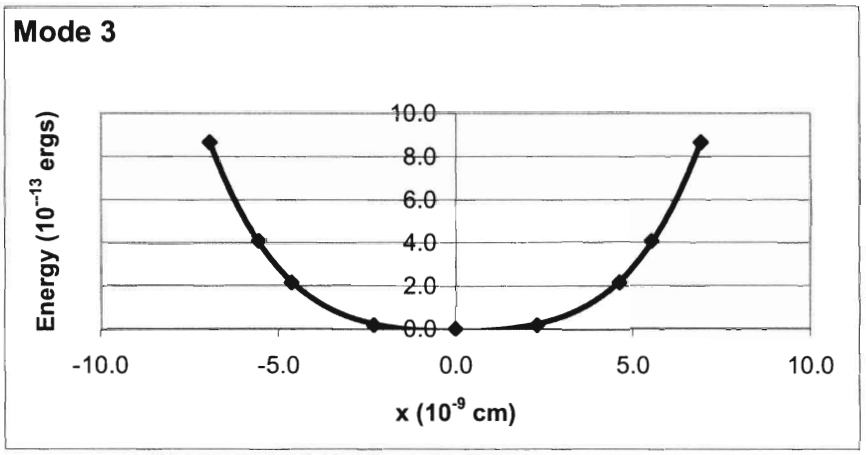

Figure 13. Water Dimer Vibrational Potential Map for Proton Acceptor Twist.
Polynomial: $y = 0.0028x^4 - 4 \times 10^{-15}x^3 + 0.0471x^2 - 7 \times 10^{-13}x - 0.0947$, $R^2 = 0.9997$.

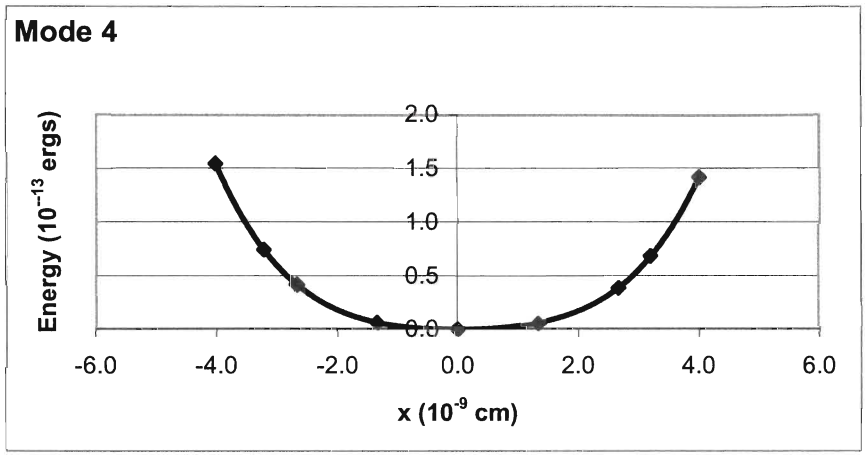

Figure 14. Water Dimer Vibrational Potential Map for Intermolecular O-O Stretch. Polynomial: $y = 0.004x^4 - 0.001x^3 + 0.0283x^2 + 0.0009x - 0.0038$, $R^2 = 1$.

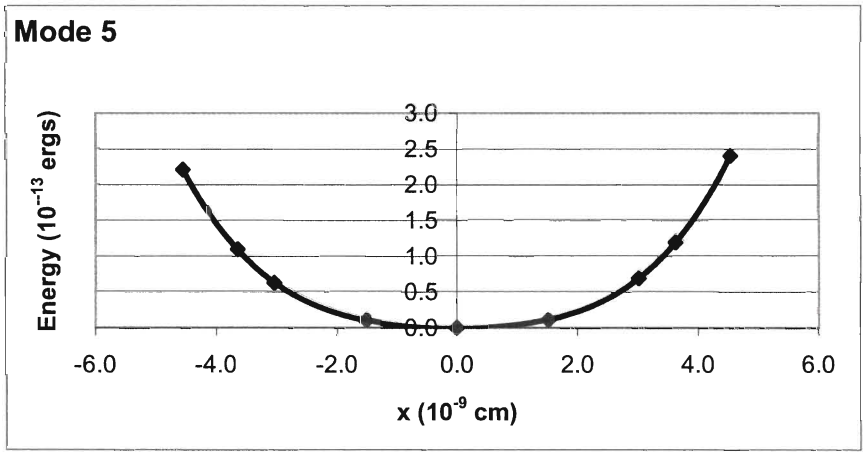

Figure 15. Water Dimer Vibrational Potential Map for In-Plane Bend. Polynomial: $y = 0.0034x^4 + 0.001x^3 + 0.042x^2 + 0.0005x - 0.0061$, $R^2 = 1$.

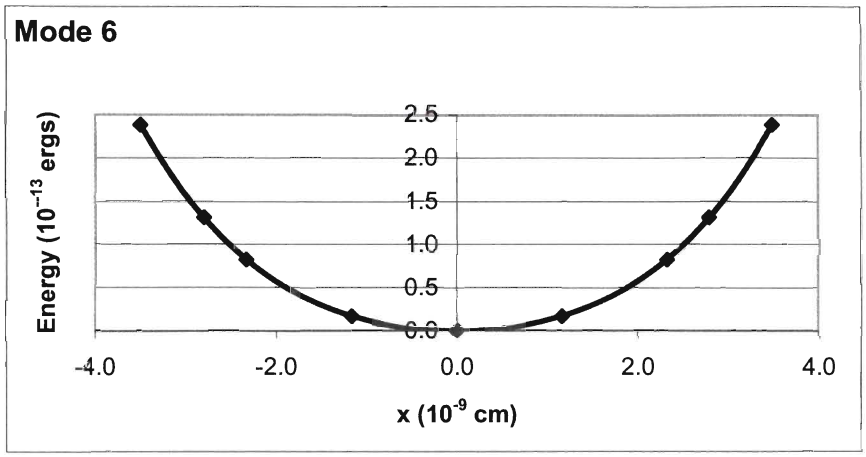

Figure 16. Water Dimer Vibrational Potential Map for Out-of-Plane Bend. Polynomial: $y = 0.0063x^4 + 7 \times 10^{-12}x^3 + 0.1193x^2 - 7 \times 10^{-11}x - 0.0061$, $R^2 = 1$.

It is possible to estimate the energy states for motions on the polynomial potential curves for each mode, by constructing a matrix representation of the Hamiltonian – kinetic and potential - in the harmonic oscillator basis. This matrix may be diagonalized directly, or the alternative "HEG" method [1] adapted by Shillady [2] may be employed. The HEG [98, 99] method requires the matrix for the q operator in a convenient basis; the harmonic oscillator basis seems natural here. Then the q matrix is diagonalized:

$$\left[T^{-1}\right][q][T] = \left[q_{diag}\right] \tag{7.3}$$

Next, the energy from the fitted polynomial $V(q)$ is evaluated at the specific values of the $\left[q_{diag}\right]$ matrix to give $\left[V_{diag}\right]$, and then the transformation is reversed (to "undiagonalize" $\left[V_{diag}\right]$) to obtain $V(q)$ in the original harmonic oscillator basis:

$$V(q) = [T]\left[V_{diag}\right]\left[T^{-1}\right] \tag{7.4}$$

Finally, $V(q)$ is added to the p^2 matrix (where p is the momentum / kinetic energy operator) to produce the approximate Hamiltonian matrix in the original harmonic

oscillator basis, and the Hamiltonian matrix is diagonalized to find the eigenvalues and eigenvectors (which provides the normal mode motions and their corresponding frequencies). This treatment is the polynomial-variational (HEG) method.

Table 38 shows a comparison of water dimer frequencies at the MP2 level for various methods. The harmonic frequencies were used to help assign mode descriptions when none were given by some authors. We assumed that the order of the harmonic mode motions (from lowest to highest frequency) should be the same as long as the basis sets used by all authors are of sufficient quality.

Looking at the intermolecular harmonic frequencies (modes 1-6), the counterpoise optimization/frequency treatment (this work) lowers these frequencies. Mode-specific polynomial fits to mapped vibrational potentials (this work) as described above (the soft mode component of the dual polynomial method) obtain frequencies that are comparable to those calculated by the VSCF methods (found in the GAMESS software) for modes 1-3. However, our frequencies are in much better agreement with experimental values than VSCF frequencies for intermolecular modes 4-6. Furthermore, our approach is much less expensive computationally than the VSCF methods.

Table 38. Summary of Water Dimer MP2 Frequencies Including Polynomial Fitting (in cm^{-1}).

Mode	Expt	Harmonic TZP [e]	VSCF [e]	CC-VSCF [e]	Harmonic 6-31+G(d,p) -CP-opt [g]	Dual Poly [g]	Poly-Var. (HEG) [h]	Barone [i]	Description [j]
1	88 [a]	142	545	419	102	433	552	78	PD torsion
2	103 [a]	161	414	309	129	237	225	122	PA wag
3	108 [a]	179	259	147	152	393	461	120	PA twist
4	143 [b]	191	451	409	170	186	655	150	Intermolec str
5	311 [c]	366	550	521	335	361	541	323	In-plane bend
6	523 [c]	674	769	732	596	623	788	525	Out-of-plane bend
7	1599 [c]	1618	1565	1564	1633	1620	1620	1608	PA OH bend
8	1616 [c]	1646	1612	1605	1650	1638	1637	1618	PD OH bend
9	3601 [d]	3799	3560	3565	3804	3677	3704	3599	PD sym OH str
10	3660 [d]	3874	3689	3647	3864	3776	3787	3666	PA sym OH str
11	3735 [d]	3982	3733	3745	3983	3953	3975	3772	PD asym OH str
12	3745 [d]	4005	3763	3724	4006	4099	4098	3779	PA asym OH str

[a] Reference [18], planar supersonic molecular beam expansion (terahertz laser vibration-rotation-tunneling spectroscopy), 5 K. [b] Reference [19], planar supersonic molecular beam expansion (terahertz laser vibration-rotation-tunneling spectroscopy), 5 K. [c] Reference [20], Neon matrix, 10 K. [d] Reference [21], molecular beam depletion spectroscopy with size selection by momentum transfer in scattering experiment (atoms under single collision conditions). [e] Reference [4], available in GAMESS software. [g] Dual method, this work: modes 7-12 calculated normally with the polynomial-perturbational method, intermolecular modes 1-6 derived from polynomial quadratic coefficients of mapped potentials as described above. [h] Reference [100], 50 basis HEG treatment. [i] Reference [20], using Barone's method [13] as found in Gaussian software. [j] When mode descriptions were not available for a given author, they are based on matching the order of that authors harmonic frequencies with those of an author who provided descriptions (in order to match all frequencies and descriptions between different authors).

Both the polynomial-variational (HEG) and VSCF methods strongly blue-shift frequencies relative to the harmonic values, while the cc-VSCF method moderates the effect. The most serious corrections to the VSCF values by cc-VSCF are found for the lowest frequencies.

For the high frequency, intramolecular vibrations the VSCF methods produce better frequencies in general than the polynomial-perturbational and polynomial-variational (HEG) methods, which do not red-shift frequencies as much as the VSCF methods. For all frequencies, compared with the polynomial-variational (HEG) approach, the VSCF methods tend to be in better agreement with measured values. However, the polynomial-variational (HEG) method is computationally much less expensive.

The method put forth by Barone [13] in the Gaussian computational software is the most sophisticated (involving multi-dimensional mode coupling and potential mapping) and time consuming of all. As can be seen by the computations of Bouteiller and Perchard [20], the results of Barone's approach are quite good, having the best agreement overall with experimental data of the methods presented in Table 38, especially for the low frequency intermolecular vibrations. Also, it always gives red-shifts from the harmonic frequencies. It is clearly the best treatment of the water dimer so far in terms of accuracy. Table 39 below further explores this method in different basis sets.

Table 39. Water Dimer Anharmonically Corrected Frequencies with Barone's Method [13] as found in Gaussian.

MP2/6-311G(d,p)		MP2/6-311+G(d,p)	
Harmonic	Barone	Harmonic	Barone
82	**-15**	133	75
144	**-20**	172	138
155	96	178	131
189	**166**	204	**142**
385	340	382	286
652	534	665	526
1657	1620	1640	1593
1703	1643	1664	1604
3835	3680	3808	3649
3892	3712	3875	3699
3984	3806	3975	3798
3999	3806	3989	3805

* Carl Trindle [private communication] - calculations conducted in this model at the MP2/6-311G(d,p) and MP2/6-311+G(d,p) levels without counterpoise corrections.

It is apparent that even Barone's method [13] can arrive at negative frequencies for some of the intermolecular modes. Table 40 provides counterpoise corrected results.

Table 40. Water Dimer Counterpoise-Corrected Anharmonic Frequencies with Barone's Method [13].

MP2/6-31+G(d,p) CP		PD=donor PA=acceptor	MP2/6-311+G(d,p) CP	
Harmonic	Anharmonic-G03	Mode	Harmonic	Anharmonic-G03
124	80	A" PA-rotn	114	56
137	107	A' PA-rotn	129	86
168	134	A" PD rotn	155	119
175	**130**	A' **diss**	156	**123**
341	285	A' H $\parallel$	307	268
598	488	A" H $\perp$	569	459
1634	1584	A' PA bend	1636	1591
1650	1596	A' PD bend	1655	1603
3801	3645	A' PD sstr	3826	3670
3860	3684	A'PA sstr	3880	3706
3979	3796	A' PD astr	3975	3797
4002	3812	A" PA astr	3995	3821

* Carl Trindle [private communication] - calculations with full CP corrections – both structure and frequencies incorporate counterpoise estimates of basis set superposition effects.

With or without corrections for BSSE, the anharmonically calculated inter-oxygen stretch, or cluster dissociation frequency (diss in Table 40), is very close that measured by Saykally [19]. Also, the anharmonically corrected frequencies are always red-shifted from the harmonic frequencies.

Multi-dimensional mode-coupling such as that found in Barone's method [13] would produce improved results, but this would also result in a geometric increase in the number of points needed to characterize the vibrations and in a correspondingly massive increase in computational time. The harmonic starting point is probably more appropriate for the intramolecular modes than it is for the intermolecular modes. Using enhanced model chemistries would probably not overturn that feature of the potential for the intermolecular vibrations (as is witnessed by the fact that the cc correction in cc-VSCF is large for the intermolecular modes and small for the intramolecular modes). A

complete departure from the harmonic oscillator basis may be necessary to obtain realistic frequencies for rovibrational modes (the lowest three modes in the case of the water dimer) which tend to have more rotational character than vibrational. Using sinusoidal potentials to model rovibrational modes could result in better matches with experimental data.

7.4 Comparison of Morse Method to Other Approaches

In Table 41 the Morse method developed in this project is compared to several different approaches from the literature. The intermolecular frequencies produced from the Morse method are in much better agreement with experimental values than the frequencies produced by the anharmonic methods found in GAMESS software (VSCF and cc-VSCF methods [4, 14, 15]), and the Morse method is much faster as well. However, the VSCF methods provide better intramolecular frequencies. VSCF [4] methods required the calculation of 4,320 single-point energies for the water dimer compared to only 24 for our custom-fitting Morse approach. On the basis of single-point energy calculations alone, our treatment is 180 times faster, and more so, because VSCF methods must then go on to make variational calculations and pair-wise mode interaction computations as well (cc-VSCF requires yet more time to arrive at corrections due to correlations between different vibrational states).

Table 41. Frequency Results for the Water Dimer from Various Methods (in cm^{-1}).

Mode	Expt	VSCF [e]	cc-VSCF [e]	Scott-Radom Scaling [f]	Muñoz-Caro / Niño [g]	Custom-Fit Morse [h]	Barone [i]	Description [j]
1	88 [a]	545	419	116	105	102	78	PD torsion
2	103 [a]	414	309	145	NA	128	122	PA wag
3	108 [a]	259	147	145	158	152	120	PA twist
4	143 [b]	451	409	159	153	168	150	Intermolec str
5	311 [c]	550	521	310	371	332	323	In-plane bend
6	523 [c]	769	732	573	639	596	525	Out-of-plane bend
7	1599 [c]	1565	1564	1694	1654	1630	1608	PA OH bend
8	1616 [c]	1612	1605	1723	1680	1648	1618	PD OH bend
9	3601 [d]	3560	3565	3674	3548	3669	3599	PD sym OH str
10	3660 [d]	3689	3647	3709	3803	3768	3666	PA sym OH str
11	3735 [d]	3733	3745	3789	3905	3899	3772	PD asym OH str
12	3745 [d]	3763	3724	3808	3769	4006	3779	PA asym OH str

[a] Reference [18], planar supersonic molecular beam expansion (terahertz laser vibration-rotation-tunneling spectroscopy), 5 K. [b] Reference [19], planar supersonic molecular beam expansion (terahertz laser vibration-rotation-tunneling spectroscopy), 5 K. [c] Reference [20], Neon matrix, 10 K. [d] Reference [21], molecular beam depletion spectroscopy with size selection by momentum transfer in scattering experiment (atoms under single collision conditions). [e] Reference [4], variational method as found in GAMESS software. [f] Harmonic frequencies scaled using Scott and Radom's 1.0127 factor for low-frequency, fundamental vibrations and for intermolecular modes (lowest eight modes) and the 0.9496 factor for high-frequency, fundamental vibrations (highest four modes), MP2/6-311G(d,p), Reference [17] [g] Reference [29], collected from various treatments. [h] Frequencies from custom fit of Morse potentials as described in this work, MP2/6-31+G(d,p)-CP-opt. [i] Reference [20], using Barone's method [13] as found in Gaussian software. [j] When mode descriptions were not available for a given author, they are based on matching the order of that authors harmonic frequencies with those of an author who provided descriptions (in order to match all frequencies and descriptions between different authors).

Relative to Scott and Radom scaling [17], better experimental agreement for the lower vibrations of both the intramolecular and intermolecular modes are achieved by custom-fitting a Morse potential.

The frequencies of Muñoz-Caro and Niño [29] are arrived at by a collection of methods involving polynomial-fitting to potential maps usually requiring five times as

many single-point energies (as required by our Morse method) beyond the equilibrium energy for a given frequency, coupled with multiple geometry re-optimizations (adding more computational expense) for the same frequency, some of which were enhanced by scaling. These elaborate treatments consume much more time than our Morse method which uses a custom-fitting approach that eliminates the need for so many single-point energies to map the potential, and our treatment optimizes the geometry only once (not multiple times for each mode). Despite the lesser sophistication of our method, our Morse frequencies agree better with the experimental results for 75 % of the modes, and this is done with a single, much faster method.

Our approach does not compete, in terms of accuracy, with the multi-dimensional coupling frequency technique [13] found in Gaussian software. However, our treatment retains a huge advantage in speed over this method, while delivering reasonably good accuracy: on the basis of single-point energy calculations alone, our Morse method is at least about 1,000 times faster than Barone's method.

7.5 Conclusions

The dual polynomial approach of combining the polynomial-perturbational method (for intramolecular modes) with derived frequencies from polynomial quadratic coefficients of mapped potentials (for intermolecular vibrations), gives intramolecular frequencies that are in good agreement with measured values and are improved estimates compared to those from the harmonic approximation (although not quite as accurate as those from the Morse method). The intermolecular modes of the dual polynomial method are of VSCF quality or better (but not as good as harmonic values) and all estimates are

positive. Also, the dual method is much faster than VSCF methods and gives bending mode predictions for water which were better than the corresponding Morse frequencies.

For the low-frequency modes the polynomial-perturbational method is not appropriate; estimated frequencies are meaningless (negative). The polynomial-variational (HEG) method, using polynomial mode-specific potentials, did not suffer from this difficulty and produced results closely comparable with the much more demanding VSCF methods. These frequencies predicted by VSCF and the polynomial-variational (HEG) methods are much larger than either the harmonic estimates or the observed values.

The Morse method produces intramolecular frequencies that agree well with experimental values and that are better than those of the dual polynomial and harmonic approximations. The intermolecular predictions are about the same as or slightly better than the harmonic frequencies. The scaling factors of Scott and Radom [17] are limited in that they are based on an "average" factor derived from a small set of "training" frequencies from a limited set of chemical systems. Our Morse method, however, takes into account each individual frequency, custom-fitting the potential of each vibration for any frequency and any chemical system. Furthermore, the scaling factors [17] are based on molecular frequencies and not on those from any complexes, which means that intermolecular frequencies have not been incorporated to enhance the scaling factors, and effects due to hydrogen bonding have been omitted as well.

Our custom-fitting Morse approach is much faster than the multi-point potential mapping/multiple geometry optimization, Taylor series methods of Muñoz-Caro and Niño [29] and more accurate as well. Barone's [13] perturbation/multi-dimensional

mode-coupling treatment provides excellent accuracy but is much more computationally expensive than the Morse method. VSCF [4, 14, 15] methods produce better intramolecular frequencies than the Morse method but our custom-fitting Morse technique gives much improved intermolecular frequencies and is computationally much faster.

CHAPTER VIII. Conclusions

This work presents computational models for the gas phase hydrogen bonded systems water-water, methanol-water, water-methanol, and methanol-methanol. Counterpoise optimizations in conjunction with full counterpoise treatment of single-point energies and frequencies, was shown to give structures, energies, and spectra of comparable quality to those achieved by methods employing larger basis sets, standard optimizations, and at most single-point counterpoise estimates of basis set superposition error (BSSE can be of the same order of magnitude as binding energies in weakly interacting systems). Our results for hydrogen bonding were in agreement with those in the literature, where the vast majority of sources report that the strongest hydrogen bonds of the systems studied in this work are to be found in the methanol dimer and the water-methanol complex, and the weakest hydrogen bonding takes place between the water dimer and the methanol-water complex.

Estimates of vibrational frequencies are generally limited to harmonic estimates derived from the second derivatives of the energy near an energy minimum. These estimates are generally in disagreement with experimental measurements, owing in part to neglect of anharmonicity. Whereas the harmonic calculation assumes that every normal mode is associated with a simple quadratic potential $V\left(q_j\right)=\frac{1}{2}k_j q_j^2$, we computed estimates of the energy at several points along each vibrational mode, $E\left(f_{ik}q_k\right)$. These points can define either a Morse fit to each mode's potential or a more general polynomial representation. Vibrational energy eigenvalues of the polynomial

potential can be estimated by perturbation theory or by variational treatment in a basis. A second order perturbational treatment for calculating vibrations was designed and tested. For very low frequency intermolecular modes this polynomial-perturbational method is not useful; the variational approach is still effective. Compared with VSCF [4, 14, 15] techniques, the dual polynomial method provided improved prediction of intermolecular modes on the whole, and the polynomial-variational (HEG) method afforded comparable soft-mode results to VSCF treatments in general. Furthermore, both dual polynomial and polynomial-varitaional (HEG) methods retain a large speed advantage over VSCF methods.

The Morse method gives much improved calculations of intermolecular frequencies compared to VSCF methods [4, 14, 15] (GAMESS software) as well as intramolecular vibrational predictions that are better than the harmonic model. The custom-fitting Morse technique is applicable to all frequencies and chemical systems, and so does not face the limitations of scaling factors [17] and has been shown to provide greater accuracy and speed versus methods using multi-point/multiple optimization potential mapping [29].

The Morse treatment provides good accuracy and is very fast compared with available algorithms for estimating anharmonicity as implemented in software from GAMESS and Gaussian. Our custom-fitting Morse technique will prove beneficial for aiding in the interpretation of experimental spectra and in the making of spectral transition predictions where experimental results are difficult to obtain. Solvation studies and thermodynamic predictions involving large clusters with many different conformations would especially benefit from the speed of this method.

Literature Cited

Literature Cited

[1] C. A. Holden, S. S. Hunnicutt, R. Sanchez-Ponce, J. M. Craig, S. C. Rutan, "Study of Complexation in Methanol/Water Mixtures by Infrared and Raman Spectroscopy and Multivariate Curve Resolution - Alternating Least-Squares Analysis" Applied Spectroscopy 57 (2003) 483.

[2] D. D. Shillady, J. Craig, S. Rutan, B. J. Rao, "Explicitly Correlated SCF Study of Anharmonic Vibrations in $(H_2O)_2$" International Journal of Quantum Chemistry 90 (2002) 1414.

[3] Pauling L, Jr. E. Wilson, Introduction to Quantum Mechanics with Applications to Chemistry. Dover Publications, Inc., New York, 1963.

[4] G. M. Chaban, J. O. Jung, R. B. Gerber, "Anharmonic Vibrational Spectroscopy of Hydrogen-Bonded Systems Directly Computed From Ab Initio Potential Surfaces: $(H_2O)_n$, N=2, 3; $Cl^-(H_2O)_n$, n=1, 2; $H^+(H_2O)_n$, n=1, 2; H_2O-CH_3OH" Journal of Physical Chemistry A 104 (2000) 2772.

[5] L. A. Curtiss, M. Blander, "Thermodynamic Properties of Gas-Phase Hydrogen-Bonded Complexes" Chemical Reviews 88 (1988) 827.

[6] R. K. Thomas, "Hydrogen Bonding in Gas Phase - Thermodynamic Properties of Hydrogen Fluoride-Ether Complexes and Their Far Infrared Spectra" Proceedings of the Royal Society of London Series A-Mathematical and Physical Sciences 322 (1971) 137.

[7] H. A. Benesi, J. H. Hildebrand, Journal of the American Chemical Society, 71, (1949), 2703.

[8] A. S. Pine, B. J. Howard, "Hydrogen-Bond Energies of the HF and HCl Dimers From Absolute Infrared Intensities" Journal of Chemical Physics 84 (1986) 590.

[9] A. C. Legon, D. J. Millen, S. C. Rogers, "Spectroscopic Investigations of Hydrogen-Bonding Interactions in the Gas-Phase .1. the Determination of the Geometry, Dissociation-Energy, Potential Constants and Electric-Dipole Moment of the Hydrogen-Bonded Heterodimer HCN...HF From Its Microwave Rotational Spectrum" Proceedings of the Royal Society of London Series A-Mathematical Physical and Engineering Sciences 370 (1980) 213.

[10] A. C. Legon, D. J. Millen, H. M. North, "Dissociation-Energies of the Hydrogen-Bonded Dimers =HF Ch_3CN, HCCCN Determined by Rotational Spectroscopy" Journal of Chemical Physics 86 (1987) 2530.

[11] J. A. Pople, H. B. Schlegel, R. Krishnan, D. J. Defrees, J. S. Binkley, M. J. Frisch, R. A. Whiteside, R. F. Hout, W. J. Hehre, "Molecular-Orbital Studies of Vibrational Frequencies" International Journal of Quantum Chemistry (1981) 269.

[12] J. A. Pople, A. P. Scott, M. W. Wong, L. Radom, "Scaling Factors for Obtaining Fundamental Vibrational Frequencies and Zero-Point Energies From HF/6-31G* and MP2/6-31G* Harmonic Frequencies" Israel Journal of Chemistry 33 (1993) 345.

[13] V. Barone, "Anharmonic Vibrational Properties by a Fully Automated Second-Order Perturbative Approach" Journal of Chemical Physics 122 (2005).

[14] J. O. Jung, R. B. Gerber, "Vibrational Wave Functions and Spectroscopy of $(H_2O)_n$, n=2, 3, 4, 5: Vibrational Self-Consistent Field With Correlation Corrections" Journal of Chemical Physics 105 (1996) 10332.

[15] G. M. Chaban, J. O. Jung, R. B. Gerber, "Ab Initio Calculation of Anharmonic Vibrational States of Polyatomic Systems: Electronic Structure Combined With Vibrational Self-Consistent Field" Journal of Chemical Physics 111 (1999) 1823.

[16] R. Burcl, S. Carter, N. C. Handy, "On the Representation of Potential Energy Surfaces of Polyatomic Molecules in Normal Coordinates: II. Parameterisation of the Force Field" Chemical Physics Letters 373 (2003) 357.

[17] A. P. Scott, L. Radom, "Harmonic Vibrational Frequencies: An Evaluation of Hartree-Fock, Moller-Plesset, Quadratic Configuration Interaction, Density Functional Theory, and Semiempirical Scale Factors" Journal of Physical Chemistry 100 (1996) 16502.

[18] L. B. Braly, K. Liu, M. G. Brown, F. N. Keutsch, R. S. Fellers, R. J. Saykally, "Terahertz Laser Spectroscopy of the Water Dimer Intermolecular Vibrations. II. $(H2O)_2$" Journal of Chemical Physics 112 (2000) 10314.

[19] F. N. Keutsch, L. B. Braly, M. G. Brown, H. A. Harker, P. B. Petersen, C. Leforestier, R. J. Saykally, "Water Dimer Hydrogen Bond Stretch, Donor Torsion Overtone, and "in-Plane Bend" Vibrations" Journal of Chemical Physics 119 (2003) 8927.

[20] Y. Bouteiller, J. P. Perchard, "The Vibrational Spectrum of (H2O)(2): Comparison Between Anharmonic Ab Initio Calculations and Neon Matrix Infrared Data Between 9000 and 90 cm^{-1}" Chemical Physics 305 (2004) 1.

[21] U. Buck, F. Huisken, "Infrared Spectroscopy of Size-Selected Water and Methanol Clusters" Chemical Reviews 100 (2000) 3863.

[22] T. R. Dyke, K. M. Mack, J. S. Muenter, "Structure of Water Dimer From Molecular-Beam Electric Resonance Spectroscopy" Journal of Chemical Physics 66 (1977) 498.

[23] S. Wuelfert, D. Herren, S. Leutwyler, "Supersonic Jet Cars Spectra of Small Water Clusters" Journal of Chemical Physics 86 (1987) 3751.

[24] Z. S. Huang, R. E. Miller, "High-Resolution Near-Infrared Spectroscopy of Water Dimer" Journal of Chemical Physics 91 (1989) 6613.

[25] G. A. Yeo, T. A. Ford, "The Combined Use of Abinitio Molecular-Orbital Theory and Matrix-Isolation Infrared-Spectroscopy in the Study of Molecular-Interactions" Structural Chemistry 3 (1992) 75.

[26] L. Fredin, B. Nelander, G. Ribbegard, "IR-Spectrum of Water Dimer in Solid Nitrogen .1. Assignment and Force-Constant Calculations" Journal of Chemical Physics 66 (1977) 4065.

[27] R. D. Amos, "Structures, Harmonic Frequencies and Infrared Intensities of the Dimers of H2O and H2S" Chemical Physics 104 (1986) 145.

[28] R. M. Bentwood, A. J. Barnes, W. J. Orvillethomas, "Studies of Intermolecular Interactions by Matrix-Isolation Vibrational Spectroscopy - Self-Association of Water" Journal of Molecular Spectroscopy 84 (1980) 391.

[29] C. Muñoz-Caro, A. Niño, "Effect of Anharmonicities on the Thermodynamic Properties of the Water Dimer" Journal of Physical Chemistry A 101 (1997) 4128.

[30] M. E. Dunn, T. M. Evans, K. N. Kirschner, G. C. Shields, "Prediction of Accurate Anharmonic Experimental Vibrational Frequencies for Water Clusters, $(H_2O)_n$, n=2-5" Journal of Physical Chemistry A 110 (2006) 303.

[31] G. M. Chaban, J. O. Jung, R. B. Gerber, "Anharmonic Vibrational Spectroscopy of Hydrogen-Bonded Systems Directly Computed From Ab Initio Potential Surfaces: $(H_2O)_n$, n=2, 3; $Cl^-(H2O)_n$, n=1, 2; $H^+(H2O)_n$, n=1, 2; H_2O-CH_3OH" Journal of Physical Chemistry A 104 (2000) 2772.

[32] N. Bakkas, Y. Bouteiller, A. Loutellier, J. P. Perchard, S. Racine, "The Water-Methanol Complexes - Matrix Induced Structural Conversion of the 1-1 Species" Chemical Physics Letters 232 (1995) 90.

[33] N. Bakkas, Y. Bouteiller, A. Loutellier, J. P. Perchard, S. Racine, "The Water-Methanol Complexes .1. A Matrix-Isolation Study and An Ab-Initio Calculation on the 1-1 Species" Journal of Chemical Physics 99 (1993) 3335.

[34] S. Carter, N. C. Handy, "A Theoretical Determination of the Rovibrational Energy-Levels of the Water Molecule" Journal of Chemical Physics 87 (1987) 4294.

[35] B. M. Tissue, 2000, http://www.chem.vt.edu/chem-ed/quantum/diatomic.html.

[36] Eyring H, Walter J: Kimball G, Quantum Chemistry. John Wiley & Sons, Inc., New York, 1967.

[37] N. R. Zhang, D. D. Shillady, "Ab-Initio Equilibrium-Constants for H_2O-H_2O and H_2O-CO_2" Journal of Chemical Physics 100 (1994) 5230.

[38] L. Kiran, W. Coleman, Journal of Chemical Education, Microsoft Excel Spreadsheet, 2005, http://jchemed.chem.wisc.edu/JCEDLib/WebWare/collection /reviewed/JCE2005p1263_2WW/index.html.

[39] I. N. Levine, Molecular Spectroscopy. John Wiley & Sons, Inc, New York, 1975.

[40] M. Fowler, 2002, http://galileo.phys.virginia.edu/classes/751.mf1i.fall02 /SimpleHarmOsc.htm.

[41] M. B. Day, K. N. Kirschner, G. C. Shields, "Global Search for Minimum Energy $(H_2O)_n$ Clusters, n=3-5" Journal of Physical Chemistry A 109 (2005) 6773.

[42] Y. Miller, G. M. Chaban, R. B. Gerber, "Ab Initio Vibrational Calculations for H_2SO_4 and H_2SO_4 • H2O: Spectroscopy and the Nature of the Anharmonic Couplings" Journal of Physical Chemistry A 109 (2005) 6565.

[43] P. Sinha, S. E. Boesch, C. M. Gu, R. A. Wheeler, A. K. Wilson, "Harmonic Vibrational Frequencies: Scaling Factors for HF, B3LYP, and MP2 Methods in Combination With Correlation Consistent Basis Sets" Journal of Physical Chemistry A 108 (2004) 9213.

[44] Y. Bouteiller, J. P. Perchard, "The Vibrational Spectrum of $(H_2O)_2$: Comparison Between Anharmonic Ab Initio Calculations and Neon Matrix Infrared Data Between 9000 and 90 cm^{-1}" Chemical Physics 305 (2004) 1.

[45] M. E. Alikhani, V. Barone, "Hydrogen-Bonding Between the Hydrogen Peroxide Molecule and the Hydroperoxy Radical (H_2O_2-HO_2): the Global Minimum" Chemical Physics Letters 391 (2004) 134.

[46] H. M. Lee, P. Tarakeshwar, J. Park, M. R. Kolaski, Y. J. Yoon, H. B. Yi, W. Y. Kim, K. S. Kim, "Insights into the Structures, Energetics, and Vibrations of Monovalent Cation-(Water)(1-6) Clusters" Journal of Physical Chemistry A 108 (2004) 2949.

[47] D. D. Shillady, J. Craig, S. Rutan, "Explicitly Correlated SCF Study of Small Hydrides" International Journal of Quantum Chemistry 85 (2001) 520.

[48] L. Ojamae, K. Hermansson, "Ab-Initio Study of Cooperativity in Water Chains - Binding-Energies and Anharmonic Frequencies" Journal of Physical Chemistry 98 (1994) 4271.

[49] K. S. Kim, B. J. Mhin, U. S. Choi, K. Lee, "Abinitio Studies of the Water Dimer Using Large Basis-Sets - the Structure and Thermodynamic Energies" Journal of Chemical Physics 97 (1992) 6649.

[50] M. M. Probst, K. Hermansson, "On Frequency-Shifts in OH Stretching Vibrations of Hydrated Cations" Journal of Chemical Physics 96 (1992) 8995.

[51] K. Ohno, M. Okimura, N. Akai, Y. Katsumoto, "The Effect of Cooperative Hydrogen Bonding on the OH Stretching-Band Shift for Water Clusters Studied by Matrix-Isolation Infrared Spectroscopy and Density Functional Theory" Physical Chemistry Chemical Physics 7 (2005) 3005.

[52] K. Diri, E. M. Myshakin, K. D. Jordan, "On the Contribution of Vibrational Anharmonicity to the Binding Energies of Water Clusters" Journal of Physical Chemistry A 109 (2005) 4005.

[53] J. P. Perchard, "Anharmonicity and Hydrogen Bonding. III. Analysis of the Near Infrared Spectrum of Water Trapped in Argon Matrix" Chemical Physics 273 (2001) 217.

[54] J. P. Perchard, "Anharmonicity and Hydrogen Bonding II - A Near Infrared Study of Water Trapped in Nitrogen Matrix" Chemical Physics 266 (2001) 109.

[55] J. P. Perchard, Z. Mielke, "Anharmonicity and Hydrogen Bonding I. A Near-Infrared Study of Methanol Trapped in Nitrogen and Argon Matrices" Chemical Physics 264 (2001) 221.

[56] M. J. T. Jordan, J. E. Del Bene, "Unraveling Environmental Effects on Hydrogen-Bonded Complexes: Matrix Effects on the Structures and Proton-Stretching Frequencies of Hydrogen-Halide Complexes With Ammonia and Trimethylamine" Journal of the American Chemical Society 122 (2000) 2101.

[57] J. E. Del Bene, M. J. T. Jordan, "Vibrational Spectroscopy of the Hydrogen Bond: an Ab Initio Quantum-Chemical Perspective" International Reviews in Physical Chemistry 18 (1999) 119.

[58] P. Carbonniere, V. Barone, "Performances of Different Density Functionals in the Computation of Vibrational Spectra Beyond the Harmonic Approximation" Chemical Physics Letters 399 (2004) 226.

[59] H. M. Cho, S. J. Singer, "Correlation Function Quantum Monte Carlo Study of the Excited Vibrational States of $H_5O_2^+$" Journal of Physical Chemistry A 108 (2004) 8691.

[60] V. Barone, "Accurate Vibrational Spectra of Large Molecules by Density Functional Computations Beyond the Harmonic Approximation: The Case of Azabenzenes" Journal of Physical Chemistry A 108 (2004) 4146.

[61] V. Barone, "Vibrational Zero-Point Energies and Thermodynamic Functions Beyond the Harmonic Approximation" Journal of Chemical Physics 120 (2004) 3059.

[62] V. Barone, "Vibrational Spectra of Large Molecules by Density Functional Computations Beyond the Harmonic Approximation: the Case of Pyrrole and Furan" Chemical Physics Letters 383 (2004) 528.

[63] D. P. Schofield, H. G. Kjaergaard, "Calculated OH-Stretching and HOH-Bending Vibrational Transitions in the Water Dimer" Physical Chemistry Chemical Physics 5 (2003) 3100.

[64] R. A. Wheeler, H. T. Dong, S. E. Boesch, "Quasiharmonic Vibrations of Water, Water Dimer, and Liquid Water From Principal Component Analysis of Quantum or QM/MM Trajectories" Chemphyschem 4 (2003) 382.

[65] G. M. Florio, T. S. Zwier, E. M. Myshakin, K. D. Jordan, E. L. Sibert, "Theoretical Modeling of the OH Stretch Infrared Spectrum of Carboxylic Acid Dimers Based on First-Principles Anharmonic Couplings" Journal of Chemical Physics 118 (2003) 1735.

[66] D. D. Shillady, J. Craig, S. Rutan, B. J. Rao, "Explicitly Correlated SCF Study of Anharmonic Vibrations in $(H_2O)_2$" International Journal of Quantum Chemistry 90 (2002) 1414.

[67] C. Trindle, D. Shillady, J. Craig, S. Rutan, "Dye Probes of Nanoclusters in Liquids" Journal of Cluster Science 12 (2001) 473.

[68] M. V. Vener, O. Kuhn, J. Sauer, "The Infrared Spectrum of the O•••H•••O Fragment of $H_5O_2^+$: Ab Initio Classical Molecular Dynamics and Quantum 4D Model Calculations" Journal of Chemical Physics 114 (2001) 240.

[69] N. J. Wright, R. B. Gerber, D. J. Tozer, "Direct Calculation of Anharmonic Vibrational States of Polyatomic Molecules Using Density Functional Theory: Spectroscopic Tests of Recently Developed Functionals" Chemical Physics Letters 324 (2000) 206.

[70] N. J. Wright, R. B. Gerber, "Direct Calculation of Anharmonic Vibrational States of Polyatomic Molecules Using Potential Energy Surfaces Calculated From Density Functional Theory" Journal of Chemical Physics 112 (2000) 2598.

[71] M. V. Vener, J. Sauer, "Quantum Anharmonic Frequencies of the O•••H•••O Fragment of the $H_5O_2^+$ Ion: a Model Three-Dimensional Study" Chemical Physics Letters 312 (1999) 591.

[72] P. Hobza, O. Bludsky, S. Suhai, "Reliable Theoretical Treatment of Molecular Clusters: Counterpoise-Corrected Potential Energy Surface and Anharmonic

Vibrational Frequencies of the Water Dimer" Physical Chemistry Chemical Physics 1 (1999) 3073.

[73] J. O. Jung, R. B. Gerber, "Vibrational Wave Functions and Spectroscopy of $(H_2O)_n$, n=2, 3, 4, 5: Vibrational Self-Consistent Field With Correlation Corrections" Journal of Chemical Physics 105 (1996) 10332.

[74] H. M. Lee, S. B. Suh, J. Y. Lee, P. Tarakeshwar, K. S. Kim, "Structures, Energies, Vibrational Spectra, and Electronic Properties of Water Monomer to Decamer" Journal of Chemical Physics 112 (2000) 9759.

[75] C. J. Tsai, K. D. Jordan, "Monte-Carlo Simulation of $(H_2O)_8$ - Evidence for A Low-Energy S4 Structure and Characterization of the Solid Reversible Liquid Transition" Journal of Chemical Physics 95 (1991) 3850.

[76] H. M. Lee, S. B. Suh, K. S. Kim, "Structures, Energies, and Vibrational Spectra of Water Undecamer and Dodecamer: An Ab Initio Study" Journal of Chemical Physics 114 (2001) 10749.

[77] Unpublished work, J. M. Craig, D. D. Shillady, Virginia Commonwealth University, 2007.

[78] G. R. Low, H. G. Kjaergaard, "Calculation of OH-Stretching Band Intensities of the Water Dimer and Trimer" Journal of Chemical Physics 110 (1999) 9104.

[79] C. Trindle, D. Shillady, J. Craig, S. Rutan, "Dye Probes of Nanoclusters in Liquids" Journal of Cluster Science 12 (2001) 473.

[80] S. B. Suh, H. M. Lee, J. Kim, J. Y. Lee, K. S. Kim, "Vibrational Spectra and Electron Detachment Energy of the Anionic Water Hexamer" Journal of Chemical Physics 113 (2000) 5273.

[81] R. Krishnan, J. S. Binkley, R. Seeger, J. A. Pople, "Self-Consistent Molecular-Orbital Methods .20. Basis Set for Correlated Wave-Functions" Journal of Chemical Physics 72 (1980) 650.

[82] J. Foresman, A. Frisch, Exploring Chemistry with Electronic Structure Methods. Gaussian, Inc, Pittsburgh, PA, 1996.

[83] F. Jensen, Introduction to Computational Chemistry. John Wiley & Sons Ltd, Chichester, West Sussex, England, 1999.

[84] Trindle C., University of Virginia, personal communication, 2007.

[85] L. A. Curtiss, D. J. Frurip, M. Blander, "Studies of Molecular Association in H_2O and D_2O Vapors by Measurement of Thermal-Conductivity" Journal of Chemical Physics 71 (1979) 2703.

[86] S. Tsuzuki, T. Uchimaru, K. Matsumura, M. Mikami, K. Tanabe, "Effects of Basis Set and Electron Correlation on the Calculated Interaction Energies of Hydrogen Bonding Complexes: MP2/cc-PV5Z Calculations of H_2O-MeOH, H_2O-Me_2O, H_2O-H_2CO, MeOH-MeOH, and HCOOH-HCOOH Complexes" Journal of Chemical Physics 110 (1999) 11906.

[87] N. Goldman, R. S. Fellers, M. G. Brown, L. B. Braly, C. J. Keoshian, C. Leforestier, R. J. Saykally, "Spectroscopic Determination of the Water Dimer Intermolecular Potential-Energy Surface" Journal of Chemical Physics 116 (2002) 10148.

[88] B. S. Jursic, "Study of the Water-Methanol Dimer With Gaussian and Complete Basis Set Ab Initio, and Density Functional Theory Methods" Journal of Molecular Structure-Theochem 466 (1999) 203.

[89] K. N. Kirschner, R. J. Woods, "Quantum Mechanical Study of the Nonbonded Forces in Water-Methanol Complexes" Journal of Physical Chemistry A 105 (2001) 4150.

[90] M. Masella, J. P. Flament, "Relation Between Cooperative Effects in Cyclic Water, Methanol/Water, and Methanol Trimers and Hydrogen Bonds in Methanol/Water, Ethanol/Water, and Dimethylether/Water Heterodimers" Journal of Chemical Physics 108 (1998) 7141.

[91] E. E. Fileti, S. Canuto, "Calculated Infrared Spectra of Hydrogen-Bonded Methanol-Water, Water-Methanol, and Methanol-Methanol Complexes" International Journal of Quantum Chemistry 104 (2005) 808.

[92] A. Bleiber, J. Sauer, "The Vibrational Frequency of the Donor OH Group in the H-Bonded Dimers of Water, Methanol and Silanol - Ab-Initio Calculations Including Anharmonicities" Chemical Physics Letters 238 (1995) 243.

[93] P. A. Stockman, G. A. Blake, F. J. Lovas, R. D. Suenram, "Microwave Rotation-Tunneling Spectroscopy of the Water-Methanol Dimer: Direct Structural Proof for the Strongest Bound Conformation" Journal of Chemical Physics 107 (1997) 3782.

[94] R. Vargas, J. Garza, R. A. Friesner, H. Stern, B. P. Hay, D. A. Dixon, "Reply to Comment on "Strength of the N-H•••O=C Bonds in Formamide and N-Methylacetamide Dimers"" Journal of Physical Chemistry A 109 (2005) 6991.

[95] M. W. Feyereisen, D. Feller, D. A. Dixon, "Hydrogen Bond Energy of the Water Dimer" Journal of Physical Chemistry 100 (1996) 2993.

[96] U. Buck, F. Huisken, "Infrared Spectroscopy of Size-Selected Water and Methanol Clusters" Chemical Reviews 100 (2000) 3863.

[97] N. Seurre, J. Sepiol, F. Lahmani, A. Zehnacker-Rentien, K. Le Barbu-Debus, "Vibrational Study of the S-0 and S-1 States of 2-Naphthyl-1-Ethanol/$(Water)_2$ and 2-Naphthyl-1-Ethanol/$(Methanol)_2$ Complexes by IR/UV Double Resonance Spectroscopy" Physical Chemistry Chemical Physics 6 (2004) 4658.

[98] D. O. Harris, G. G. Engerholm, W. D. Gwinn, "Calculation of Matrix Elements for 1-Dimensional Quantum-Mechanical Problems and Application to Anharmonic Oscillators" Journal of Chemical Physics 43 (1965) 1515.

[99] E. Yurtsever, O. Yilmaz, D. D. Shillady, "Sturmian Basis Matrix Solution of Vibrational Potentials" Chemical Physics Letters 85 (1982) 111.

[100] Unpublished work, D. Shillady, Virginia Commonwealth University, Trindle C, University of Virginia, 2007.

APPENDIX

A.1 First and Second Order Perturbation Theory (Expanded Formalism)

A.1.1 First Order Correction

Let us suppose that we have a vibrational system whose energy and wavefunction are unknown, as given by the equation

$$H\psi = E\psi \tag{A.1}$$

Suppose also that we have a vibrational system that has already been solved, where n is the ground state

$$H^0\psi_n^0 = E_n^0\psi_n^0 \tag{A.2}$$

This is our reference system. Next, we define a perturbation of the reference system and write the components of the system to be solved in terms perturbed reference system as follows. For the Hamiltonian, this is

$$H = H^{(0)} + \lambda V \quad \text{where} \lim_{\lambda \to 0} H = H^0 \tag{A.3}$$

Here the reference Hamiltonian (0^{th} order) is perturbed by adding the quantity λV, the perturbation. λ is a coefficient that determines the size of the perturbation. Similarly, to define the unknown wavefunction in terms of the perturbed reference wave function we have

$$\psi_n = \psi_n^{(0)} + \lambda\psi_n^{(1)} + \lambda^2\psi_n^{(2)} + \lambda^3\psi_n^{(3)} + \ldots \text{ where } \lim_{\lambda\to 0}\psi_n = \psi_n^{(0)} \tag{A.4}$$

Likewise for the energy

$$E_n = E_n^{(0)} + \lambda E_n^{(1)} + \lambda^2 E_n^{(2)} + \lambda^3 E_n^{(3)} + \ldots \tag{A.5}$$

Now substituting the above expressions for H, Ψ_n, and E_n into the system that we wish solve

$$H\psi_n - E_n\psi_n = 0 \tag{A.6}$$

gives a power series. Collecting like terms according to the power of λ we have

$$(H^{(0)}\psi_n^{(0)} - E_n^{(0)}\psi_n^{(0)})\lambda^0 + (H^{(0)}\psi_n^{(1)} + V\psi_n^{(0)} - E_n^{(0)}\psi_n^{(1)} - E_n^{(1)}\psi_n^{(0)})\lambda$$
$$+(H^{(0)}\psi_n^{(2)} + V\psi_n^{(1)} - E_n^{(0)}\psi_n^{(2)} - E_n^{(1)}\psi_n^{(1)} - E_n^{(2)}\psi_n^{(0)})\lambda^2 + \ldots = 0 \tag{A.7}$$

As we are only interested in the terms through the second order (for a second order perturbative treatment), we will ignore terms with a higher power of λ. In order for the equation to be true, each term must equal zero. This produces

$$(H^{(0)}\psi_n^{(0)} - E_n^{(0)}\psi_n^{(0)}) = 0 \tag{A.8}$$

$$(H^{(0)}\psi_n^{(1)} + V\psi_n^{(0)} - E_n^{(0)}\psi_n^{(1)} - E_n^{(1)}\psi_n^{(0)}) = 0 \tag{A.9}$$

$$(H^{(0)}\psi_n^{(2)} + V\psi_n^{(1)} - E_n^{(0)}\psi_n^{(2)} - E_n^{(1)}\psi_n^{(1)} - E_n^{(2)}\psi_n^{(0)}) = 0 \tag{A.10}$$

Taking a look at the first order equation and rearranging gives

$$(H^{(0)} - E_n^{(0)})\psi_n^{(1)} = (E_n^{(1)} - V)\psi_n^{(0)} \tag{A.11}$$

Now $\Psi_n^{(1)}$ is the first order correction to the wavefunction and can be defined in terms of the sum of the unperturbed wavefunctions of all states (other than the n^{th} state, due to orthogonality) as follows

$$\psi_n^{(1)} = \sum_{n \neq k} a_{nk}\psi_k^{(0)} \tag{A.12}$$

where each a is the respective coefficient of mixing for each $\Psi_k^{(0)}$. Substituting the right hand of equation (A.12) into where $\Psi_n^{(1)}$ appears in the first order equation (equation (A.9)) produces

$$(H^{(0)} - E_n^{(0)})\sum_{k \neq n} a_{nk}\psi_k^{(0)} = (E_n^{(1)} - V)\psi_n^{(0)} \tag{A.13}$$

Recalling that

$$H^{(0)}\psi_k^{(0)} = E_k^{(0)}\psi_k^{(0)} \tag{A.14}$$

We now have

$$\sum_{k \neq n}(E_k^{(0)} - E_n^{(0)})a_{nk}\psi_k^{(0)} = (E_n^{(1)} - V)\psi_n^{(0)} \tag{A.15}$$

To arrive at the first order correction of the energy, multiply both sides of the equation by

$\langle \psi_n^{(0)} |$ from the left and integrate. We are now left with

$$\sum_{k \neq n} (E_k^{(0)} - E_n^{(0)}) a_{nk} \langle \psi_n^{(0)} | \psi_k^{(0)} \rangle = 0 = E_n^{(1)} - \langle \psi_n^{(0)} | V | \psi_n^{(0)} \rangle \tag{A.16}$$

which simplifies to

$$E_n^{(1)} = \langle \psi_n^{(0)} | V | \psi_n^{(0)} \rangle \tag{A.17}$$

So we now have the first order correction to the energy. To obtain the first order correction to the wave function, $\Psi_n^{(1)}$ we multiply the first order equation (A.15) by $\langle \psi_k^0 |$ from the left and integrate. We arrive at

$$a_{nk}(E_k^{(0} - E_n^{(0)}) = -\langle \psi_k^{(0)} | V | \psi_n^{(0)} \rangle \tag{A.18}$$

Solving for a_{nk} we obtain

$$a_{nk} = -\frac{\langle \psi_k^{(0)} | V | \psi_n^{(0)} \rangle}{E_k^{(0)} - E_n^{(0)}}, \quad k \neq n \tag{A.19}$$

Substituting this expression for a into equation (A.12) for the first order correction to the wavefunction results in

$$\psi_n^{(1)} = \left[-\sum_{k \neq n} \frac{\langle \psi_k^{(0)*} | V | \psi_n^{(0)} \rangle}{(E_k^{(0)} - E_n^{(0)})} \right] | \psi_k^{(0)} \rangle \tag{A.20}$$

We now have both the first order correction to the energy and the first order correction to the wavefunction in hand.

A.1.2 Second Order Correction

To solve for the second order correction to the energy we make use of the second order equation from above

$$H^{(0)}\psi_n^{(2)} + V\psi_n^{(1)} - E_n^{(0)}\psi_n^{(2)} - E_n^{(1)}\psi_n^{(1)} - E_n^{(2)}\psi_n^{(0)} = 0 \tag{A.21}$$

Multiplying this equation by $\langle \psi_n^{(0)} |$ and integrating we arrive at

$$\langle \psi_n^{(0)} | H^{(0)} | \psi_n^{(2)} \rangle + \langle \psi_n^{(0)} | V | \psi_n^{(1)} \rangle = E_n^{(0)} \langle \psi_n^{(0)} | \psi_n^{(2)} \rangle + E_n^{(1)} \langle \psi_n^{(0)} | \psi_n^{(1)} \rangle + E_n^{(2)} \tag{A.22}$$

Now, keeping in mind that all corrections to the n^{th} order wavefunction are orthogonal to the reference wavefunction (which is 0^{th} order) we are left with

$$E_n^{(2)} = \langle \psi_n^{(0)} | V | \psi_n^{(1)} \rangle = -\sum_{k \neq n} \frac{\langle \psi_n^{(0)} | V | \psi_k^{(0)} \rangle \langle \psi_k^{(0)} | V | \psi_n^{(0)} \rangle}{E_k^{(0)} - E_n^{(0)}} \tag{A.23}$$

after substituting equation (A.8) in for $\Psi_n^{(1)}$.

A.2 Perturbing the Harmonic Oscillator (Expanded Formalism)

Here we present in detail the polynomial method developed in this work. We begin with the Schroedinger equation for the quantum mechanical harmonic oscillator [39]

$$\left(\frac{-\hbar^2}{2m} \frac{d^2}{dx^2} + \frac{kx^2}{2} \right) \Psi = E\Psi \tag{A.24}$$

where the quadratic potential operator, $\frac{kx^2}{2}$, is separable from the kinetic operator, m is the effective mass, and k is the force constant. The quadratic potential describes the normal mode motions according to the harmonic model. The harmonic frequencies are computed from the diagonalized mass-weighted Hessian (force constant) matrix represented by

$$k_{ij} = \left(\frac{d^2V}{dx_i dx_j} \right) \tag{A.25}$$

The resulting eigenvectors are the normal mode motions of each atom, and the eigenvalues provide the vibrational energies.

For the perturbed harmonic oscillator

$$\left(\frac{-\hbar^2}{2m} \frac{d^2}{dx^2} + \frac{kx^2}{2} + \beta x^3 + \gamma x^4 \right) \Psi = E\Psi \tag{A.26}$$

Let us define the unit of energy as $\hbar\omega/2$ and multiply equation (A.11) above by $\left(\frac{2}{\hbar\omega} \right)$, where $\omega = 2\pi\nu$. This gives us the expression

$$\left(\left(\frac{2}{\hbar\omega} \right) \frac{-\hbar^2}{2m} \frac{d^2}{dx^2} + \left(\frac{2}{\hbar\omega} \right) \frac{kx^2}{2} + \left(\frac{2}{\hbar\omega} \right) \beta x^3 + \left(\frac{2}{\hbar\omega} \right) \gamma x^4 \right) \Psi = \left(\frac{2}{\hbar\omega} \right) E\Psi \tag{A.27}$$

Now we may define the quantity ε to be $\left(\frac{2E}{\hbar\omega} \right)$ and simplify

$$\left(\frac{-\hbar}{m\omega} \frac{d^2}{dx^2} + \frac{kx^2}{\hbar\omega} + \left(\frac{2}{\hbar\omega} \right) \beta x^3 + \left(\frac{2}{\hbar\omega} \right) \gamma x^4 \right) \Psi = \varepsilon\Psi \tag{A.28}$$

In equation (A.12) above, we wish to simplify terms by gathering constants and the variable x into a single variable q. More importantly this will put x in terms of the unitless length, q. [40] For the first term on the left hand side of equation (A.12), we make the following substitution

$$\left(\frac{-\hbar}{m\omega}\frac{d^2}{dx^2}\right)=\frac{-d^2}{dq^2} \tag{A.29}$$

In order for this to be true, q must be

$$q=\sqrt{\frac{m\omega}{\hbar}}x \tag{A.30}$$

Check:

$$\left(\frac{-\hbar}{m\omega}\frac{d^2}{dx^2}\right)=\frac{-d^2}{d\left(\frac{m\omega}{\hbar}x\right)^2}=\frac{-d^2}{dq^2} \tag{A.31}$$

From equation (A.13) we also see that x must be

$$x=\sqrt{\frac{\hbar}{m\omega}}q \tag{A.32}$$

Substituting this expression wherever x appears in the remaining terms produces

$$\left(\frac{-d^2}{dq^2}+\frac{k}{\hbar\omega}\frac{\hbar}{m\omega}q^2+\left(\frac{2}{\hbar\omega}\right)\beta\left(\frac{\hbar}{m\omega}\right)^{\frac{3}{2}}q^3+\left(\frac{2}{\hbar\omega}\right)\gamma\left(\frac{\hbar}{m\omega}\right)^2q^4\right)\Psi=\varepsilon\Psi \tag{A.33}$$

Recall that $k=m\omega^2$ and substitute this expression for k

$$\left(\frac{-d^2}{dq^2}+\frac{m\omega^2}{\hbar\omega}\frac{\hbar}{m\omega}q^2+\left(\frac{2}{\hbar\omega}\right)\beta\left(\frac{\hbar}{m\omega}\right)^{\frac{3}{2}}q^3+\left(\frac{2}{\hbar\omega}\right)\gamma\left(\frac{\hbar}{m\omega}\right)^2q^4\right)\Psi=\varepsilon\Psi \tag{A.34}$$

Canceling and rearranging:

$$\left(\frac{-d^2}{dq^2}+q^2+\beta\left(\frac{2}{\hbar\omega}\right)\left(\frac{\hbar}{m\omega}\right)^{\frac{3}{2}}q^3+\gamma\left(\frac{2}{\hbar\omega}\right)\left(\frac{\hbar}{m\omega}\right)^2 q^4\right)\Psi=\varepsilon\Psi \tag{A.35}$$

Our perturbation takes the form of a polynomial

$$V(q)=Bq^3+Cq^4 \tag{A.36}$$

Recognize that we now have this same form in equation (A.15) above, where

$$B=\beta\left(\frac{2}{\hbar\omega}\right)\left(\frac{\hbar}{m\omega}\right)^{\frac{3}{2}} \tag{A.37}$$

and

$$C=\gamma\left(\frac{2}{\hbar\omega}\right)\left(\frac{\hbar}{m\omega}\right)^2 \tag{A.38}$$

This leaves us with the perturbed harmonic oscillator in terms of q, the desired unitless length and with the energy in units of $\hbar\omega/2$

$$\left(\frac{-d^2}{dq^2}+q^2+Bq^3+Cq^4\right)\Psi=\varepsilon\Psi \tag{A.39}$$

VITA

John Michael Craig was born at the Camp Zama Army Base in Kanagawa Ken, Tokyo, Japan on December 10, 1969. He graduated from Mills E. Godwin High School in Richmond, Virginia in 1988 and attended J. Sergeant Reynolds Community College where he obtained his A.S. degree in engineering, in 1996. He then went on to complete his B.S. (ACS) degree in chemistry at Virginia Commonwealth University in 1998. He enrolled in the chemistry graduate program at VCU in August of 1998 and joined Dr. Donald Shillady's research group in February of 2000. He is co-author on four publications and has presented his research at scientific meetings.

Publications

Holden C.A., Hunnicutt S.S., Sanchez-Ponce R., Craig, J. M., Rutan, S. C. "Study of complexation in methanol/water mixtures by infrared and Raman spectroscopy and multivariate curve resolution - alternating least-squares analysis." Applied Spectroscopy, 2003, 57 (5), pp. 483-490.

Shillady, D.D., Craig, J., Rutan, S., Rao, B. J. "Explicitly correlated SCF study of anharmonic vibrations in $(H_2O)_2$." International Journal of Quantum Chemistry, 2002, 90 (4-5), pp. 1414-1420.

Shillady, D.D., Craig, J., Rutan, S. "Explicitly correlated SCF study of small hydrides." International Journal of Quantum Chemistry, 2001, 85 (4-5), pp. 520-528.

Trindle, C., Shillady, D., Craig, J., Rutan, S. "Dye probes of nanoclusters in liquids." Journal of Cluster Science, 2001, 12 (3), pp. 473-486.

Presentations

Craig, J., Shillady, D., Rutan, S., Hunnicutt, S., and Bezemer, E. "Theoretical Investigation of the Structure and Vibrational Frequencies of Homogeneous and Heterogeneous Clusters of HPLC Solvents: Water, Methanol, and Acetonitrile." Oral presentation at the ACS National Meeting. Summer 2002, Boston, MA.

Trindle, C., Shillady, D., Craig, J., and Rutan, S. "Dye Probes of Nanoclusters in Liquids." Poster presented at the Virginia ACS Meeting, Fall 2000, Richmond, VA.